DNA Damage Induction by Bilirubin Induced Oxidative Stress and Activation of DNA Repair Pathways by Bilirubin

Thesis

DNA damage induction by bilirubin induced oxidative stress and activation of DNA repair pathways by bilirubin

Vipin Singh Rawat

This thesis is submitted for the degree of Doctor of Philosophy in the Faculty of Life Sciences of the Open University, UK

International Centre for Genetic Engineering and Biotechnology (ICGEB), Trieste, Italy

Director of Studies- Dr. Andrés Fernando Muro

External supervisor- Dr. Eduard Ayuso

Submitted March, 2018

Acknowledgements

First of all, I would like to thank Dr.Andrés Fernando Muro, for giving me the opportunity to work in his lab. The healthy discussion with him about the work and science ignited me both as a scientist as well as person. I would also like to thank the ICGEB for providing me fellowships and other supports.

I would also like to say my special thanks to Prof. Claudio Tiribelli's lab, especially Dr. Silvia Gazzin, Eleonora Vianello and Sandra Leal for all the help during initial part of the project.

I would also like to thank all the past and present colleagues of the Mouse Molecular Genetics lab, Fabiola Porro, Sandra Iaconcig, Alessia De Caneva, Luka Bockor, Simone Vodret, Luisa Costessi, Guilia Bortolussi, Giulia De Sabbata, Joseph Olajide, Michela Lisjak and Riccardo Sola for all the help in the lab.

My gratitude also goes to Jayashree thatte for helping me in every possible way.

I also would like to thank my PhD check point examiners Prof. Banks and Prof. Burrone. My special thanks to Marco Bestagno for all the help in FACS experiments.

Finally, I would like to thank my Mother and other family members for all the patience and constant support during all these years.

Table of contents

List of Figures

List of Tables **56**

Abbreviations

ABRs	Auditory brainstem response
AD	Alzheimer's disease
ALS	Amylotrophic lateral sclerosis
Alt- EJ	Alternative end joining
APLF	Aprataxin-and-PNK-like factor
ATF-3 and 4	Activating transcription factors 3& 4
ATF6	Activating transcription factor 6
ATM	Ataxia telangiectasia mutated
ATR	Ataxia telangiectasia and Rad3- related
BAEP	Brain auditory evoked potential
BER	Base-excision repair pathway
Bf	Free bilirubin
BIND	Bilirubin induced neurological dysfunction
CDKs	Cyclin dependent kinase
CHOP	C/EBP homologous protein
CH_3OH	Methanol
$CHCl_3$	Chloroform
CNS	Central nervous system
DMSO	Dimethyl sulphoxide

DMEM	Dulbecco's modified Eagle's medium
DNA	Deoxyribonucleic acid
DNA PKcs	DNA-dependent protein kinase, Catalytic subunit
DR5	Death receptor
DSB	Double stranded break
DSBR	Double stranded break repair
EMEM/F12	Eagle's minimum essential medium F12
ER stress	Endoplasmic reticulum stress
FCS	Fetal calf serum
GGR	Global genome repair
GRP78	Glucose-regulated protein 78
HD	Huntington disease
H_2O_2	Hydrogen peroxide
HO-1	Heme oxygenase-1
HR	Homologous recombination
HRP	Horse radish peroxidase
IL1β	Interleukin-1 β
IL6	Interleukin-6
IRE1	Inositol requiring 1

INFγ	Interferon- γ
mRNA	Messenger RNA
MMEJ	Micro homology mediated end- joining
MMR	Mismatch repair
Mrp-2	Multidrug resistance protein-2
MTT	3(4,5-dimethylthiazolyl-2)-2,5diphenyl tetrazolium
NAC	N-acetyl cysteine
NaCl	Sodium chloride
NaHCO3	Sodium bicarbonate
Na_2HPO_4	Sodium phosphate dibasic
$NaH_2PO_4.H_2O$	Sodium dihydrogen monophosphate mohohydrate
NER	Nucleotide-excision repair
NFKβ	Nuclear factor kappa-light-chain-enhancer of B-cells
NHEJ	Non-homologous end joining
Nrf-2	Nuclear factor (erythroid-derived 2)-like 2
NP-40	Nonidet P-40
PBS	Phosphate buffer saline
PCs	Purkinje cells

PD	Parkinson's disease
PERK	Protein kinase RNA – like endoplasmic reticulum kinase
PFA	Paraformaldehyde
PI	Propidium iodide
RNS	Reactive nitrogen species
ROS	Reactive oxygen species
RPA	Replication protein-A
SSBs	Single stranded breaks
SSBR	Single-stranded break repair pathway
TB	Total bilirubin
TCR	Transcription coupled repair
TNFα	Tumour necrosis factor-α
TSB	Total serum bilirubin
UCB	Unconjugated bilirubin
UGT1A1	Uridine glucuronosyl transferase 1A1
UPR	Unfolded protein response
WRN	Werner
XLF	Xrcc4 like factor
Xrcc4	X-ray cross complementing protein-4
8-OH G	8-hydroxy guanine

Abstract

“Kernicterus” due to hyperbilirubinemia is one of main cause of irreversible brain damage in low and middle income countries. Deaths due to “kernicterus” are ranked within the top 3 causes of neonatal death in African countries. Neonates experiencing permanent or temporary absence or reduced activity of Uridine diphosphate-glucuronosyl-transferase A1 (UGT1A1) enzyme present increased levels of total unconjugated bilirubin (UCB) in the blood. When the bilirubin binding capacity of serum albumin is saturated, this results in the increase in the free fraction of bilirubin (Bf). The excess of Bf is accumulated in lipid-rich tissues such as the brain, where it may reach toxic levels causing bilirubin-induced encephalopathy in jaundiced newborns and patients with Crigler-Najjar syndrome Type I, leading to kernicterus if not promptly treated. Bilirubin causes severe neurological dysfunction by affecting several different cellular pathways such as, induction of oxidative stress, endoplasmic reticulum (ER) stress, autophagy, neuroinflammation and DNA damage.

The work done in this thesis focus on the DNA damaging effect of bilirubin on neuronal (SH SY 5Y) and non-neuronal (HeLa) cells and the effect of bilirubin on the different double stranded break (DSB) repair pathways was investigated using HeLa DR GFP and HeLa cell lines.

Bilirubin exposure led to time-dependent increase in DNA damage in neuronal cells. Treatment with the anti-oxidant N-acetylcysteine (NAC) caused a dose-dependent decrease in DNA damage, suggesting a key role of oxidative stress in bilirubin-induced DNA damage.

In the second part of this work, I studied the effect of bilirubin on different DSB repair pathways using HeLa cell lines. Treatment with

bilirubin modulated Homologous Recombination (HR) in a time-dependent manner. In fact, treatment with different doses of bilirubin led to a dose-dependent increase in HR. Bilirubin-induced increase in HR was reversed by addition of NAC, suggesting the important role of oxidative stress in bilirubin-induced modulation of HR. DNA damage analysis after bilirubin treatment showed an increase in DNA damage in HeLa cells. Unexpectedly, bilirubin-induced DNA damage had no effect on the cell cycle profile. Similarly, exposure to bilirubin concentrations similar to those found in patients led to an increase in the Non-Homologous End Joining (NHEJ) pathway. These results suggest the general increase in DSB repair pathways by bilirubin.

INTRODUCTION

1.1 Bilirubin metabolism

Bilirubin is the final product of heme catabolism in mammals. About 80% of heme is haemoglobin derived, while the remaining 20% is derived from myoglobin and other heme-containing proteins such as cytochromes, catalase and peroxidase (Sticova and Jirsa, 2013). It can also be generated due to inefficient erythropoiesis in the bone marrow (London et al., 1950). Mainly occurring in the reticulo-endothelial system, the prosthetic heme groups are oxidized into biliverdin by heme oxygenase (HO-1) and then reduced into bilirubin by biliverdin reductase (Figure 1).

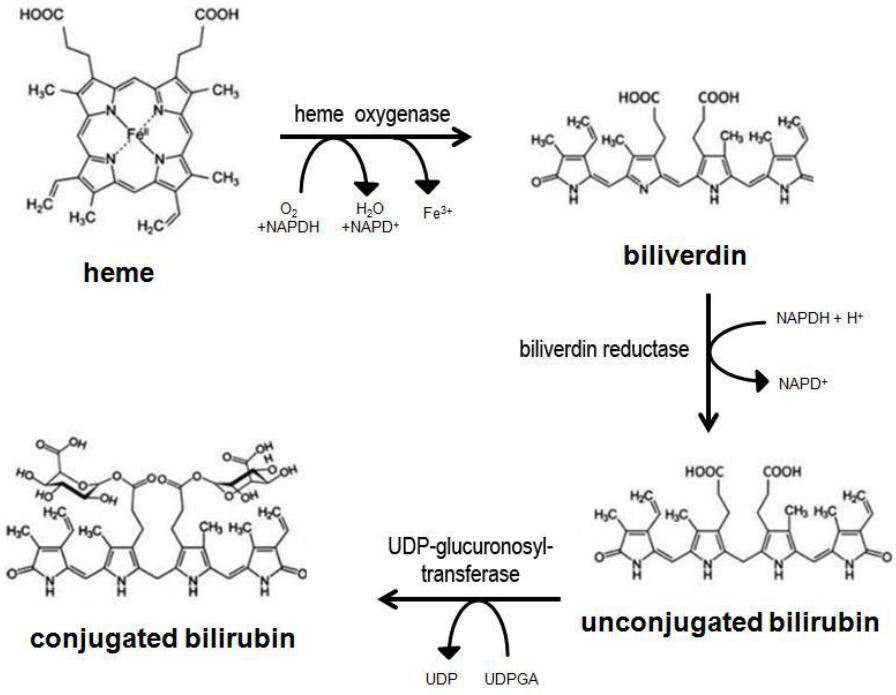

Figure 1. Metabolism of bilirubin. The structures of heme, biliverdin, unconjugated and conjugated bilirubin are shown, along with the enzyme catalysing each step. Adapted from (Jangi et al., 2013).

Bilirubin is water insoluble in nature. It circulates in the plasma as serum albumin bound form. Unconjugated bilirubin (UCB) is taken rapidly by hepatocytes where it is conjugated to glucuronic acid and converted into bilirubin mono and diglucuronides by the endoplasmic

reticulum localized enzyme UDP-glucuronosyl transferase A1 (UGT1A1) (Figure 2) (Bosma, 2003; Jangi et al., 2013). Bilirubin conjugation increases its solubility and is necessary for its safe disposal from the body through the bile fluid, thus, preventing its accumulation to toxic levels in plasma and lipid-rich tissues, such as the brain. The conjugated form of bilirubin is transported out from hepatocytes to the bile fluid by active transporters such as multidrug-associated resistance protein 2 (Mrp2 or ABCC2) (Erlinger et al., 2014; Jemnitz et al., 2010; Keppler, 2011). Bacterial β-glucuronidase present in the intestine partially deconjugates bilirubin, followed by degradation to urobilinogen and stercobilinogen, and their respective oxidation products (Maki et al., 1962; Maki et al., 1964). A fraction of the intestinal bilirubin is absorbed by enterocytes to reach the liver in adults. This enterohepatic cycle may contribute to an increase of plasma bilirubin in neonates (Vitek and Carey, 2003). Under physiological conditions, a significant portion of bilirubin glucuronides enters into the blood stream through the ABCC3 transporter followed by re-entry into downstream hepatocytes via OATP1B1/3. This process helps to prevent the saturation of biliary excretion capacity of upstream hepatocytes (van de Steeg et al., 2012).

The liver is the main organ of UGT1A1 expression, although it is also found at much lower levels in a few extra-hepatic tissues like kidney, intestine and skin (Fisher et al., 2001; Fujiwara et al., 2015; Sumida et al., 2013).

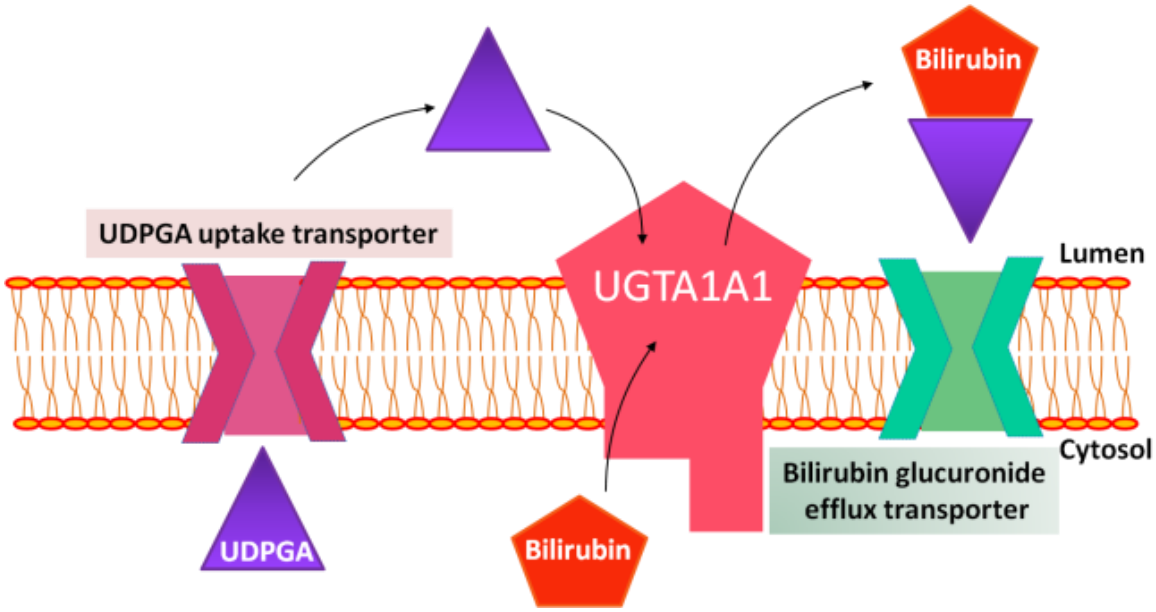

Figure 2. Bilirubin conjugation in hepatocytes. Bilirubin is conjugated with glucuronic acid in the lumen of the endoplasmic reticulum. Bilirubin glucuronides are then transported out from the lumen to the cytosol by the bilirubin glucuronide efflux transporter. Adapted from (Erlinger et al., 2014).

1.2 Hyperbilirubinemia conditions

Hyperbilirubinemia can be broadly categorised into genetic and non-genetic types, according to the main causes of the condition:

1.2.1 Genetic hyperbilirubinemia

Crigler-Najjar syndrome type I (CNSI)

CNSI is a very rare recessive condition affecting about 0.6-1 in 1 million live newborns. It is caused by mutations in UGT1A1 gene that result in the complete absence of the UGT1A1 enzyme. Due to absence of UGT1A1, bilirubin glucuronidation does not occur, causing severe hyperbilirubinemia, with neurotoxicity followed by death due to kernicterus, if untreated (Bosma, 2003; Crigler and Najjar, 1952).

Crigler-Najjar syndrome type II (CNSII)

CNSII is a milder form of the disease, which is characterised by low level or activity of UGT1A1 enzyme due to non-inactivating mutations in the gene that reduce the activity of the enzyme (Arias, 1962). Studies in CNSII patients with mild hyperbilirubinemia showed that their bile contains mostly unconjugated bilirubin, monoglucuronides and a small fraction of diglucuronides (Sinaasappel and Jansen, 1991). Phenobarbitol-induced UGT1A1 expression is sufficient to prevent bilirubin-induced encephalopathy, by reducing the levels of plasma bilirubin (Yaffe et al., 1966).

Gilbert syndrome

Gilbert syndrome affects 3-13% of the populations (Owens and Evans, 1975; Travan et al., 2014). It is the mildest form of genetic hyperbilirubinemia with at least 50% reduction in hepatic biliubin UGT1A1 enzyme activity (Auclair et al., 1976). The most common genotype in the Caucasian population is the presence of two extra TA bases in TATAA box in the promoter region of UGT1A1 gene. The presence of the extra TA dinucleotide in the promoter region decreases the RNA polymerase affinity to promoter, which leads to reduced gene expression (Bosma et al., 1995; Monaghan et al., 1996). Other genetic conditions include blood related disorders like ABO incompatibility and Glucose-6 phosphate dehydrogenase deficiency. These conditions aggravate the hyperbilirubinemia by increased hemolysis and altered metabolism (Kaplan et al., 2000; Kaplan et al., 1997).

1.2.2 Non-genetic hyperbilirubinemia

The most common cause of non-genetic hyperbilirubinemia is the delayed induction of the UGT1A1 enzyme after birth, which is more pronounced in pre-term babies. Hyperbilirubinemia may be further aggravated by other conditions, such as increased breakdown of fetal erythrocytes, inefficient transport of serum albumin to liver, leading to acute bilirubin encephalopathy (Bhutani and Wong, 2013; Greco et al., 2016).

Several non-genetic factors can also affect bilirubin metabolism. Pathological conditions like sepsis, viral infection, hypoxia, or hepatic disorders may affect liver function by impairing the glucuronidation system and, thereby, increasing serum unconjugated bilirubin levels. Another possible cause of hyperbilirubinemia is related to breast milk

feeding. Breast milk reduces the expression of the intestinal UGT1A1, thus contributing to the elevated level of UCB during early neonatal days when the expression of liver enzyme is very low (Fujiwara et al., 2012). Neonatal jaundice may be further complicated by the β-glucuronidase enzyme of breast milk, due to increased bilirubin de-conjugation and reabsorption in the gut. In addition, inadequate breast milk consumption may result in dehydration, further complicating the condition of the newborn.

1.3 Free bilirubin (Bf) concept

Most clinical laboratories biochemically measures total serum bilirubin (TSB) into direct and indirect fraction. The direct fraction consists of bilirubin mono and di-glucuronides, while indirect bilirubin (UCB) is made up of the fraction left after subtraction of direct bilirubin from total bilirubin (Smith et al.).

Bilirubin has poorly aqueous solubility at physiological pH and needs to enter the liver in order to get conjugated by the UGT1A1 enzyme in hepatocytes. Due to its high binding affinity to serum albumin, bilirubin travels in the bloodstream bound to albumin (Ostrow et al., 1994). As the level of TB increases, the bilirubin-binding capacity of serum albumin gets saturated resulting in the increase in the UCB free fraction (Bf), which is not bound to albumin (Wennberg et al., 1979). Bf is usually less than 0.1% of the total plasma bilirubin. Due to its lipophilic nature, this small fraction of total bilirubin (Bf) can cross lipid-rich membranes. This is particularly important in hyperbilirubinemic conditions, as Bf may cross the blood-brain-barrier (BBB), accumulating in specific brain regions, causing severe neurotoxicity and, eventually, permanent brain damage (Ostrow et al., 2004). Bf is the

main player in bilirubin-induced encephalopathy in jaundiced newborns and patients with Crigler-Najjar syndrome Type I and II (Ahlfors and Wennberg, 2004; Ihara et al., 1999; Wennberg et al., 2006). Studies in hyperbilirubinemic animals showed Bf to be a major determinant of bilirubin-induced toxicity (Wennberg and Hance, 1986). In premature neonates with hyperbilirubinemia induced encepthalopathy, Bf is a more sensitive marker than TB (Amin et al., 2001). Recently, our lab showed that administration of human serum albumin to a genetic mouse model of neonatal hyperbilirubinemia resulted in increased plasma serum bilirubin binding capacity, leading to the mobilisation of bilirubin from tissues to plasma (Vodret et al., 2015). This resulted in the reduction of plasma Bf, forebrain and cerebellum bilirubin levels, saving the life of the hyperbilirubinemic pups. Unfortunately, free bilirubin is not measured regularly in jaundiced patients due to unavailability of sensitive and accurate measurement methods (Ahlfors et al., 2006; Amin and Lamola, 2011).

1.4 Bilirubin-induced neurological dysfunction (BIND)

Neonatal hyperbilirubinemia and jaundice affects about 85% of the newborns. It is usually a benign and transitional condition for the majority of neonates. However, increased levels of UCB may cause serious brain damage to a small proportion of newborns when mild bilirubin encephalopathy is followed by acute bilirubin encephalopathy (kernicterus) (Watchko and Tiribelli, 2013). In recent years, the interest in bilirubin-induced encephalopathy reawakened due to increase in its prevalence, associated to reduced monitoring consequent to early discharge of mothers and neonates from the hospitals (Bhutani and Wong, 2013; Kaplan and Hammerman, 2005). Newborns with

prolonged bilirubin exposure experience clinical symptoms like lethargy, opthalmoplegia (ocular muscles paralysis), high pitch crying, opisthotonus (bowed body and rigid extremities or dystonia), and seizures, as well as mental retardation, and often death by kernicterus (Shapiro, 2003; Smitherman et al., 2006). The regions targeted by bilirubin in developing brain includes basal ganglia, cochlear and occulomotor nuclei, cerebellum that includes granular and Purkinje neurons (Lauer and Spector, 2011; Watchko, 2006). Even moderate levels of UCB have been associated with developmental delay, attention-deficit disorders, autism, and isolated neural hearing loss (Shapiro, 2010). Exposure to high levels of bilirubin for long time may lead to severe neurological sequelae and it could have permanent impact on infant's learning and memory.

Severity of BIND can be measured by magnetic resonance (Refaey et al., 2017), images of brain (Shah et al., 2003), or by brain auditory evoked potential (BAEPs, or auditory brainstem response ABRs), as the auditory system is particularly sensitive to bilirubin toxicity (Shapiro and Nakamura, 2001). Hence, response to auditory stimuli represents a reliable method to investigate the neuronal activity.

So, detailed identification of different neurological events and new molecular targets triggering bilirubin toxicity will help to better understand and management of BIND.

1.5 Kernicterus

'Kernicterus' is defined as the condition of irreversible brain damage produced by prolonged exposure to bilirubin. This term was coined by

Christian Schmorl in 1903 which means “yellow kern”, kern represents the most severely affected part of brain .i.e. nuclear region.

The incidence of kernicterus is variable in different parts of world, with 10 per 100,000 live births in the western world, while in low-income and middle-income countries it rises up to73 per 100,000 live births (Bhutani and Wong, 2013; Greco et al., 2016). Death due to kernicterus in Africa is ranked amongst the top 3 causes of death in newborns (Olusanya et al., 2014). The incidence rise in preterm infants born before 30 weeks of gestation (1.8 per 1000 live births) (Morioka et al., 2015). Increased incidence of kernicterus in America and rest of the world during 1980s and 1990s has been linked to early hospital discharge, the influence of managed care, increase in number of breast feeding infants and inappropriate breastfeeding during first week of life (Moerschel et al., 2008).

1.6 Mechanisms of bilirubin toxicity

1.6.1 Neurodegeneration

Neurodegeneration is the term used to describe the progressive loss of neuronal structure and function, including the death of neurons. Since neurons are post mitotic in nature, neurodegeneration strongly affects the central nervous system (CNS). Most of the attention, nowadays, is focussed on neurodegenerative diseases like Alzheimer’s disease (AD), Parkinson’s disease (PD), Huntington disease (HD) and Amylotrophic lateral sclerosis (ALS) (Brettschneider et al., 2015). In humans, most of the clinical and physiological features overlap between different neurodegenerative diseases, leading to misdiagnosis of the disease,

neurodegeneration being the shared feature. To avoid the problems with the phenotypic mis-identification of neurodegenerative diseases, animal models serve as useful tools to better characterize neurodegeneration (Harvey et al., 2011). Despite many efforts, the causes and key mechanisms initiating neurodegeneration are not yet well understood.

Neurodegenerative diseases are not merely characterised by altered neuronal function. They are also caused by events that can affect the integrity of neurons and development, such as lack of oxygen, leading to loss of dendrites and extensive fragmentation of the dendritic arbour (Wen et al., 2013), and traumatic brain injury (Petzold et al., 2011), resulting in neuronal cell death.

Neurodegeneration can be also caused by severe hyperbilirubinemia. Although neonatal jaundice is a benign and transient form of hyperbilirubinemia, bilirubin may raise up to neurotoxic levels. High lipid content of neuronal cells makes them particularly vulnerable to bilirubin due to high affinity of bilirubin to lipid rich membranes, especially myelin-rich membranes (Watchko and Tiribelli, 2013). UCB treatment reduced viability of dividing neuronal precursor cells, while neurogenesis is reduced without affecting astrogliogenesis (Fernandes et al., 2009). Differentiating hippocampal cells showed reduced neuronal arborization, dendritic output and axonal arborization after exposure to bilirubin (Fernandes et al., 2009). Bilirubin treatment inhibits cytochrome c activity in immature neuronal cells. In addition, bilirubin treatment impairs cellular oxygen consumption and collapses mitochondrial membrane potential that leads to apoptosis of neuronal cells (Vaz et al., 2010). Another report showed that exposure of primary rat neurons to bilirubin dissipates the mitochondrial membrane potential, leading to cellular energy failure followed by cytochrome c release and

activation of caspases and programmed cell death (Rodrigues et al., 2000). Bilirubin decreases cell viability by altering the redox status of cells (Tell and Gustincich, 2009). *In vivo* studies showed extensive Purkinje cells (PCs) degeneration in mouse models of hyperbilirubinemia (Barateiro et al., 2012; Bortolussi et al., 2014a; Bortolussi et al., 2012). In Gunn rats, acute hyperbilirubinemia leads to the impairment of presynapsis of glutaminergic neurons (Haustein et al., 2010).

1.6.2 Oxidative stress

Oxidative stress is the term used to define the state where imbalance of the antioxidant system occurs, with excessive incorporation/over production of free radicals/reactive oxygen species (ROS) from environment to the living system. Although oxygen is very important for life, impaired oxygen metabolism and ROS over-production is involved in several neurodegenerative diseases like AD, PD, and others (Uttara et al., 2009). Free radicals are chemical entities with unpaired electrons (McCord, 2000). They can be the by-product of aerobic respiration, by-products released from chemical reactions, or generated from electromagnetic radiations. The presence of unpaired electrons makes them extremely unstable, which in turn, become stable after transferring the unpaired electron to other molecules. However, these free radicals may be detrimental to cells due to their ability to oxidise proteins, DNA and lipid molecules of the cells. The levels of free radicals are tightly regulated by the cellular machinery. To overcome the detrimental effect of free radicals, cells have several enzymes involved in the antioxidant response like superoxide dismutase, glutathione peroxidase, catalase, thioredoxin, glutathione transferases, and HO1 (Cho et al., 2002). In

addition to enzymes of antioxidant system, non-enzymatic anti-oxidant molecules like β-carotene, vitamin C and E, uric acid and glutathione also helps to scavenge the free radicals (Birben et al., 2012).

One of the most extensively studied gene of the antioxidant system is the nuclear factor (erythroid-derived 2)-like 2 (Nrf2) (Jung et al., 2017). Oxidative stress leads to the transport of Nrf2 from cytoplasm to nucleus, where it binds to the antioxidant response element (ARE) in the upstream region of genes of the antioxidant system, such as glutathione transferases, oxidoreductases and HO-1 (Nguyen et al., 2009; Nguyen et al., 2003). HO-1, being an enzyme of antioxidant system, also plays an important role in bilirubin catabolism.

Mildly elevated concentrations of bilirubin are considered beneficial due to its antioxidant property (Stocker et al., 1987). Neonates having physiological jaundice have lower oxidative stress compared to controls (Kumar et al., 2007). However, higher concentrations of bilirubin lead to oxidative stress. Oxidative stress has been shown to play an important role in bilirubin neurotoxicity *in vitro*, through the increase in the level of glutathione in cells (Giraudi et al., 2011). Treatment of synaptosomal vesicles from gerbil cortical brain tissue with bilirubin leads to oxidative stress, loss of membrane asymmetry and functionality, lipid and protein oxidation and calcium intrusion (Brito et al., 2004). Treatment of Hepa 1c1c7 cells with bilirubin leads to oxidative stress, loss of mitochondrial membrane potential and caspase9 activation (Oakes and Bend, 2005; Seubert et al., 2002). *In vitro* experiments with HeLa cells and mouse embryonic fibroblasts (MEFs) showed bilirubin-induced oxidative stress after treatment with 80nM Bf (Cesaratto et al., 2007). Treatment with bilirubin creates ROS in SH SY 5Y cells and results in the overexpression of DJ-1 protein, a protein involved in various cellular

processes including oxidative stress (Deganuto et al., 2010). Sulphadimethoxine-induced hyperbilirubinemia in pups of Gunn rats causes lipid peroxidation, as determined by the levels of 4-hydroxy-2-nonenal (Bortolussi et al., 2015; Daood et al., 2012).UCB treatment leads to oxidative stress and apoptosis of neurones and astrocytes (Brito et al., 2008a; Brito et al., 2008b; Silva et al., 2001; Vaz et al., 2011). Similarly, bilirubin induces oxidative stress in SH SY 5Y and immature cortical neuronal cells (Qaisiya et al., 2014; Vaz et al., 2010). Research from our group has shown bilirubin-induced disturbance in the antioxidant system in the cerebellum of the C57BL/6 *Ugt1*$^{-/-}$ mouse model. 2D-gel electrophoresis and expression analysis of the cerebellum revealed increased expression of Nrf2 and lower expression of SOD1 (Bortolussi et al., 2015). Another interesting result includes the increased oxidation of peroxidase 2 and 6 upon bilirubin exposure. The perturbation in the antioxidant machinery of neuronal cells leads to their death (Bortolussi et al., 2015). Bilirubin induced oxidative stress was shown in another mouse model of hyperbilirubinemia. They observed an increase in oxidised glutathione and HO-1 protein levels in these animals (Yueh et al., 2014).

1.6.3 Endoplasmic reticulum stress

The endoplasmic reticulum (ER) is a specialized organelle of cells that contains several chaperones and detectors to facilitate protein folding and to detect the presence of misfolded/unfolded proteins, respectively. The ER has a strong oxidising environment to form disulfide bonds, and it may acts as a source of free radicals, suggesting a strong link between ER and oxidative stress (Malhotra and Kaufman, 2007). Depending on

the type of stress, ER stress response can be activated by one of the following proteins/pathways, or by their combination (Figure 3).

a) Inositol requiring 1 (IRE1).

b) Protein kinase RNA – like endoplasmic reticulum kinase (PERK).

c) Activating transcription factor 6 (ATF6).

Each of the above-mentioned proteins makes a different signalling network, which gets activated depending upon the type of stress (Doyle et al., 2011). The activation of unfolded protein response delays the translation process in order to clear the unfolded proteins and induces the expression of proteins involved in cell survival and protein degradation.

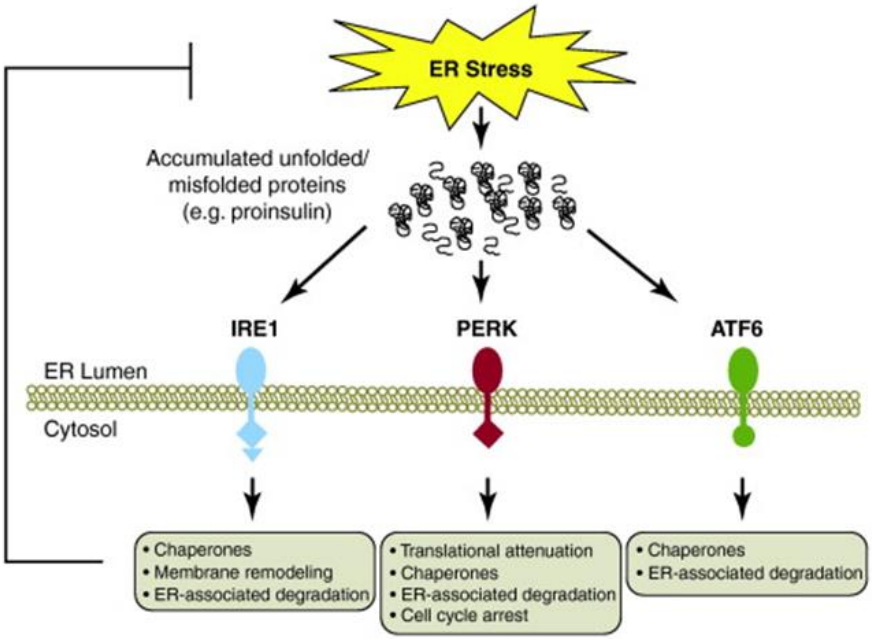

Figure 3. Endoplasmic reticulum stress signalling. ER stress activates three different master regulators (IRE1, PERK and ATF6) of ER stress in response to the accumulation of unfolded proteins. All three tranducers activate downstream targets that alleviate ER stress (Fonseca et al., 2011).

The accumulation of unfolded proteins stimulates ER stress, consequently the ER chaperone glucose-regulated protein 78 (GRP78) gets separated from IRE1, PERK and ATF6 (Doyle et al., 2011). GRP78 also helps newly synthesized proteins to get folded correctly.

Generally, the main role of this pathway is to restore the normal function of the cells by the activation of UPR target genes. However, if the ER stress sustains for longer time, then cells cannot attain the steady state. In this case, accumulation of unfolded proteins ends up with the activation of the apoptotic pathway. Activation of the C/EBP homologous protein (CHOP) and CD95/Fas leads to apoptosis by activating caspases (Li et al., 2014; Peter et al., 2015). In cancer cell lines, activation of ER stress leads to the increased transcription of important regulators like death receptor 5 (DR5), activating transcription factors 3 (ATF3) and 4 (ATF4), and CHOP. The activation of these genes results in apoptosis induced by the upregulation of caspase 9, caspase 8 and caspase 3 (Liu et al., 2012). ER stress is one of the main contributors to neurodegenerative diseases. Infact, neurodegenerative diseases like HD, AD, PD, and ALS are characterised by accumulation of aggregated proteins that affect ER stability.

ER homeostasis is also impaired by treatment of cells with bilirubin. Treatment of oligodendrocytes with bilirubin leads to the activation of ER stress by the overexpression of GRP78, IRE1 and ATF6 (Barateiro et al., 2012). Trancriptomic analysis of neuroblastoma cells after bilirubin treatment showed upregulation of ER stress-related genes such as CHOP and ATF3 (Calligaris et al., 2009). Another study showed ATF6, CHOP and GRP78 upregulation at mRNA level by bilirubin treatment of neuroblastoma cells. GRP78 was upregulated at protein level in neuroblastoma cells after bilirubin treatment; while ATF6 was

not upregulated at protein level. ER stress inhibition increases the survival of neuronal cells suggesting ER stress as one of the mechanism responsible for neurotoxicity (Qaisiya et al., 2017a). *In vivo* studies from our lab showed the upregulation of ATF3, CD95/Fas and CHOP, with the highest expression at the most aggressive stage of bilirubin toxicity. Immunofluorescence analysis of brain sections of hyperbilirubinemic mutant mice during early stages showed increased levels of CHOP in all the layers of the cerebellum. During later stages, CHOP and CD95/Fas was localised mostly in Purkinje cells. CHOP was localised mostly in severely degenerating Purkinje cells that were surrounded by microglia cells, suggesting microglia activation (Vodret et al., 2017). Microarray analysis of hepatoma cells treated with bilirubin showed the activation of ER stress, as revealed by overexpression of GRP78, ATF3, CHOP and PERK activation by phosphorylation (Oakes and Bend, 2010).

1.6.4 Neuroinflammation

Neuroinflammation is the general term used to describe inflammation in the brain and spinal cord. The CNS immune surveillance is mainly provided by glia (microglia, astrocytes, macrophages and oligodendrocytes) and endothelial cells. CNS inflammation normally acts as a protective mechanism of neuronal cells from stress. However, prolonged activation of inflammatory response may further result in the damage of neurons by the activation of glial cells. Migrating microglial/macrophages cells can either repair or exacerbate the situation, depending on their activation status. The ratio between M1 and M2 microglia cells determine the response, whether pro-inflammatory or anti-inflammatory. M1 microglia is pro-inflammatory and is associated with clearance of dead tissues (Kigerl et al., 2009;

Martinez et al., 2006), whilst M2 microglia is anti-inflammatory and are involved in repair of injured tissues by reducing the inflammatory mediators (Kigerl et al., 2009; Martinez et al., 2006).

Neurodegeneration is a common feature of several neurodegenerative diseases (Frank-Cannon et al., 2009). Activated microglia cells and their relative inflammatory markers accumulate at the site of neurodegeneration. Studies have been performed to verify the effect of bilirubin on the activation of glia cells. Bilirubin exposure activate astrocytes (Falcao et al., 2007; Fernandes et al., 2007; Fernandes et al., 2006; Fernandes et al., 2004) and microglia, resulting in the release of IL1β, IL6, TNFα, NFKβ, interferon γ (INFγ), and glutamate (Fernandes and Brites, 2009; Gordo et al., 2006; Silva et al., 2010). Activated microglia and astrocytes are also present in the brain of Gunn rats (Liaury et al., 2012; Mikoshiba et al., 1980). Activated glia cells are also found in a Ugt1a1 knockout mouse model (Barateiro et al., 2016; Vodret et al., 2017; Yueh et al., 2014). Bilirubin treatment leads to the expression of neuroinflammatory cytokines like IL-8, TNFα and NFκB in neuroblastoma cells (Qaisiya et al., 2017a). *In vivo* study in mutant animals found activation of microglia and astrocytes in cerebellum. Inflammatory regulators and TNFα were upregulated in mutant animals during most aggressive stage of bilirubin toxicity at mRNA level. Immunofluorescent analysis in cerebellum from mutant animals showed expression of TNFα in both astrocytes and microglia during the most severe stage of bilirubin toxicity. More detailed analysis into the type of microglia activated during neuroinflammation revealed activation of pro-inflammatory M1 microglia with a parallel decrease in anti-inflammatory M2 type microglia (Vodret et al., 2017).

1.6.5 Autophagy

Autophagy is a process of self degradation of a portion of the cytoplasm by the lysosome. During starvation, cells activate autophagy to increase the supply of nutrients to cells (Kuma et al., 2004). Basal autophagic activity is normally considered as a pro-survival mechanism, protecting cells from different types of stress (Scott et al., 2007). Autophagy is dysregulated in several neurodegenerative diseases like spinocerebellar ataxia (SCA), PD and HD (Calligaris et al., 2009; Rubinsztein et al., 2005).

In vitro experiments showed autophagy activation in cells by bilirubin treatment. Bilirubin-treated neuroblastoma cells overexpress the regulators of autophagy such as GABARAPL1 (GABA (A) or ATG8), and WIPI1 (WD repeat domain, phosphoinositide interacting 1 gene or Atg18) (Calligaris et al., 2009). Brain microvascular endothelial cells (BMEC) overexpress LC3 after exposure to bilirubin (Palmela et al., 2012). *In vitro* experiments in SH SY 5Y cells showed autophagy activation after bilirubin treatment (Qaisiya et al., 2017b). Hyperbilirubinemic mutant mice have activation of autophagy during the most aggressive stages of bilirubin toxicity suggesting autophagy may be a pro-survival mechanism used by cells against bilirubin-induced stress (Vodret et al., 2017).

1.6.6 DNA damage

As already mentioned above (Section 1.6.2), bilirubin can induce oxidative stress. Higher rate of oxidative metabolism in the brain accompanied by lower expression of antioxidant enzymes in neurons, compared to other somatic tissues, make them extremely susceptible to

oxidative stress. As a result, numerous oxidative lesions may accumulate in neurons due to the above-mentioned factors (Brooks, 2000). Association between oxidative stress and markers of oxidative stress have been already proven. In addition, DNA damage has been found to be an important factor to initiate neuronal cell death in several neuropathological diseases (Gabbita et al., 1998; Mattson, 2000). A previous study showed increased levels of 8-OH G (marker of DNA damage) in neonates even with lower bilirubin concentration (Basu et al., 2014). Bilirubin exposure results in DNA strand breaks in lymphocytes (Khan and Poduval, 2012). Bilirubin also induces double stranded breaks (DSBs) in the presence of Cu (Frock et al.) ions due to the generation of reactive oxygen species (ROS) (Asad et al., 1999). Treatment of SH SY 5Y cells with bilirubin leads to DNA damage and reduction in growth of cells. Levels of 8-OH G were upregulated after bilirubin treatment (Deganuto et al., 2010).

1.7 DNA damage in neurodegenerative diseases

Accumulation of DNA damage in neurons is a common feature of neurodegenerative diseases that includes ataxias, AD, PD, and HD (Kulkarni and Wilson, 2008; Rass et al., 2007). Higher rate of mitochondrial and nuclear DNA damage is attributed to the higher rate of mitochondrial respiration and ROS production (Weissman et al., 2007). Defects in base excision repair (BER) and single stranded break repair (SSBR) pathways trigger neuronal dysfunction and degeneration (Caldecott, 2008; Rass et al., 2007). The limited capacity of neurons of being replaced during adult stages and the accumulation of damaged, but irreplaceable, terminally differentiated neurons make them particularly vulnerable to DNA damage. In addition, neuronal cells

being in the G0 phase of the cell cycle utilize mostly the error-prone NHEJ to repair DNA damage (Rass et al., 2007). Neurons are highly transcriptionally active and oxidative stress can block transcription. This leads to shortage of transcripts in neuronal cells in normal ageing individuals that result in degeneration and apoptosis of neuronal cells (Ljungman and Lane, 2004).

1.8 DNA damage response

The main objective of every life form is to duplicate the genetic material followed by its transmission to the next generation with extreme fidelity. Duplication of genetic material should be done precisely, despite being exposed continuously to several exogenous and endogenous DNA damaging agents. To overcome the damaging effects of these agents, cells have developed different signalling mechanisms to recognise DNA damage, signal its presence, followed by repair of the damage. Cells having defects in these mechanisms are extremely sensitive to many types of DNA damaging reagents (Jackson and Bartek, 2009). DNA can be damaged by mis-incorporation of bases during the normal replication of the cells. DNA strand breaks can also be generated by aborted topoisomerase I and II activity. DNA can be damaged by reactive oxygen species (ROS) generated as by-products of the oxidative metabolism. ROS can be also generated by several environmental toxins, as well as by heavy metal-mediated Fenton reaction (Valko et al., 2006). ROS and reactive nitrogen species (Bernstein and Landing) can also be generated by neutrophils and macrophages during inflammation and infections (Kawanishi and Hiraku, 2006). These species can attack the DNA, leading to the formation of DNA adducts. These modified bases can impair base pairing, block DNA replication

and transcription, resulting in the loss of bases followed by single stranded breaks (SSBs) formation. DSBs can be generated when two SSBs are present in immediate proximity or when the DNA replication apparatus meets these SSBs or any other type of DNA lesion. Although DSBs are not so frequent like other lesions listed above, they are extremely deleterious to cells (Khanna and Jackson, 2001).

To counteract against the deleterious effect of DNA damage, cells have evolved distinct mechanism to detect the DNA damage, signal their presence and finally promote their repair (Harper and Elledge, 2007; Harrison and Haber, 2006).

1.9 DNA repair pathways

The diversity of DNA damaging lesions makes compulsory for cells to have multiple DNA repair pathways (Figure 4). Some lesions get repaired simply by a series of catalytic events catalyzed by a set of multiple proteins. During mismatch repair (MMR), mismatches, insertions/deletions loops lead to single stranded breakage that get finally repaired with the participation of polymerases, nucleases and ligases (Jiricny, 2006). In the case of the base-excision repair (BER) pathway, detection of mismatches and insertion/deletions loops by DNA glycosylase removes the damaged base before getting repaired by nucleases, polymerases and ligases (David et al., 2007). The nucleotide-excision repair pathway (NER) system recognises lesions that distort the DNA helix. NER operates by two different sub-pathways: transcription-coupled NER and global NER. Transcription-coupled NER repairs DNA lesions that block transcription, while global NER focuses on the helix distorting lesions that spread over the whole genome (Hoeijmakers, 2001).

The DSB repair pathway includes Non-Homologous End Joining (NHEJ) pathway (Lieber, 2008; Shibata, 2017) and Homologous Recombination (HR) (San Filippo et al., 2008). The NHEJ gets activated after DSB ends recognition by the Ku protein followed by binding and activation of the protein kinase DNA-PKcs. DNA PKcs activation leads to the recruitment and activation of end-processing enzymes, polymerases and DNA ligase IV (Baumann and West, 1998). Non-canonical Ku-independent NHEJ pathways includes micro homology mediated end joining (MMEJ) or alternative end joining (Alt- EJ). Activation of these Ku-independent pathways always results in deletions (Boulton and Jackson, 1996; Liang et al., 1996; McVey and Lee, 2008). Despite being error prone, NHEJ and Alt-EJ occurs in all phases of cell cycle. In contrast, HR can occur only during the S and G2 phases of the cell cycle due to the requirement of template strand to repair the damage precisely (San Filippo et al., 2008). The HR pathway is initiated by ssDNA formation. ssDNA formation is catalyzed by Mre11-Rad50-NBS1 (MRN) complex. In the next step, ssDNA invade the intact template strand, process which is catalyzed by Rad51, Brca1 and Brca2 proteins. After strand exchange, substrate resolution occurs with the help of polymerases, helicases and ligases (Figure 4) (Jackson and Bartek, 2009).

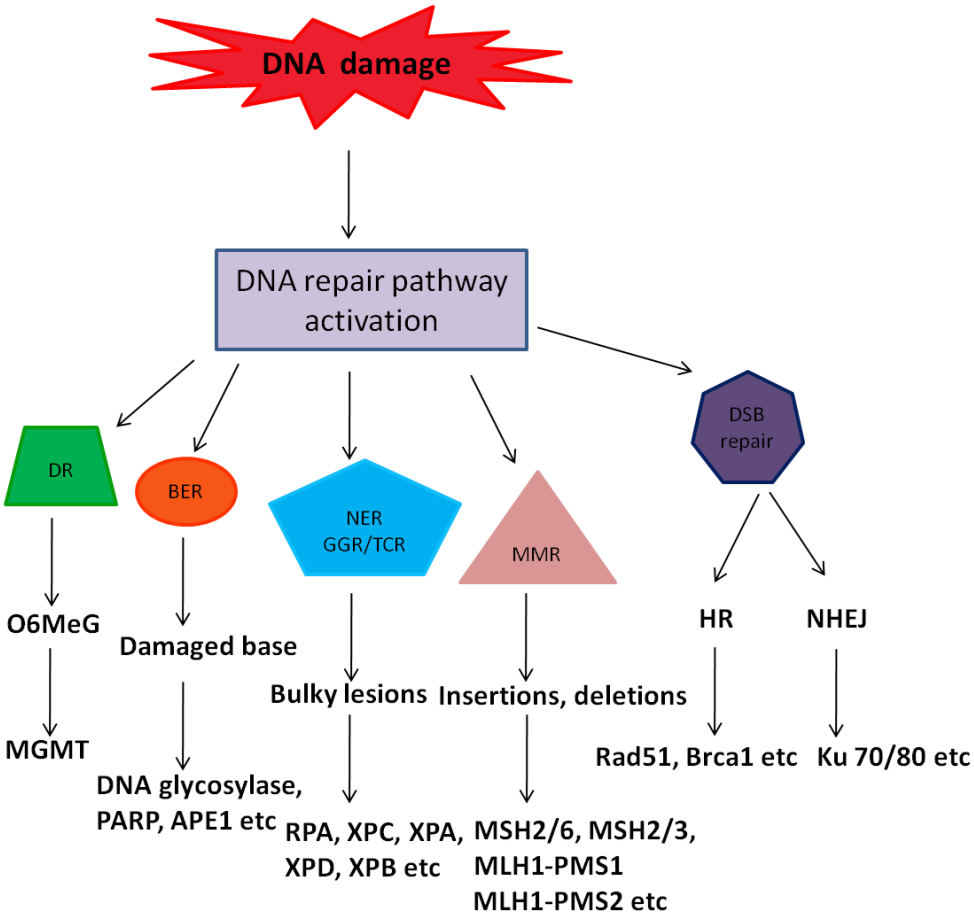

Figure 4. Different DNA repair pathways. DR: represents direct enzymatic repair, MGMT- O6-alkylguanine-DNA-alkyltrasferase, BER-Base excision repair, NER-nucleotide excision repair, GGR-Global genome repair, TCR-Transcription coupled repair, MMR-Mis-match repair, DSBR-Double stranded break repair, HR-Homologous Recombination, NHEJ-Non-Homologous End Joining. Adapted from (Damia and D'Incalci, 2007).

1.9.1 DNA damage and cell cycle checkpoints

The two most important DNA damage response (DDR) sensor protein kinases present in cells are Ataxia Telangiectasia mutated (ATM) and Ataxia Telangiectasia and Rad-3 related(ATR). ATM gets activated by double stranded breaks while ATR gets activated by Replication protein A (RPA) coated-ssDNA (Bartek and Lukas, 2007; Cimprich and Cortez, 2008; Shiloh, 2003). After recognition of DNA damage, ATM and ATR signal further downstream to activate CHK2 and CHK1 respectively. CHK1 and CHK2, along with ATM and ATR function to reduce the activity of cyclin dependent kinases (CDKs), by different mechanisms, activation of P53 is the most common one (Bartek and Lukas, 2007; Kastan and Bartek, 2004; Riley et al., 2008). Inhibition of CDKs leads to the slowing down or arrest of cell cycle at G1/S, intra S and G2/M checkpoint, giving time to the cell to repair the DNA before replication and mitosis initiates.

1.9.2 Homologous Recombination

The HR pathway plays an important role in the repair of DNA double stranded breaks. It uses the intact homologous sequence as template for repair (Heyer et al., 2010) (Figure 5). The repair process of the damaged piece of DNA requires the close proximity between undamaged homologous sequence and the damaged DNA sequence during S and G2 phases of cell cycle (Renkawitz et al., 2014; Weiner et al., 2009). HR can be divided into three substages: pre-synaptic, synaptic and post-synaptic phases.

The pre-synaptic phase is initiated by the binding of Mre11-Rad50-Xrs2 (MRX) complex in *S cerevisae* and Mre11-Rad50-Nbs1 (MRN)

complex in humans to the broken DNA termini (Lee et al., 2003; Paull and Gellert, 1999; Stracker and Petrini, 2011; Trujillo et al., 2003). In the next step, Mre11 together with CtIP initiates the 5'-3' resection at the broken DNA ends (Sartori et al., 2007; Symington and Gautier, 2011; Williams et al., 2007). The resection step is further continued by the concerted action of Exo1 (exonuclease 1), and the helicase-endonuclease activity of the Sgs-Top3-Rmi1 (STR)-Dna2 complex (BLM-TopoIIIα-RMI1/RMI2 (BTR)-DNA2 complex 1 (Cejka et al., 2010; Niu et al., 2010; Symington and Gautier, 2011). After end resection, the ssDNA binding protein Replication protein A (RPA) coats the ssDNA to minimize the secondary structure formation facilitating Rad51 loading. Rad51 binding to ssDNA leads to the formation of a presynaptic nucleoprotein, which can pair with the intact strand of sister chromatid after homologous sequence has been found during homology search (Fanning et al., 2006; Heyer et al., 2010).

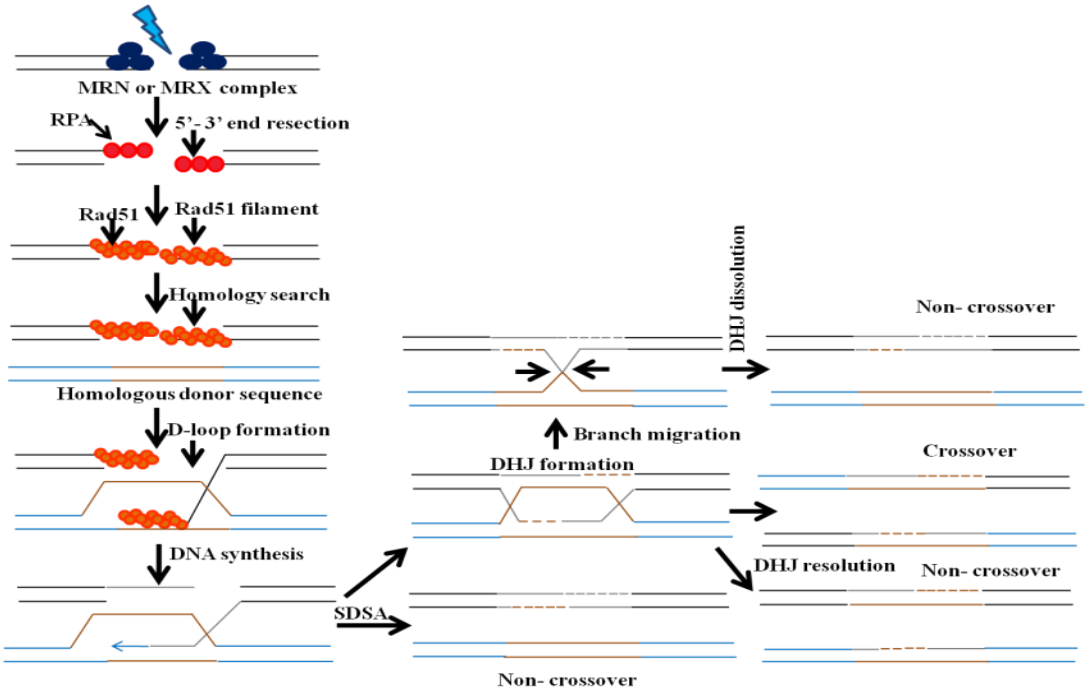

Figure 5. The Homologous Recombination pathway. Homologous Recombination pathway is divided into presynaptic (includes 5'-3' end resection, Rad51 filament formation and homology search), synaptic (this phase is characterised by D-loop formation) and post-synaptic phases resulting in different types of recombination products (this phase includes all steps after D-loop formation). Adapted from (Renkawitz et al., 2014).

Next is the synaptic phase, which is characterised by DNA strand exchange between the target DNA and Rad51 nucleofilament to form a structure known as displacement loop (D-loop). The D-loop consists of the heteroduplex DNA and the displaced strand of the donor DNA (Heyer et al., 2010; Shinohara et al., 1992). The next step is the post-synaptic phase, in which DNA synthesis starts at the 3' end of broken ends. During classic DSB repair pathways, the second end of the DSB aligns with the D-loop to form a double holiday junction (Ferguson and Holloman, 1996; Heyer et al., 2010; Nassif et al., 1994). In the next phase, resolvases such as Yen1 (GEN1) or the Mus8-Mms4 complex (MUS81-EME1) can either generate a crossover product or a non-crossover product from these symmetrical structures (Figure 5) (Heyer et al., 2010).

1.9.3 Homologous recombination reporter cell line (HeLa DR-GFP)

A very useful tool for the study of homologous recombination is the HeLa DR-GFP stable cell line. It contains a single integration site of a reporter construct, which has two differentially inactivated versions of tandemly repeated (DR) GFP, developed by Maria Jasin (Pierce et al., 1999). The upstream GFP gene (Cassette I) is interrupted by a Isce1 restriction enzyme site, a rare-cutting endonuclease (Jasin, 1996). Introduction of the Isce1 site leads to the formation of two in frame stop codons in Casette I, thereby inactivating Casette I. The downstream GFP fragment (Casette II) is truncated at 5' and 3' ends, resulting in a truncated, inactive, GFP product (502 bp).

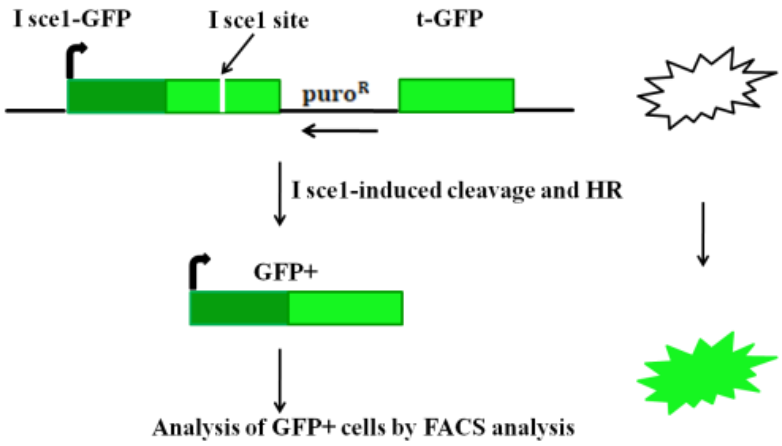

Figure 6. HeLa DR-GFP cell line. The HeLa DR-GFP cell line is a stable clone containing a single insertion of a recombination-reporter cassette. It is composed by an upstream GFP fragment interrupted by Isce1 site that leads to the introduction of two STOP codons. Downstream of the Isce1 GFP fragment, the t-GFP fragment is present, with both the 5' and 3' termini truncated. Transfection of the cells with plasmid encoding Isce1 leads to the Homologous Recombination between two fragments that lead to GFP expression. Adapted from (Cuozzo et al., 2007).

Transient transfection of cells with a plasmid encoding Isce1 induces Homologous Recombination between the two cassettes and production of active GFP, that can be quantified by flow cytometry (Figure 6) (Cuozzo et al., 2007).

1.9.4 Non- Homologous End Joining (NHEJ)

NHEJ is one of main DSB repair pathway of cells. It involves the re-ligation of the broken ends of the DNA (Weterings and Chen, 2008). NHEJ can mediate the ligation of any type of DNA ends. However, in contrast to HR, NHEJ does not require a homologous template to repair the DNA damage. Since NHEJ does not require a template, it is not restricted to a particular cell cycle phase.

The NHEJ can be divided into four sequential steps: 1) **DNA end recognition by Ku heterodimer**. The Ku heterodimer is composed of Ku70 and Ku80 at the DNA breakage site. The Ku heterodimer then acts as a scaffold for the recruitment of other NHEJ proteins. The Ku heterodimer has been shown to recruit directly and indirectly different NHEJ factors to DSBs like DNA-PKcs (Uematsu et al., 2007), X-ray cross complementing protein-4 (Xrcc4) (Costantini et al., 2007; Mari et al., 2006; Nick McElhinny et al., 2000), Xrcc4 like factor (XLF) (Yano et al., 2008), Aprataxin-and-PNK-like factor (APLF) (Grundy et al., 2013; Kanno et al., 2007; Macrae et al., 2008); 2) **DNA end bridging and promotion of end stability.** After DSB, Ku heterodimer binds to the broken DNA ends and maintains their stability because non-specific processing of DNA ends could lead to chromosomal aberrations and, thus, genomic instability. After recruitment of DNA-PKcs to DSBs ends, it forms a distinct structure at the broken DNA ends, which is likely to play an important role in the formation of the synaptic complex

that holds together the ends of the broken DNA ends (Cary et al., 1997). Other proteins include XRCC4 and XLF, that play an important role in stabilizing the broken DNA ends (Andres et al., 2012; Hammel et al., 2011; Hammel et al., 2010; Malivert et al., 2010); 3) **End processing.** In this step, processing of DNA ends occurs to create DNA ends that can be ligated. Depending on the type of break, different end processing enzymes may be required. Different end-processing enzymes involved in NHEJ pathway include Artemis, PKNP, APLF, Polymerase μ and λ, Werner (WRN), aprataxin, and Ku. PNKP, Aprataxin and Ku are some of the factors that remove blocking end groups in order to make broken DNA ends accessible for ligation. DSBs can have non-ligatable 5' hydroxyl and 3' phosphate groups. PNKP is an enzyme that contains both kinase and phosphatase activity. The kinase domain of PNKP add phosphate group to the 5' OH while phosphates domain removes 3' phosphate group. Another protein is Aprataxin, histidine triad family member remove adenylate group covalently linked to 5' phosphate termini (Ahel et al., 2006). Another research showed that Ku has 5' deoxyribose-5-phosphate (5'-dRP)/AP lyase enzymatic activity (Roberts et al., 2010). Ku removes abasic sites near DSBs *in vitro* and this activity was highest when the abasic site was within a short 5' overhang at DSB end. The proteins involved in resecting DNA ends in NHEJ are Artemis, WRN and APLF. Artemis has a number of nucleolytic activities, that includes 5' endonuclease activity that nick a 5' overhang and ultimately leaving blunt duplex, 5'-3' exonuclease activity on single-stranded DNA and removal of 3' phosphoglycolate group from the DNA termini (Ma et al., 2002; Povirk et al., 2007). DNA-PKcs/ATM binding and phosphorylation activate Artemis. DNA-PKcs mediated phosphorylation of Artemis is required for its endonuclease activity (Ma et al., 2002). Another protein, Werner (WRN), interacts

with both the Ku heterodimer and XRCC4, and both proteins stimulate the 3'-5' exonuclease but not the 3'-5' helicase activity (Cooper et al., 2000; Kusumoto et al., 2008; Perry et al., 2006). APLF activity on ssDNA or DNA overhangs is not modulated by another core NHEJ factors. APLF can resect 3' overhangs in *in vitro* end joining assays to permit ligation of DNA ends by XRCC4- DNA ligase IV (Li et al., 2011). Filing of gaps is performed by Family X polymerases which include DNA polymerases μ and λ in the presence of complex DNA damages (Moon et al., 2007). DNA polymerase μ is involved in template dependent synthesis in presence of dNTPs and rNTPs. DNA polymerase μ can polymerize across a discontinuous template strand in the presence of Ku, XRCC4/ DNA ligase IV (Nick McElhinny et al., 2005). The activity of Polymerase λ is not dependent on template and lyase activity of Polymerase λ removes a damaged base (Ramadan et al., 2004); 4) **Ligation of broken ends and dissolution of NHEJ complex.** In the final step, ligation of broken DNA ends by DNA ligase IV occurs. DNA ligase IV ligation activity is modulated by XRCC4. Adenylation of DNA ligase IV by XRCC4 stimulates its activity (Figure 7) (Grawunder et al., 1997).

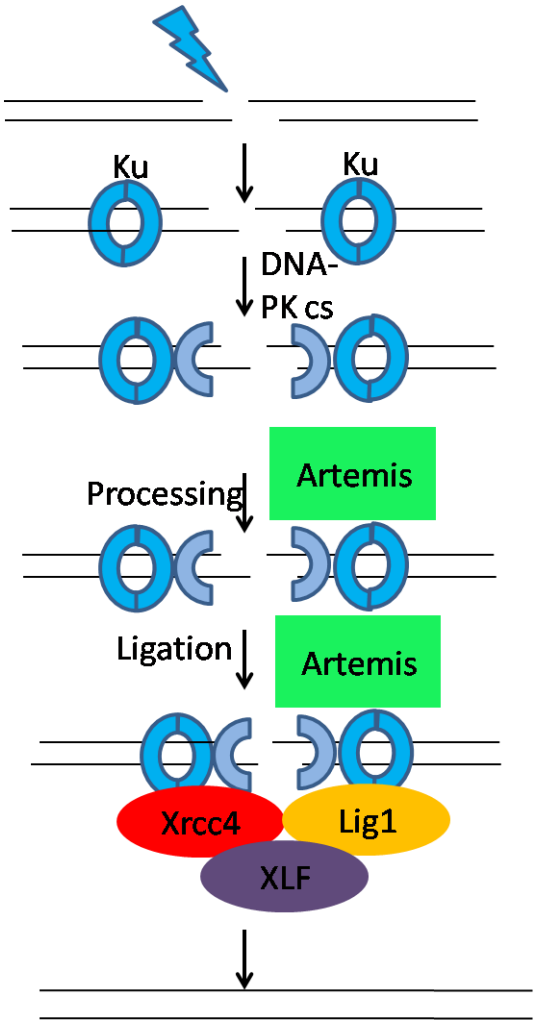

Figure 7. Non Homologous End-Joining (NHEJ). NHEJ is divided into four sequential steps- 1) DNA end recognition. 2). DNA end bridging and promotion of end stability. 3). End processing. 4). Ligation of broken DNA ends and promotion of end stability. Adapted from (Davis and Chen, 2013).

1.9.5 NHEJ substrate vector (pIM EJ5-GFP)

The pIM EJ5-GFP reporter cassette can detect multiple NHEJ events. It consists of a promoter which is separated from the GFP gene by a puromycin gene (Figure 8). The puromycin cassette is flanked by two Isce1 restriction enzyme sites that are present in the same orientation. After removal of the puromycin cassette by Isce1-induced DSB, formation of overhangs occurs followed by end-joining. This end-joining process restores GFP expression by placing GFP cassette next to the promoter. An Isce1 resistant site could form during end-joining of overhangs due to error prone nature of the NHEJ pathway. However, NHEJ could reconstitute the Isce1 site without any error after end-joining. In this case, the Isce1 site could be targeted again by Isce1 enzyme that may form an Isce1 resistant site due to error prone mechanism of NHEJ (Figure 8). In any case, presence or absence of the Isce1 site after end joining does not affect the GFP expression (Bennardo et al., 2008).

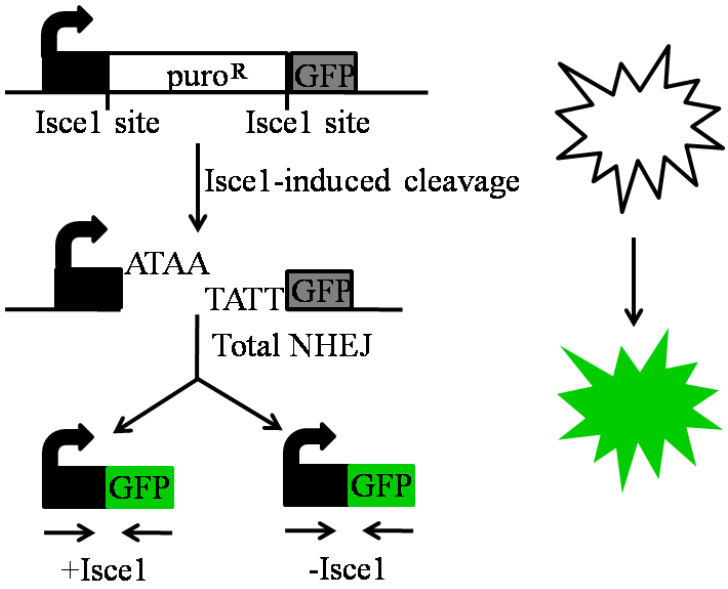

Figure 8. pIM EJ5-GFP repoter plasmid. pIM EJ5-GFP plasmid consists of a promoter which is separated from GFP gene by puromycin gene. Puromycin gene is flanked by Isce1 site. GFP gene fragment placed downstream of the puromycin gene. Isce1 induced DSB leads to the joining of the GFP fragment with the promoter that leads to GFP expression. Adapted from (Bennardo et al., 2008).

1.10 Concept of genome editing

The genome editing field had an exceptional development consequent to the development of site-specific nucleases that can be used, combined with the discovery that targeted DSBs could be used to activate the endogenous cellular DNA repair machinery. The DBSs in the genome can be repaired by one of the two pathways: Homologous recombination (HR) and Non-Homologous end joining (NHEJ) (Takata et al., 1998). Targeted double stranded break using site-specific nucleases can be used for gene knockout, gene knock-in and gene correction.

1.10.1 Site-specific nucleases

The successful implementation of site-specific genome editing relies on the introduction of targeted DSB in the genome using one of the following systems: meganucleases, transcription activator-like effector (TALE)-nucleases (TALENs), zinc-finger nucleases (ZFNs) and more recent one, CRISPR/Cas9 system.

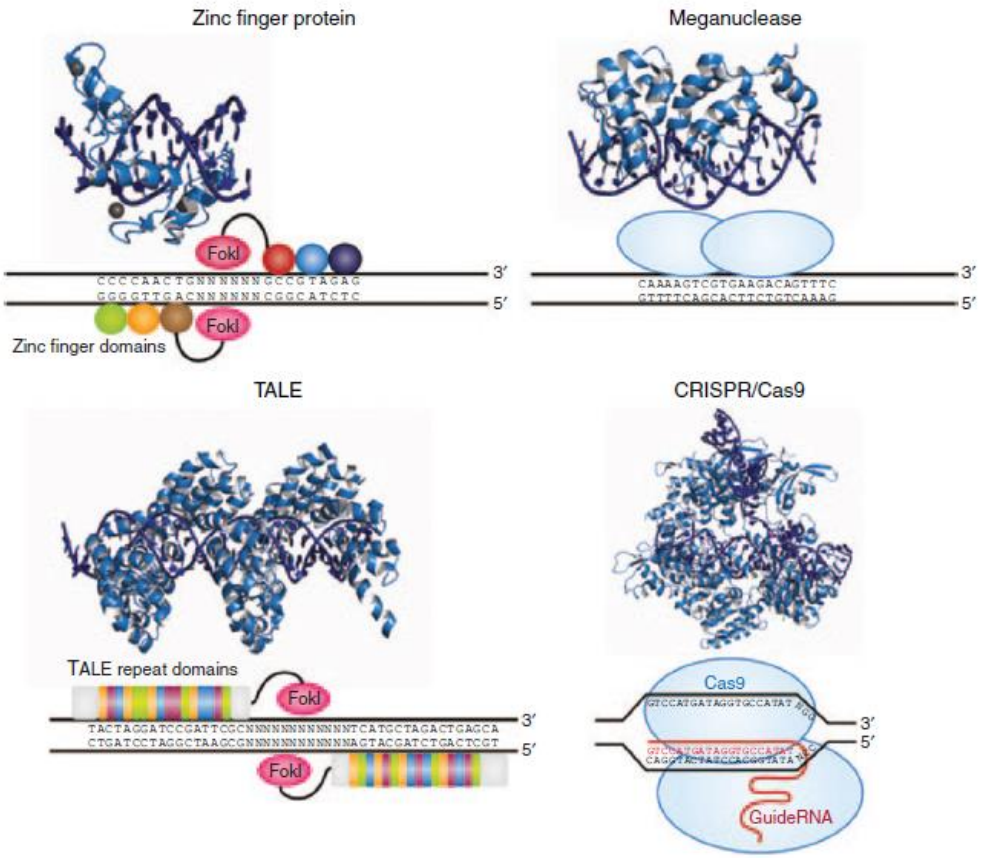

Figure 9. Most commonly used site-specific nucleases used for genome editing (Maeder and Gersbach, 2016).

1.10.2 Meganucleases

Meganuclease technology involves the re-engineering of the DNA binding specificity of homing endonucleases such as I-Cre1 and I-Sce1 (Chevalier and Stoddard, 2001). These homing endonucleases could be re-engineered to target novel sequences (Rosen et al., 2006; Smith et al., 2006). Several studies showed the use of meganucleases in genome editing (Dupuy et al., 2013; Gurlevik et al., 2013). However, difficulty in separating the DNA binding and cleavage domain accompanied by the difficulty in engineering proteins with novel specificity limited the use of meganucleases.

1.10.3 Zinc-finger nucleases (ZFNs)

Zinc-finger (ZF) proteins are the most abundant class of transcription factors and the Cys2-His2 zinc-finger domain represents one of the most common DNA-binding domains encoded in the human genome (Tupler et al., 2001). Crystal structure of Zif268 suggests that zinc fingers form a compact ββα structure in the presence of zinc atom where the α-helical portion of each finger makes contact with 3 or 4 bp in the major groove of the DNA (Lee et al., 1989; Pavletich and Pabo, 1991). Tandem zinc finger motifs wrap around the DNA to recognize DNA sequences such that 3 finger modules/domains binds a 9 bp target site. The modular structure of Zif268 suggests its use as a probable framework for the engineering of novel DNA-binding motifs (Gersbach et al., 2014). The designing of Zinc fingers with unique specificity based on simple rules had some success during initial attempts (Desjarlais and Berg, 1992). Later on, combinatorial libraries combined with selection-based methods proved to be a more effective strategy to generate individual finger with novel DNA binding specificities (Rebar and Pabo, 1994);

(Choo and Klug, 1994). After initial success, designing of multi-finger arrays with novel target sites with unique specificity in a complex genome was a challenging task. This type of approach depends on the collections of single finger modules identified in naturally occurring proteins (Bae et al., 2003) or selected to bind specific 3 base pair target sites (Segal et al., 1999), which are then linked together in tandem to generate novel DNA binding proteins (Beerli et al., 2000). In another approach, known as OPEN, new proteins are selected from the random libraries (Maeder et al., 2008). Other approaches included those used by Sigma-Aldrich Compo Zr platform and Sangamo biosciences (Gupta et al., 2012; Sander et al., 2011b).

The birth of zinc-finger nucleases (ZFN) technology was made possible by the observation that the DNA binding domain and the DNA cleavage domain of the Fok1 endonuclease can function independently from each other (Li et al., 1992). Zinc finger nucleases were designed after replacing the Fok1 DNA binding domain with the zinc finger domain with novel DNA binding specificities (Kim and Chandrasegaran, 1994). Since Fok1 nucleases act as a dimer, two ZFNs binding opposite strands are required to create a DSB (Smith et al., 2000). This technology has been successfully used to perform genome editing in human somatic cells (Moehle et al., 2007; Urnov et al., 2005), pluripotent stem cells (Lombardo et al., 2007), mice (Anguela et al., 2013; Sharma et al., 2015) HIV patients (Tebas et al., 2014).

1.10.4 Transcription activator like effector nucleases (TALENs)

The discovery of the DNA recognition code of TALE proteins from the plant pathogen Xanthomonas provided a new way to design sequence-

specific nucleases (Boch et al., 2009). Each of the highly conserved 30-35 amino acid long TALE repeat binds a single base pair in the DNA with specificity determined by two hypervariable residues (Deng et al., 2012). These TALE repeats can be linked together in an array with custom DNA-binding specificities (Miller et al., 2011; Zhang et al., 2011). Several procedures exist for engineering TALE arrays. The simplest one involves the cloning of the TALE array from different plasmids, each containing one TALE repeat (Sander et al., 2011a). Another method used for cloning TALE arrays is Golden-Gate cloning platform, where multiple pieces are cloned simultaneously in the same reaction (Morbitzer et al., 2011). High-throughput methods include solid phase assembly or ligation independent cloning (Briggs et al., 2012; Schmid-Burgk et al., 2013).

Similar to ZFNs, each TALE monomer is fused to the DNA cleavage domain of the Fok1 endonuclease in order to selectively cleave double stranded DNA after dimerization (Mussolino et al., 2011). TALENs have been shown to induce HDR and NHEJ in both human somatic cells and pluripotent stem cells (Hockemeyer et al., 2011; Reyon et al., 2012). TALENs can be designed to target any sequence with the only restriction of the presence of 5' T, specified by the N-terminal domain for each array. The unlimited targeting range of TALEN combined with ease of generation makes them an attractive tool for genome editing. However, the large size of TALENs limits their application for *in vivo* genome editing using available viral delivery vehicles. In addition, the presence of tandem repeats in TALENs makes it difficult to package inside the viral vectors (Holkers et al., 2013).

1.10.5 CRISPR/Cas9 nucleases

CRISPR/Cas9 are RNA guided nucleases derived from an adaptive immune system used by bacteria against invading plasmids and viruses. Work done by several groups over the years discovered the mechanism of insertion of short sequences of foreign nucleic acid into the CRISPR loci (Barrangou et al., 2007). The inserted foreign DNA undergoes transcription and processing into CRISPRRNA (crRNAs), which along with a trans-activating crRNAs (tracrRNAs) forms a complex with CRISPR associated (Cas) nuclease. The resulting ribonucleoprotein complex eventually loads on to the target sequence through Watson-Crick base pairing followed by DNA cleavage. Further studies by Doudna, Charpentier and colleagues showed that this system could be reduced to only two components by forming a fusion between crRNA and tracrRNA into a single guide RNA (gRNA). Additionally, they also showed that targeting of Cas proteins to another locus could be achieved by changing only a small portion of gRNA (Jinek et al., 2012). After this discovery, several publications demonstrated the CRISPR/Cas-mediated genome editing in mammalian cells (Cong et al., 2013; Jinek et al., 2013; Mali et al., 2013).

The only limitation of the CRISPR/Cas system is the requirement of protospacer associated motif (PAM) located immediately 3’ to the target site. The PAM sequence is specific to the Cas protein derived from a particular species, such as the PAM sequence 5’ NGG is required for binding and cleavage by Cas9 derived from *Streptococcus pyogenes* (Chylinski et al., 2014);(Sternberg et al., 2014).

1.11 miRNA screening to find novel modulators of homologous recombination

Micro RNA (miRNA) represents a subset of small, endogenous, regulatory RNAs of 21-25 nucleotides in length(Wahid et al., 2010). The miRNA genes are transcribed to generate primary miRNA (pri-miRNA). This pri-miRNA is further processed by DROSHA within the nucleus into precursor miRNA (pre-miRNA). During the next phase, the pre-miRNA is exported out of nucleus into the cytoplasm by exportin-5 (Exp-5). In the cytoplasm, these pre-miRNAs further get processed into mature miRNA by DICER, that finally loads the miRNA onto the Argonaute (Ago) protein to produce the RNA-induced silencing complex (RISC) (Wahid et al., 2010).

A number of miRNAs have a role in several different cellular processes such as cell proliferation, cell death, fat metabolism, neuronal patterning, hematopoietic differentiation and immunity (He and Hannon, 2004).

Recently, miRNAs have emerged as one of the regulatory factors that influence HDR (Wei et al., 2012). Some studies highlight the fact that cells defective in miRNA biogenesis have uncontrolled cell cycle checkpoint and DNA repair (Huen and Chen, 2010; Pothof et al., 2009). Some miRNA such as miR-16, miR-24, miR-138, miR-183-96-182 cluster, miR-155, miR-1255b, miR-148b and miR-193b have been implicated in DNA damage response (DDR) and DNA repair (Choi et al., 2014; Gasparini et al., 2014; Moskwa et al., 2011; Wang et al., 2012; Wei et al., 2012). Similarly, miR-196b enhances the radiosensitivity of gastric cells by targeting Rad23b (Shen et al., 2018). These finding suggests the important role of miRNA in DDR pathways.

miRNA regulatory network is highly complex since a single miRNA can target many transcripts and a single transcript can be targeted by many miRNA (Brodersen and Voinnet, 2009). So far, the precise role of miRNA in DDR is poorly understood.

Several miRNA-based therapeutics have reached clinical trials. miR-34 mimic reached clinical phase I trials for treating cancer, while miR-122 has reached clinical trials phase II to treat hepatitis (Rupaimoole and Slack, 2017). Based on all the previous work that showed important roles of different miRNAs during HR, supported by its safe use during pre-clinical and clinical trials, makes the use of different miRNA mimics and Anti-miR as an attractive tool to modulate HR. For this purpose, a hi-throughput miRNA screening platform was planned to investigate the miRNA that modulate HR using special liver reporter stable cell line.

For miRNA screening, HR reporter cells line were planned to get transfected with a library of miRNA mimics (Dharmacon) using a standard reverse-transfection protocol. Analysis of HR positive cells using an ImageXpress Micro high-content screening microscope (Molecular Devices) was programmed to be done 3 days after transfection (Eulalio et al., 2012).

MATERIALS AND METHODS

2.1 Bilirubin purification protocol

1. All the glass wares were washed sequentially with $CH_3OH/CHCl_3$ 2:1, $CHCl_3$, CH_3OH and dried.
2. Bilirubin dissolution: 100 mg of commercial bilirubin (Sigma Aldrich-B 4126) was dissolved in $CHCl_3$ (stabilized with ethyl alcohol, Carlo Erba, 438613) in a conical flask. Nitrogen gas was bubbled into the solution. Solution was warmed up to 60°C to allow complete dissolution of bilirubin. Temperature was always maintained above the boiling point of $CHCl_3$ (62°C).
3. Bilirubin filtration: Completely dissolved solution (amber coloured without any red precipitate) was filtered through a filter paper (Whatman 40 ashless, diameter: 11 cm- WHA1442110) pre treated with $CHCl_3$ in a separatory funnel. Finally, filter paper was washed with $CHCl_3$ again to remove most of the absorbed bilirubin.
4. Washing: 250 ml of $NaHCO_3$ (Sigma Aldrich-S5761) 0.1 M was added into the separatory funnel and shaken vigorously several times. Two miscible solutions were allowed to make two different layers. Aqueous solution and lipid interface were removed using a Pasteur pipette connected to a vacuum pump. This process was repeated again until lipid interface gets completely removed. Next, 20% NaCl (Sigma Aldrich-433209) was added to reach same volume as $CHCl_3$. Finally, bilirubin solution was washed two times with miliQ water.
5. Filtration: After washing, organic phase was filtered as done in step 3 into a conical flask. During this step, the filter paper in the funnel was always filled about 1/3 volume of $CHCl_3$. UCB solution was added into the $CHCl_3$ solution and then the filter paper was washed

with $CHCl_3$. $CHCl_3$ layer was always maintained in the filter cone layer.

6. Crystallization: Nitrogen gas was bubbled into the flask with lower half of flask immersed in hot water (60-70°C). CH_3OH (Sigma Aldrich-322415) was added drop wise up to 1:7 of initial volume of UCB solution. This process replaces the $CHCl_3$ with CH_3OH until total volume reduces to 1/5 of its original amount. At this point, solution started to become slightly cloudy with red crystals. The addition of CH_3OH was continued till all the $CHCl_3$ was evaporated from the solution and final volume was 1/20 of the original volume. Next, solution was kept in room temperature to allow crystal formation. After 10 min incubation at room temperature, centrifugation was done to remove CH_3OH. Now, crystals were washed twice with CH_3OH and allowed to dry. The purification was stopped at this step and dried bilirubin was stored at -20 °C.
7. Secondary bilirubin dissolution: Bilirubin was again dissolved in $CHCl_3$ and transferred into separatory funnel. Nitrogen gas was bubbled into the solution.
8. Preparation of washing solution: Washing solution was prepared by mixing 122 ml of 0.2 M Na_2HPO_4 (Sigma Aldrich-255793), 78 ml of 0.2 M $NaH_2PO_4 \cdot H_2O$ (Sigma Aldrich- 71507). pH was adjusted to 7. Then add 0.1 M NaCl in 1:1 ratio.
9. Washing: Equal amount of washing buffer and UCB-Chloroform solution were added into the separatory funnel. Washes were done as mentioned above in the washing section. Washing with phosphate buffer were done 3 times followed by two washes with the mili Q water.
10. Bilirubin concentration determination: Concentration of bilirubin was determined by adding 20 µl of bilirubin sample into 980 µl of

$CHCl_3$ in a glass cuvette. $CHCl_3$ was used as blank. Absorbance was determined at 453 nm. Concentration of bilirubin was determined using equation given below:

Absorbance x9.74 x dilution factor (50) = µg/ml x 1000/585 = µM.

11. Fractionation: The bilirubin solution was aliquoted into several amber glass tubes. Different aliquots were made, i.e. 1mg, 5mg, 100 µg, 50 µg, 200 µg etc. Bilirubin was dried under gentle nitrogen gas in the presence of heat. These amber glass tubes were then stored at -20 °C under dark conditions.

2.2 Bf determination

Basic principle: The principle of this method is based on the fact that unbound bilirubin is oxidised to colourless compound by peroxide (H_2O_2) in the presence of peroxidase (HRP) (Sigma Aldrich-P8125) with 1st order kinetic; while albumin-bound form is protected from oxidation. In order to determine Bf, Kp of HRP enzyme was determined first by calculating the decrease in Abs_{440} following addition of HRP and H_2O_2 to 1-3 µM bilirubin.

2.2.1 Kp determination: Reagents: 1µg of bilirubin was dissolved in 340 µl of DMSO. 2mg of HRP was dissolved in 2ml PBS buffer. 5µg/ml working solution was prepared by mixing 100 µl of stock solution in 20 ml PBS buffer. 550mM H_2O_2 was prepared by mixing 200 µl to 6ml PBS.

Protocol:

1. 200 µl of bilirubin solution was added into 2.8 ml PBS and mix properly. Absorbance was measured at 440 nm.
2. 10 µl of H2O2 was added to the bilirubin solution. 2-3 concentrationsof H_2O_2 were tested to make sure if the concentration was not rate limiting.
3. 110 µl of diluted HRP solution was added to the bilirubin solution and mixed properly. Absorbance was measured at 440 nm and change in absorbance was measured for 60 seconds. Kp was calculated using this formula:

   Kp= V_o/ ([Bf]x[HRP]), where V_o= initial oxidation velocity, can be represented as ΔAbs/min.

2.2.2 Bf determination:

1. 1µg of bilirubin was dissolved in 340 µl of DMSO. Bilirubin stock solution was added to culture medium to create different bilirubin: albumin ratio ranging from 0.2-1. Initial absorbance was calculated by measuring the absorbance at 468 nm.

2. 10µl of 250 nM of H_2O_2 was added to the medium and mixed properly.

3. 25 µl of different concentration of HRP (0.6-2.5 µg/ml) was added to the medium and mixed properly. Absorbance was determined at 468 nm and change in absorbance was calculated for 30 secs.
4. After calculating change in Abs using different HRP concentration, Bf was calculated using the formula:

   Apparent Bf: ΔAbs/min /Kp x [HRP]

5. The swift change in Abs reflects the true Bf, but rate of oxidation after that represents “apparent Bf”. Apparent Bf represents the steady state

equilibirium between bilirubin-albumin dissociation and enzyme oxidation. In order to determine real Bf, the assay was done at 2-3 HRP enzyme concentration. 1/ [apparent Bf] is proportional to 1/ Bf+ [HRP], and Bf was determined by making a plot between concentration of HRP used and 1/apparent Bf, where y intercept in the plot represents real Bf.

2.3 Cell culture and treatment with bilirubin

HeLa DR GFP cells were kindly gifted by Dr. E. Avvedimento (Cuozzo et al., 2007). HeLa DR GFP and HeLa cells were cultured in Dulbecco's modified Eagle's medium (DMEM, Thermo Fischer Scientific, GIBCO) supplemented with 10% Fetal calf serum (FCS) and 1% antibiotic & antimycotic solution (Sigma Aldrich-A5955).

SH SY 5Y cells were cultured in Eagle's minimum essential medium F12 (EMEM/F12, Sigma Aldrich) medium supplied with 15% FCS, 1% antibiotic & antimycotic solution (Sigma Aldrich-A5955), 1% MEM non-essential amino acid solution (Sigma Aldrich M7145).

For bilirubin treatment, bilirubin was dissolved in DMSO (17ul per 50 µg of bilirubin). Appropriate amount of UCB solution was added to DMEM and EMEM/F12 media and bilirubin concentration in media was calculated by taking absorbance at 468 nm using spectrophotometer. After confirming the required amount of bilirubin in culture media, it was added to cells.

2.4 Cell viability by MTT assay

The MTT assay is employed to calculate cellular viability spectrophotometrically. The yellow MTT (3-(4, 5-dimethylthiazolyl-

2)-2,5-diphenyltetrazolium bromide) reagent is reduced by metabolically active cells, by dehydrogenase enzymes, to generate reducing equivalents such as NADH and NADPH. The resulting intracellular purple formazan is solubilized and quantified by spectrophotometry. Reduction in cellular viabilty can be seen by decrease in absorbance.

1. 80,000 SH SY 5Y cells/well were seeded in 24 well plate one day before experiment.
2. After 14-16h, media was removed and cells were washed twice with PBS and 70 nM and 140 nM of bilirubin was added to cells, ranging from 1h, 4h and24h. Bilirubin containing culture medium was prepared as described in section 2.3.3. Cellular viability was determined using 3(4, 5-dimethylthiazolyl 2)2, 5 diphenyl tetrazolium (MTT) assay at respective time points. 5 mg/ml stock of MTT (Sigma Aldrich) was prepared by dissolving MTT in PBS. The stock solution of MTT was finally diluted in growth medium to a final concentration of 0.5 mg/mL. The cells were incubated with the MTT solution for 1h at 37 °C.

4. After incubation, the medium was discarded, the MTT formazan crystals were dissolved in 400 µl of DMSO, and the plate was shaken gently for 15 min and absorbance was recorded at 562 nm using Bio-Rad iMark microplate reader. Results were expressed as percentage of control cells (cells exposed to media only) which was considered as 100% viability.

To check the viability of HeLa DR GFP cells, 50,000 cells were plated in 24 wells culture plate one day before experiment. After 14-16h, media was removed from cells and washed twice with PBS and

140 nM of bilirubin was added to cells for different time intervals ranging from 1h, 4h and 24h as described in section 2.3. Cell viability was determined using MTT test as discussed above.

2.5 Plasmids used for transfection

The pCBA Isce1 plasmid was purchased from Addgene (#26477); the pHRG-TK plasmid was purchased from Promega; the pIM EJ5-GFP plasmid was purchased from Addgene (#44026).

The pCBA Isce1 plasmid is an expression vector that contains the I-SceI endonuclease cDNA under the transcriptional control of the CMV enhancer and chicken β-actin promoter; it has the β-globin poly-A signal. It is used to introduce a DSB at a genomic Isce1 site. The pHRG-TK is a Renilla luciferase expression vector,with the HSV TK promoter and SV-40 poly-A signal; the pIM EJ5-GFP is a NHEJ substrate vector having the CMV enhancer and chicken β-actin promoter, and β-globin poly-A signal.

2.6 HeLa DR GFP cells transfection and bilirubin treatment

1. For transfection of HeLa DR GFP cells, 50,000 cells were seeded in 24 wells plates 24h before transfection.
2. After 14-16h, cells were transfected with 300 ng of plasmid encoding Isce1 (pCBA Isce1) using Effectine tranfection reagent (Qiagen-301427) according to manufacturer protocol in the case of time-course experiments. Transfection complexes were removed 6-7h after transfection and cells were washed twice with PBS and bilirubin was added to cells as described above in section 2.3.

Bilirubin containing media was removed after different time points (24h and 48h and cells were washed with phosphate buffer saline (PBS) two times and new media was added to cells. For all the other experiments, cells were co-transfected with 300 ng of plasmid encoding Isce1 (pCBA Isce1) and 10 ng of plasmid encoding renilla (pHRG TK Renilla). Transfection complexes were removed 6-7h after transfection and cells were washed twice with PBS and bilirubin was added to cells as discussed above in section 2.3. In the case of NAC experiments, Cells were pre-treated with 2 mM NAC (Sigma Aldrich) for 1h, followed by co-treatment with bilirubin using protocol discussed above in section 2.3. Fresh NAC was added after every 24h.

3. Cells were analysed for GFP fluorescence 72h post-transfection using FL1 channel in BD FACS Calibur cell analyser. Dead cells were excluded from the analysis by using proper gating of the live cells.
4. For the time course experiment, data were normalised for the transfection efficiency by calculating the overall transfection efficiency after transfecting the cells with the EGFP plasmid in parallel wells. In order to do normalisation, total percentage of GFP positive cells per condition was divided by the calculated transfection efficiency. The value of DMSO treated cells were taken as 1 after normalisation for transfection efficiency. While for all other experiments involving HeLa DR GFP cells, cells were co-transfected with the pHRG-TK plasmid and data were normalised using the renilla luciferase activity determined in the same well. In order to do normalisation, the total percentage of GFP positive cells per condition was divided by renilla luciferase activity of same well. The value of Isce1 DMSO sample was taken as 1 after normalisation for transfection efficiency.

2.7 HeLa cells transfection and bilirubin treatment

1. For transfection of HeLa cells, 80,000 cells were seeded in 24 wells plates 24h before transfection.
2. After 14-16h, cells were co-transfected with 100 ng of NHEJ plasmid pIM EJ5- GFP, 300ng of plasmid encoding Isce1 (pCBA Isce1) and 10 ng of plasmid encoding renilla (pHRG TK renilla) using Effectine transfection reagent (Qiagen- 301427) according to manufacturer protocol. Transfection complexes were removed 6-7h after transfection. Cells were washed twice with PBS and bilirubin was added as discussed above in section 2.3.
3. Cells were analysed for GFP fluorescence 72h post-transfection using FL1 channel in BD FACS Calibur cell analyser. Dead cells were excluded from the analysis by using proper gating of the live cells.
4. Data was normalised using the renilla luciferase activity corresponds to same well. In order to do normalisation, total percentage of GFP positive cells per condition was divided by renilla luciferase activity of same well. The value of Isce1 DMSO was taken as 1 after normalisation for transfection efficiency**.**

2.8 SDS PAGE and Western Blot analysis

1. For Western Blot analysis, 150,000 SH SY 5Y cells were seeded in 35 mm culture dishes one day before experiment.
2. After 14-16h, bilirubin containing culture media was added to cells. In the case of NAC experiments, cells were pre-treated with different concentrations of NAC (0.1, 0.3 and 0.4 mM) followed by co-treatment with bilirubin for 30h. Cells were harvested at respective time points after bilirubin treatment in RIPA buffer (150 mM NaCl, 5 mM 0.5 mM EDTA (pH-8), 50 mM Tris (pH-8), 1% NP-40, 0.5% Sodium

deoxycholate, 0.1% SDS) containing SIGMAFAST (SigmaAldrich) protease inhibitor, Serine/Threonine-phosphatase inhibitor 1mM SodiumFluoride (NAF) and 1mM Tyrosine phosphatase inhibitor Sodium orthovanadate (Na_3VO_4).

3. Protein concentration was determined using Bradford reagent (Bio Rad).

4. Total protein lysate (50 µg) was loaded on 12 % SDS PAGE gel and transfer-ed into nitrocellulose membrane (GE healthcare lifescience-AMERSHAM) using wet transfer. The correct transfer of protein was confirmed by Ponceau (Sigma Aldrich) staining. Ponceau stain was cleaned using water. Blots were blocked in appropriate blocking solution (5% BSA for γH2AX antibody, 5% milk for P53 and Actin) for 1h at room temperature. Blots were incubated in appropriate primary antibody O/N at 4 ^{o} C (Table 1).

5. Next day blots were washed 3 times with TBS 0.2% Tween-20 for 10 minutes and incubated with secondary antibody for 1h at room temperature followed by 3 washing with TBS 0.2% Tween-20 for 10 minutes (Table 1). After washing steps, blots were developed with ECL reagent (Amersham Biosciences).

6.Images were taken in Uvitech Cambridge ECL machine. Densitometry analysis of protein bands were done using Quantity one software (Bio-Rad).

For HeLa DR GFP cells, cells were transfected and treated with bilirubin as discussed in section 2.6. Cells were harvested 72h post transfection in RIPA buffer. Western Blot was done as discussed above for SH SY 5Y cells.

Table 1: **List of all antibodies used for Western Blot-** Antibody name, company name, dilution and MWs are given.

Antibody	Company	MW	Dilution		2º Antibody
			WB	IF	
γH2AX	Millipore(Clone JBW301)	17	1:2000	1:200	Anti-Mouse (DAKO for WB), (Thermo Scientific) for IF.
Actin	Sigma Aldrich (A5060)	42	1:2000		Anti-Rabbit (DAKO)
P53	Santacruz biotechnology (DO-1)	53	1:2000		Anti-Rabbit (DAKO)

2.9 Immunofluorescence analysis

1. For Immunofluorescence analysis, 150,000 SH SY 5Y cells were seeded in 35 mm culture dishes.
2. After 14-16h, SH SY 5Y cells were treated with 140 nM bilirubin. In the case of NAC treatment, cells were co-treated with bilirubin and 0.4 mM NAC for 30h as discussed above in section 2.8.
3. After 30h, media was removed and cells were washed twice with PBS. It was followed by fixing of cells in ice cold 4% paraformaldehyde (PFA) for 10 min at room temperature. After 10min, PFA was removed and cells were washed thrice with PBS.

4. Next, cells were permeabilized using PBS Tween-20 0.1% for 10 mins. After 10 min, PBS Tween-20 0.1% was removed and cells were washed twice with PBS.
5. After permeabilization, cells were blocked in 2% goat serum in PBS for 1h at room temperature.
6. After blocking, cells were incubated in primary antibody at 37^{o} C for 2h (Table 1). After this, cells were washed thrice with PBS for 5 minutes.
7. After washing step, cells were incubated for 20 minutes at 37^{o} C with anti-mouse secondary antibody (Alexa Fluor 488- Thermo Fischer Scientific) followed by 3 times washing with PBS. Nuclei were visualized using TO- PRO-3 iodide dye (T3605). Images were acquired using Zeiss Meta confocal micro scope using 63X oil objective. At least, 10 images per slide were taken. Quantification was done after counting percentage of cells containing 10> foci in total of 200 cells.

1. For immunofluorescence analysis of HeLa DR GFP cells, 50,000 cells were seeded in 24 well culture plate.
2. After 14-16h, cells were transfected and treated with bilirubin as discussed in section 2.6.
3. Media was removed 72h post transfection and cells were washed twice with PBS. It was followed by fixing of cells in ice cold 4% Paraformaldehyde (PFA) for 10 min at room temperature. After 10min, PFA was removed and cells were washed twice with PBS.
4. Next, cells were permeabilized using PBS Tween-20 0.1% for 10 mins. After 10 min, PBS Tween-20 0.1% was removed and cells were washed thrice with PBS.
5. After permeabilization, cells were blocked in 2% Bovine serum albumin in PBS for 1h at room temperature.

6. After blocking, cells were incubated in primary antibody at 37° C for 2h (Table 1). After this, cells were washed thrice with PBS for 5 minutes.
7. After washing step, cells were incubated for 20 minutes at 37° C anti mouse

secondary antibody (Rabbit anti mouse Rhodamine-Thermo Fischer Scientific) followed by 3 times washing with PBS. Nuclei were visualized using TO-PRO-Iodide dye (T3605). Images were acquired using Zeiss Meta confocal Microscope using 63X oil objective. At least, 10 images per slide were taken. Quantification was done after counting percentage of cells containing 10> foci in total of 200 cells.

2.10 Cell cycle analysis

1. HeLa cells were treated with 140 nM of Bilirubin for 48h as discussed in section 2.3.
2. After 48h of treatment with bilirubin, media was removed and cells were washed twice with PBS. Next, cells were trypsinized and washed two times with PBS.
3. After washing, cells were resuspended in 200 µl PBS and 800 µl of ethanol and tubes were inverted several times and stored O/N at 20° C.
4. Next day, cells were spin down, the pellet was washed two times with PBS and resuspended in 1 ml of PI solution in sodium citrate (5 µg/µl),which guarantees an osmotic shock to the cells. Add 10-20 ul of 0.1% NP40 stock solution (in order to allow the permeabilization of the cells) and RNAse (0.5 mg/ml) to degrade the RNA and allow a clear identification of cell cycle phases.
5. 5000 cells were analysed for cell cycle analysis using FACS Calibur cell analyser.

2.11 Effect of bilirubin on etoposide induced DNA damage.

1. HeLa cells were treated with 140 nM of Bilirubin for 24h as discussed in section 2.3.
2. After 24h of treatment with bilirubin, media was removed and cells were washed twice with PBS. Next, cells were treated with 100 µM etoposide for 2h.
3. After 2h, etopsoide was removed and cells were treated again with 140 nM free bilirubin for different time intervals. Cells were harvested at different time points and western blot was done to check the level of γH2AX.

2.12 Subcloning of new codon optimised Exon4 to generate a new donor AAV vector

Digestion of pUC57 new codon optimised Exon4 and PBK plasmids was done using the protocol given below:

0.5 µl (500 ng) pUC57 Exon4 plasmid/PBK

0.5 µl BamHI (0.5 U) (New England Biolabs)

1.5 µl 10X buffer (New England Biolabs)

12.5 µl Water

The digested product was checked on 1% Agarose gel. Both the plasmids were dephosphorylated at 5’ end to prevent self ligation after treatment with calf intestinal phosphatase at 37 degree celsius for 60 minutes. Then the enzyme was inactivated after incubation at 65 degree celsius for 20 minutes.

The digested pUC57 Exon4 plasmid (insert) was then ligated directly without purification into BamHI digested PBK plasmid backbone (vector) using the protocol given below:

Vector – 1 µl (33 ng)

Insert- 3 µl (50 ng)

Ligase buffer (10X) - 1.5 µl

T4 ligase- 0.5 µl (0.5 U)

Water- 9 µl

Vector – 2 µl (66 ng)

Insert- 4 µl (200 ng)

Ligase buffer (10X) - 1.5 µl

T4 ligase- 0.5 µl (0.5 U)

Water- 7 µl

Self ligation control reaction

Vector – 1 µl (33 ng)

Ligase buffer (10X) - 1.5 µl

T4 ligase- 0.5 µl (0.5 U)

Water- 12 µl

Undigested control reaction

Vector – 1 µl (33 ng)

Ligase buffer (10X) - 1.5 µl

Water- 13 µl

All the ligation mixtures were incubated at RT for 4-5h and transformed into DH5αcompetent cells. The competent cells were stored at -20 degree celsius and thawed in ice for 10 minutes. After thawing of cells, 4 µl of β-mercaptoethanol (1.42M) was added to 100 µl of competent cells in order to increase the competence of cells. Next, half of the ligation mixture from each reaction was added to competent cells and mixed properly and kept incubated on ice for 15-20 minutes. After incubation on ice, heat shock at 42 degree celsius for 1 minute in a water bath was given to the competent cells. After heat shock, bacteria were kept on ice for 5 minutes. After this, warm LB media was added to the cells and incubated for 1h at 37 degree celsius in order to allow bacteria to recover and express the antibiotic resistance gene. After the incubation period end, cells were plated in LB agar containing plate with appropriate antibiotics (ampicillin/kanamycin) and let them grow overnight at 37 degree celsius.

The positive clones were confirmed by restriction digestion. Different plasmids were isolated from bacterial colonies using Promega plasmid

isolation kit. The presence of insert in different plasmids was confirmed by restriction digestion protocol as given below:

1 (1µg) PBK Exon4 plasmid

1 µl BamHI (1U) (New England Biolabs)

2 µl 10X buffer (New England Biolabs)

11 µl Water

The digested product was checked on 1% Agarose gel.

To clone new Exon4 into AAV vector in order to generated new codon-optimised vector plasmid, the old AAV donor vector was digested with BamHI enzyme to replace old Exon4 with new codon optimised Exon4.

1 (1µg) pAAV old Exon4 plasmid

1 µl BamHI (1U) (New England Biolabs)

2 µl 10X buffer (New England Biolabs)

11 µl Water

The digested product was checked on 1% Agarose gel. The pAAV old donor was dephosphorylated at 5’ end to prevent self ligation after treatment with calf intestinal phosphatase at 37 degree celsius for 60 minutes. Then the enzyme was inactivated after incubation at 65 degree celsius for 20 minutes.

Next, Exon4 derived from PBK new Exon4 plasmid (insert) digested with BamHI as done above, was cloned directly without purification step into BamHI digested pAAV old donor vector (Vector) using the protocol given below:

Vector - 2 µl (15 ng)

Insert- 1.8 µl (60 ng)

Ligase buffer (10X) - 1.5 µl

T4 ligase- 0.5 µl (0.5 U)

Water- 9 µl

Self ligation control reaction

Vector – 2 µl (15 ng)

Ligase buffer (10X) - 1.5 µl

T4 ligase- 0.5 µl (0.5 U)

Water- 12 µl

Undigested control reaction

Vector – 1 µl (33 ng)

Ligase buffer (10X) - 1.5 µl

Water- 13 µl

All the ligation mixtures were incubated at RT for 4-5h and transformed into XL1 Gold competent cells in order to prevent recombination between ITRs of pAAV vector. The protocol used for transformation was the same as described above.

The positive clones were confirmed by restriction digestion. Different plasmids were isolated from bacterial colonies using Promega plasmid isolation kit. The presences of the insert in different plasmids were confirmed by restriction digestion as described below:

1 (1µg) pAAV new Exon4 donor plasmid

1 µl NcoI (1U) (New England Biolabs)

2 µl 10X buffer (New England Biolabs)

11 µl Water

The digested product was checked on 1% Agarose gel.

Orientation of the positive clone was checked using restriction digestion as described below:

2 µl (1µg) pAAV new Exon4 donor plasmid

1 µl SacI (1U) (New England Biolabs)

2 µl 10X buffer (New England Biolabs)

10 µl Water

The digested product was checked on 1% Agarose gel.

2.13 TALEN activity analysis in wild type animals using genomic PCR followed by restriction digestion

Genomic PCR was done from genomic DNA isolated from the liver of TALEN treated mice using the protocol given below:

gDNA- 3 µl

10X polymerase Buffer- 5 µl

$MgCl_2$(50 nM) - 8.4 µl

dNTP (25 mM) - 2.5 µl

UGTF3- 1.7 µl

UGT9934 Rev- 1.7 µl

Taq polymerase- 0.75 µl

Water- 26.95 µl

95- 30 min

95- 30 sec
60- 40 sec
72- 40 sec
} 35 cycles

72- 3 min

The genomic PCR product was confirmed after running in 1% agarose gel.

The genomic PCR products were then digested with NcoI restriction enzyme in order to investigate the presence of NcoI resistant site due to TALEN activity and NHEJ DSB DNA repair.

7 µl genomic PCR product

0.5 µl NcoI HF (0.5U) (New England Biolabs)

2 µl 10X buffer (New England Biolabs)

10.5 µl Water

The digested product was checked on 1% Agarose gel.

Primers used for genomic PCR:

Primer name	**Sequence (5'-3')**
UGTF3	ACTCGGGCATTCATCACACACTCTGG
UGT9934 Rev	GCTGTAAGACAATCTTCTCC

2.14 gRNA activity analysis in Hep3B cells using the pGL3 EXON4 reporter plasmid

Four different gRNAs targeting Exon4 of Ugt1 locus were designed. The gRNA-coding oligonucleotides were purchased from Eurofin Genomics in the form of lyophilized, non-phosphorylated single-stranded oligonucleotides, and were resuspended inwater to obtain a stock concentration of 1µg/µl. Next, 5'-phosphorylation of every single-stranded oligonucleotide was performed by setting up reaction containing water, 100 ng/µl single-stranded oligonucleotide, 1X PNK buffer (Roche), 66 µM ATP (Roche), and 10 U of Poly-Nucleotide Kinase (Roche). The reaction mixture was further incubated at 37 degree celsius for 1h. After 1h-incubation, 10 U of PNK was added, and the reaction was incubated again for 1h at 37°C.

Once phosphorylated, complementary oligonucleotides were annealedtogether to generate the phosphorylated double-stranded oligonucleotides to be cloned into pX601 plasmid vector (Addgene) . In order to anneal oligos, equal volumes of complementary phosphorylated oligos were mixed together and incubated for 5 minutes in a 95°C water bath. After this the water bath was cooled down to room-temperature. pX601 plasmid digested with BsaI restriction enzyme was finally used to clone annealed oligos. The presence of the corresponding gRNA was further confirmed by sequencing analysis.

For gRNA activity analysis 70,000 Hep3B cells were seeded in 24 well culture plates 14-16h before transfection. Next day Hep3B cells were co-transfected with different concentrations of gRNA, 400 ng of pGL3 EXON4 and 40 ng renilla plasmid using lipofectamine reagent according to manufacturer protocol. The activity of different gRNAs was calculated after measuring luciferase activity.

2.15 TALEN activity analysis in Hep3B cells using the pGL3 EXON4 reporter plasmid

For gRNA activity analysis 70,000 Hep3B cell were seeded in 24 well culture plate 14-16h before transfection. Next day Hep3B cells were co-transfected with different concentrations of NcoI targeting TALEN pairs, 400 ng of pcDNA5 EXON4 and 40 ng renilla plasmid using lipofectamine reagent according to manufacturer protocol. The activity of TALEN was calculated after measuring luciferase activity.

2.16 Subcloning of Luciferase and LuciFeExon4Ferase into pcDNA5/FRT plasmid

In order to clone the Luciferase encoding gene into the pcDNA5/FRT plasmid, the pGL3 Luciferase plasmid was digested according to the protocol given below:

0.5 (1µg) pGL3 luciferase plasmid

1 µl HindIII (1U) (New England Biolabs)

1 µl XbaI (1U) (New England Biolabs)

2 µl 10X buffer (New England Biolabs)

15.5 µl Water

The digestion of the pGL3 control plasmid was confirmed after running in 0.8% agarose gel.

In the next step, luciferase insert derived from pGL3 plasmid was cloned directly without purification step into PBK vector digested with HindIII and XbaI.

Vector - 1 µl (40 ng)

Insert- 4 µl (80 ng)

Ligase buffer (10X) - 1.5 µl

T4 ligase- 0.5 µl (0.5 U)

Water- 8 µl

Vector- 1 µl (40 ng)

Insert- 8 µl (160 ng)

Ligase buffer (10X) - 1.5 µl

T4 ligase- 0.5 µl (0.5 U)

Water- 4 µl

Self ligation control reaction

Vector – 1 µl (40 ng)

Ligase buffer (10X) - 1.5 µl

T4 ligase- 0.5 µl (0.5 U)

Water- 12 µl

Undigested control reaction

Vector – 1 µl (40 ng)

Ligase buffer (10X) - 1.5 µl

Water- 12.5 µl

All the ligation mixtures were incubated at RT for 4-5h and transformed into DH5α competent cells as done before.

The positive clones were confirmed by restriction digestion using the protocol given below:

5 µl (1µg) PBK luciferase plasmid

1 µl HindIII (1U) (New England Biolabs)

1 µl XbaI (1U) (New England Biolabs)

2 µl 10X buffer (New England Biolabs)

11 µl Water

The digestion of the PBK luciferase plasmids was confirmed after running in 0.8% agarose gel.

In the next step, the luciferase insert derived from the PBK luciferase plasmid digested with HindIII and NotI was cloned directly without purification step into pcDNA5/FRT vector digested with HindIII and NotI enzymes. Ligation was performed using the protocol given below:

Vector - 1 µl (20 ng)

Insert- 4 µl (80 ng)

Ligase buffer (10X) - 1.5 µl

T4 ligase- 0.5 µl (0.5 U)

Water- 8 µl

Vector- 1 µl (40 ng)

Insert- 8 µl (160 ng)

Ligase buffer (10X) - 1.5 µl

T4 ligase- 0.5 µl (0.5 U)

Water- 4 µl

Self ligation control reaction

Vector – 1 µl (40 ng)

Ligase buffer (10X) - 1.5 µl

T4 ligase- 0.5 µl (0.5 U)

Water- 12 µl

Undigested control reaction

Vector – 1 µl (40 ng)

Ligase buffer (10X) - 1.5 µl

Water- 12.5 µl

All the ligation mixtures were incubated at RT for 4-5h and transformed into DH5αcompetent cells as done before.

The positive clones were confirmed by restriction digestion using the protocol given below:

0.5 µl (1µg) PBK luciferase plasmid	0.5 µl (1µg) PBK luciferase plasmid
1 µl HindIII (1U) (New England Biolabs)	1 µl HindIII (1U) (New England Biolabs)
1 µl SpeI (1U) (New England Biolabs)	1 µl PstI (1U) (New England Biolabs)
2 µl 10X buffer (New England Biolabs)	2 µl 10X buffer (New England Biolabs)
15.5 µl Water	15.5 µl Water

Next, LuciFeExon4Ferase was subcloned from pGL3LuciFeExon4Ferase was subcloned into pcDNA5/FRT. First, pGL3LuciFeExon4Ferase was digested with HindIII and XbaI as given below:

2 µl (1µg) PBK luciferase plasmid

1 µl HindIII (1U) (New England Biolabs)

1 µl XbaI (1U) (New England Biolabs)

2 µl 10X buffer (New England Biolabs)

14 µl Water

The digestion of pGL3LuciFeExon4Ferase was confirmed by running the digestion product on 0.8% gel.

The digested product was then directly cloned without purification step into HindIII and XbaI digested PBK vector.

Vector - 1 µl (16 ng)	Vector- 1 µl (16 ng)
Insert- 4 µl (70 ng)	Insert- 8 µl (140 ng)

Ligase buffer (10X) - 1.5 µl	Ligase buffer (10X) - 1.5 µl
T4 ligase- 0.5 µl (0.5 U)	T4 ligase- 0.5 µl (0.5 U)
Water- 8 µl	Water- 4 µl

Self ligation control reaction	**Undigested control reaction**
Vector – 1 µl (16 ng)	Vector – 1 µl (16 ng)
Ligase buffer (10X) - 1.5 µl	Ligase buffer (10X) - 1.5 µl
T4 ligase- 0.5 µl (0.5 U)	Water- 12.5 µl
Water- 12 µl	

All the ligation mixtures were incubated at RT for 4-5h and transformed into DH5αcompetent cells as described before.

The positive clones were confirmed by restriction digestion using the protocol given below:

3 µl (1µg) PBK LuciLuciFeExon4Feraseplasmid

1 µl HindIII (1U) (New England Biolabs)

1 µl XbaI (1U) (New England Biolabs)

2 µl 10X buffer (New England Biolabs)

13 µl Water

The digestion of the PBK LuciFeExon4Ferase plasmid was confirmed by running the digestion product on 0.8% gel.

The HindIII and NotI digested product was then directly cloned without purification step into HindIII+ NotI digested pcDNA5/FRT vector.

Vector - 1 µl (30 ng)	Vector- 1 µl (30 ng)
Insert- 3 µl (90 ng)	Insert- 6 µl (180 ng)
Ligase buffer (10X) - 1.5 µl	Ligase buffer (10X) - 1.5 µl
T4 ligase- 0.5 µl (0.5 U)	T4 ligase- 0.5 µl (0.5 U)

Water- 9 µl

Water- 6 µl

Self ligation control reaction

Undigested control reaction

Vector – 1 µl (30 ng)

Ligase buffer (10X) - 1.5 µl

T4 ligase- 0.5 µl (0.5 U)

Water- 12 µl

Vector – 1 µl (16 ng)

Ligase buffer (10X) - 1.5 µl

Water- 12.5 µl

All the ligation mixtures were incubated at RT for 4-5h and transformed into DH5αcompetent cells as done before.

The positive clones were confirmed by restriction digestion using protocol given below:

3 µl (1µg) pcDNA5 LuciFeExon4Ferase plasmid

1 µl HindIII (1U) (New England Biolabs)

1 µl XcmI (1U) (New England Biolabs)

2 µl 10X buffer (New England Biolabs)

13 µl Water

3 µl (1µg) pcDNA5 LuciFeExon4Ferase plasmid

1 µl BamHI (1U) (New England Biolabs)

2 µl 10X buffer (New England Biolabs)

14 µl Water

The digestion of pcDNA5 LuciFeExon4Ferasewas confirmed by running the digestion product on 0.8% agarose gel.

2.17 Luciferase and LuciFeExon4Ferase stable clone generation

To generate luciferase stable clone, Hep3B cells were used. Due to the absence of any antibiotics resistance gene in pcDNA5/FRT plasmid, we decided to co-transfect the cells with pBABE plasmid containing hygromycin resistance gene. In a pilot experiment, 200 µg/ml was used to kill untransfected cells. In order to generate the luciferase stable clone, Hep3B cells were co-transfected with 14 µg of pcDNA5 Luciferase and 1.4 µg pBABE plasmids in a 10 cm cell culture plate using lipofectamine reagent according to manufacturer instructions. The cells were exposed to hygromycin pressure 5 days after transfection for 10 days to kill untranfected cells. After 10 days of antibiotic pressure, cells were serially diluted to get single cells clones.

Only 9 clones survived the hygromycin pressure after serial dilution and the activity of individual clones was determined using the luciferase assay.

To generate LuciFeExon4Ferasestable clone Hep3B cells were co-transfected with 16µg of pcDNA5 LuciFeExon4Ferase and 1.6 µg pBABE plasmid in a 10 cm cell culture plate using lipofectamine reagent according to manufacturer instructions. The cells were exposed to hygromycin pressure 5 days after transfection for 10 days to kill untranfected cells. After 10 days of antibiotic pressure, cells were serially diluted to get single cells clones.

Only 11 clones survived the hygromycin pressure after serial dilution and the activity of individual clones were determined using luciferase assay after co-transfecting all the individual clones with 700 ng Nco targeting TALEN pairs and 40 ng renilla plasmid in 24-well cell culture plate using lipofectamine reagent according to manufacturer

instructions. The activities of individual clones were determined by the luciferase assay.

2.18 Subcloning of luciferase and LuciFeExon4Ferase into pcDNA3 plasmid

Sucloning of luciferase and LuciFeExon4Ferase into pcDNA3 plasmid was done using PBK luciferase and PBK LuciFeExon4Ferase plasmids cloned in Section 2.5.

The PBK clone was digested with HindIII and XbaI using protocol given below:

5 µl (1µg) PBK luciferase plasmid

1 µl HindIII (1U) (New England Biolabs)

1 µl XbaI (1U) (New England Biolabs)

2 µl 10X buffer (New England Biolabs)

11 µl Water

The digestion of PBK clones was confirmed by running the digestion reactions on 1% agarose gel.

Next, The HindIII and XbaI digested product was then directly cloned without purification step into HindIII and XbaI digested pcDNA3 vector.

Vector – 1 µl (60 ng)	Vector- 1 µl (60 ng)
Insert- 2.27 µl (22.25 ng)	Insert- 4.54µl (22.25ng)
Ligase buffer (10X) - 1.5 µl	Ligase buffer (10X) - 1.5 µl
T4 ligase- 1 µl (1 U)	T4 ligase- 1 µl (1 U)
Water- 9.23 µl	Water- 6.96 µl

Self ligation control reaction	**Undigested control reaction**
Vector – 1 µl (60 ng)	Vector – 1 µl (60 ng)
Ligase buffer (10X) - 1.5 µl	Ligase buffer (10X) - 1.5 µl
T4 ligase- 1 µl (1 U)	Water- 12.5 µl
Water- 11.5 µl	

All the ligation mixtures were incubated at RT for 4-5h and transformed into DH5α competent cells as done before.

The positive clones were confirmed by restriction digestion using protocol given below:

2 µl (1µg) pCDNA3 luciferase plasmid plasmid	2 µl (1µg) pCDNA3 luciferase
1 µl HindIII (1U) (New England Biolabs)	1 µl HindIII(1U) (New England Biolabs)
1 µl XbaI (1U) (New England Biolabs)	1 µl XcmI (1U) (New England Biolabs)
2 µl 10X buffer (New England Biolabs)	2 µl 10X buffer (New England Biolabs)
14 µl Water	14 µl Water
2 µl (1µg) pcDNA3 luciferase plasmid	
1 µl NdeI (1U) (New England Biolabs)	
1 µl XcmI (1U) (New England Biolabs)	
2 µl 10X buffer (New England Biolabs)	
14 µl Water	

Next, in order to clone LuciFeExon4Ferase construct into the pcDNA3 vector, the PBK clones were digested with HindIII and XbaI using protocol given below:

5 µl (1µg) PBK LuciFeExon4Feraseplasmid

1 µl HindIII (1U) (New England Biolabs)

1 µl XbaI (1U) (New England Biolabs)

2 µl 10X buffer (New England Biolabs)

11 µl Water

The digestion of PBK clones were confirmed by running the digestion reactions on 1% agarose gel.

Next, The HindIII and XbaI digested product was then directly cloned without purification step into HindIII and XbaI digested pcDNA3 vector.

Vector – 1 µl (60 ng)

Insert- 1.48 µl (55.75 ng)

Ligase buffer (10X) - 1.5 µl

T4 ligase- 1 µl (1 U)

Water- 10.02 µl

Vector- 1 µl (60 ng)

Insert- 2.96 µl (55.75 ng)

Ligase buffer (10X) - 1.5 µl

T4 ligase- 1 µl (1 U)

Water- 8.54 µl

Self ligation control reaction

Vector – 1 µl (60 ng)

Ligase buffer (10X) - 1.5 µl

T4 ligase- 1 µl (1 U)

Water- 11.5 µl

Undigested control reaction

Vector – 1 µl (60 ng)

Ligase buffer (10X) - 1.5 µl

Water- 12.5 µl

All the ligation mixtures were incubated at RT for 4-5 h and transformed into DH5α competent cells as describedbefore.

The positive clones were confirmed by restriction digestion using the protocol given below:

2 µl (1µg) pcDNA3LuciFeExon4Ferase plasmid

1 µl HindIII (1U) (New England Biolabs)

1 µl XbaI (1U) (New England Biolabs)

2 µl 10X buffer (New England Biolabs)

14 µl Water

2 µl (1µg) pcDNA3LuciFeExon4Ferase plasmid

1 µl HindIII (1U) (New England Biolabs)

1 µl XcmI (1U) (New England Biolabs)

2 µl 10X buffer (New England Biolabs)

14 µl Water

2.19 Statistical analysis

The Graph pad Prism package was used to analyse the data. Data was always represented as mean ± SD. $P<0.05$ were considered significant. Depending on experimental design, Student's *t*-test, one-way and two-way ANOVA with Bonferroni's *post-hoc* comparison test were used and are indicated in the legends.

AIM of the Thesis

The aim of my PhD thesis was to investigate the effects of bilirubin on the DNA damage and DNA repair pathways. Previous studies showed the induction of oxidative stress as one of the mechanisms of bilirubin induced neurotoxicity.

The first part of this thesis focused on the DNA damaging effect of bilirubin on neuronal cells. To this end, I investigated the time-dependent effect of bilirubin-induced DNA damage and next, the involvement of oxidative stress on bilirubin-induced DNA damage.

The second part of the thesis focused on the effects of bilirubin on double stranded-break repair pathways, using HeLa cell lines. In particular, I was interested to study time and dose-dependent increase in Homologous Recombination, mediated by bilirubin-induced oxidative stress. Furthermore, I investigated the effects of bilirubin on the NHEJ repair pathway.

RESULTS

Section I

Results

3.1 Bf determination for *in vitro* experiments

Bilirubin toxicity depends on the amount of Bf. Bf concentrations above 70 nM are normally considered as toxic to human cells. In order to perform *in vitro* experiments with bilirubin, Bf was quantified using modified peroxidase assay as described in the Materials and Methods Section.

Therefore, in order to perform *in vitro* experiments treating different cell lines with bilirubin, it was first required to prepare culture media (with 10% or 15% fetal calf serum, FCS, depending on the cell type) containing different amounts of TB that leads to the desired Bf. Consequently, since different FCS stocks may have variations in both albumin concentration and its affinity for bilirubin, resulting in different Bf for the same theoretical FCS concentration, I determined the Bf for the stock of fetal calf serum utilized in all experiments done in the present thesis.

The modified peroxidase assay involves minimum dilution of the sample, minimizing the effect of albumin dilution on binding affinity. This method is based on the fact that Bf gets oxidised to a colourless compound by peroxide, with first order kinetics; while albumin-bound bilirubin remains protected from oxidation. Bf determination was done with at least three (0.025-0.05 µg/ml) different enzymatic concentrations. Apparent Bf was calculated applying the formula given below, where Kp is the rate constant for the HRP enzyme used, ΔAbs corresponds to the change in absorbance over 30 seconds (Roca et al., 2006). True Bf can be calculated from the apparent Bf by making a plot of 1/Apparent Bf vs HRP concentration used, where the“y intercept” of the plot corresponds to the real Bf.

Apparent Bf = ΔAbs/min/Kp x [HRP]

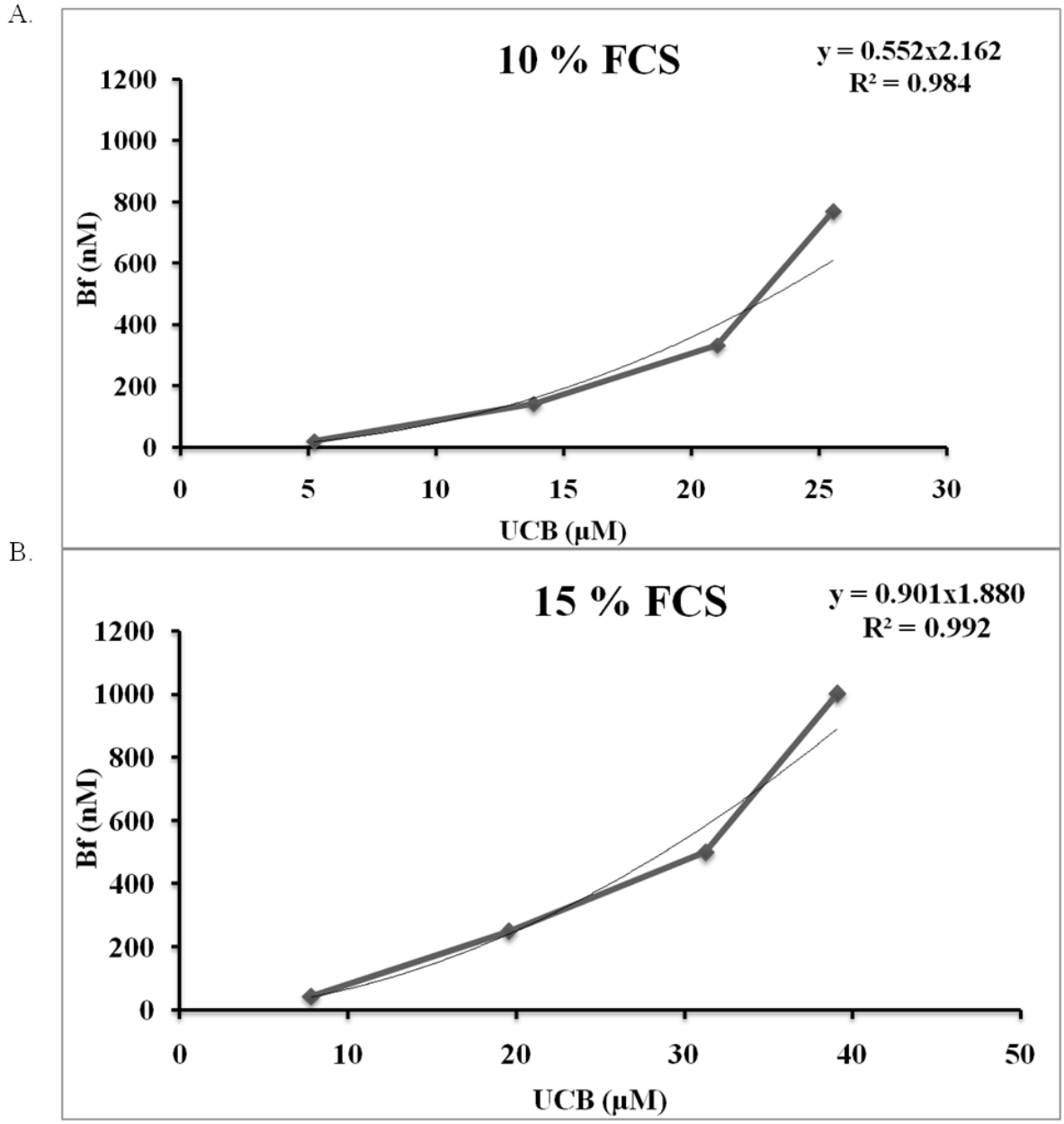

Figure 10. Bf determination in two different types of culture media (DMEM with 10% FCS and EMEM/F12 with 15% FCS) by modified peroxidase assay. A). Bf determination in 10% FCS containing DMEM media. B). Bf determination in 15% FCS containing EMEM/F12 media. X-axis corresponds to total bilirubin concentration while Y-axis corresponds to Bf concentration (this assay has been performed only once, as recommended by Prof. Tiribelli's lab).

Using the modified peroxidase method, Bf was determined in DMEM media with 10% FCS and EMEM/F12 with 15% FCS (used to culture HeLa and SH SY 5Y cells respectively; Figure 10. Different molar ratios of bilirubin/albumin were used to calculate the Bf.

3.2 Bilirubin-induced toxicity in immature neuronal (SH SY5Y) cells

For bilirubin related studies of neurotoxicity, we used the SH SY 5Y cell line (Qaisiya et al., 2017a; Qaisiya et al., 2014). In order to check the cytotoxicity of bilirubin, SH SY 5Y cells were treated with 70 nM and 140 nM of Bf for different time intervals (1h, 4h and 24h). The MTT test was done to check the viability of cells in each of the respective time points. After one hour, viability was reduced to 91% and 82% with 70 nM and 140 nM Bf, respectively. Viability was further reduced to 80% and 75% after 4h treatment with 70nM and 140 nM respectively. After 24h, viability with 70 nM treatment was 81%, while it was reduced to 69% in the case of 140 nM treatment (Figure 11). Viability at 140 nM compared to 70 nM showed a trend of decrease in viability at all time points studied. Based on our results and published data (Qaisiya et al., 2017a; Qaisiya et al., 2014), 140 nM Bf was chosen for subsequent studies to check bilirubin-induced DNA damage.

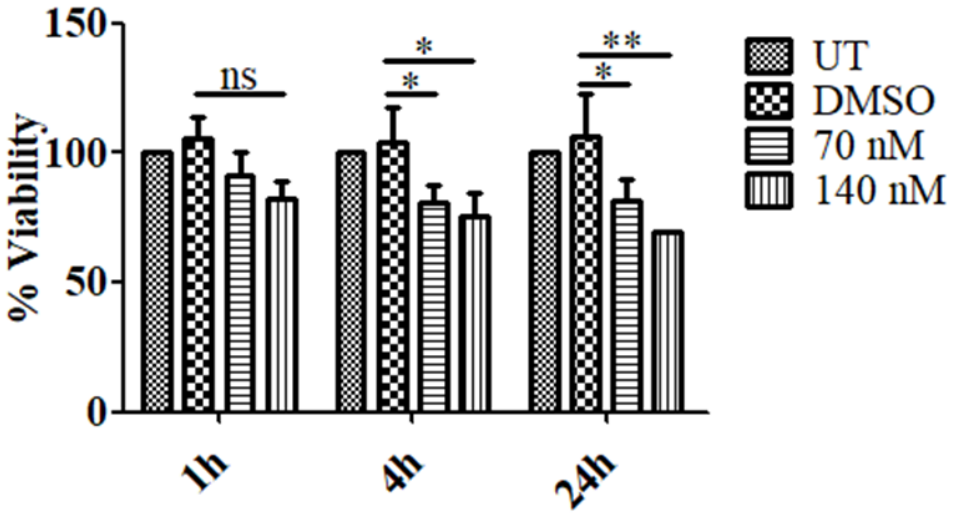

Figure 11. MTT test to check the viability of SH SY 5Y cells. SH SY 5Y cells were treated with 70 nM and 140 nM Bf for different time intervals ranging from 1h, 4h and 24h. Cell viability was assessed using MTT reagent corresponding to respective time point. Viability of untreated cells were considered as 100%. DMSO acts as a solvent for bilirubin and used as a control. Values are represented as mean ± SD. ** represents $P < 0.01$; * $P < 0.05$; ns, non-significant. Two-way ANOVA with Bonferroni's *post hoc* test was used to perform statistical analysis.

However, the cellular viability after bilirubin treatment could be confirmed by other well-known methods such as Lactate dehydrgenase (LDH) release, Caspase-3 cleavage Western blot and Annexin-propidium iodide (PI) staining. MTT may not represents the appropriate assay to check cellular viability after bilirubin treatment due to the direct effect of bilirubin on mitochondria (Vaz et al., 2010). Because, MTT test directly measures the mitochondrial activity and bilirubin toxicity affects mitochondria (Rodrigues et al., 2000), measurement of cellular viability after bilirubin treatment by MTT test may result in an inaccurate value of cellular viability.

3.3 Bilirubin-induced DNA damage in immature neuronal (SH SY 5Y) cells

Oxidative stress is one of the mechanisms involved in bilirubin-induced neuronal cell death. The accumulation of DNA damage due to bilirubin induced oxidative stress may play an important role in neurodegeneration. Accumulation of increased oxidative DNA damage in mitochondrial and nuclear DNA derived from post-martem brain regions of several neurodegenerative diseases tempted us to investigate the induction of DNA damage by bilirubin induced oxidative stress (Coppede and Migliore, 2015). In addition to oxidative base modifications, ROS can also create DSBs. The involvement of DSBs in neurodegeneration was first seen in AD during 1990s (Mullaart et al., 1990).Similarly, human amyloid precursor protein (APP) trangenic mice, had increased neuronal DSBs than control mice (Suberbielle et al., 2013). However, studying the contribution of DNA damage during neurodegeneration represents a complex question. It is not clear whether DNA damage cause neurodegeneration or it occurs as a consequence to

neurodegeneration. So, based on previous studies, we started to investigate the induction of DNA damage by bilirubin induced oxidative stress in immature neuronal cells. Since, immature neuronal cells represents the most severely affected cells in the brain due to high bilirubin levels (Bortolussi et al., 2012), induction of DNA damage by bilirubin induced oxidative stress may contribute to neuronal cell death by delayed cellular response to DNA damage such as apoptosis and senescence (Borges et al., 2008).

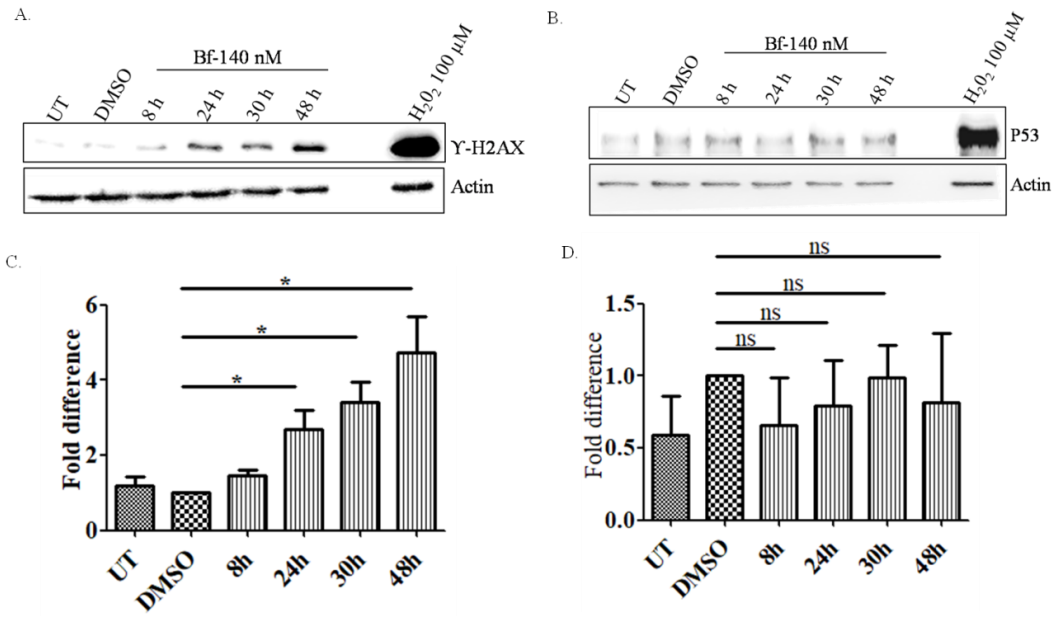

Figure 12. Western Blot analysis to check DNA damage induction by bilirbin. SH SY 5Y cells were treated with 140 nM bilirubin for different time intervals. DMSO acts as solvent for bilirubin and was added as control. A). Cells were harvested at different time intervals after bilirubin treatment and DNA damage was assessed by checking the level of γH2AX using Western Blot. Graph in Panel C represents quantification from 3 independent experiments as shown in Panel A. B). P53 levels were checked in the same samples after bilirubin treatment using Western Blot analysis. Graphs in Panel D represents the quantification from 3 independent experiments as shown in Panel B.Values are represented as mean ± SD. * represents $P < 0.05$, ns represents non-significant. Student's *t-test* was used to perform statistical analysis.

Phosphorylated H2AX (γH2AX) is the most commonly used marker to assess induction of double stranded DNA breaks and single stranded DNA accumulation generated during replication stress (Ward and Chen, 2001). In response to ionizing radiation and DNA damage chemotherapeutic reagents, DSBs are generated that results in the rapid phosphorylation of H2AX (γH2AX) at Ser 139. The phosphoryaltion of H2AX is abudant, rapidly spread over the damaged chromatin that highly correlated with the number of DSBs, making it a good marker for double-stranded break and its repair (Sharma et al., 2012). In addition, H2AX get phosphorylated by ATR in reponse to ssDNA formed during replication stress (Ward and Chen, 2001). Due to the phosphorylation of H2AX during DSBs and replication stress, it cannot be considered as a reliable marker specfically for DSBs. Another method that can be used to detect DNA damage in individual cells is the comet assay. This assay can be done under neutral and alkaline conditions. The comet assay done under alkaline conditions can detect single stranded breaks, double stranded breaks and alkali-labile lesions. Double stranded breaks can be detected specifically by neutral comet assay (Olive and Banath, 2006). However, comet assay was not performed in this thesis.

In order to assess bilirubin-induced DNA damage by oxidative stress, SH SY 5Y cells were treated with 140 nM Bf for different time intervals ranging from 8h to 48h. Cells were harvested at the respective time points and the level of γH2AX was determined by Western Blot analysis using γH2AX-specific antibody.

Bilirubin treatment leads to DNA damage induction, with an evident increase in the γH2AX signal already after 24h of treatment. There was a time dependent increase in DNA damage in SH SY 5Y cells with maximum DNA damage at 48h after bilirubin treatment (4-5 folds)

(Figure 12A). Next, I checked the level of P53 to determine if it is activated after DNA damage induced by bilirubin. P53 activation after DNA damage could lead to a delay in cell cycle progresion to allow the repair of the damaged DNA. Alternatively, if the DNA damage is irreparable, cells could undergo apoptosis. Interestingly, P53 protein levels were not modulated after the induction of DNA damage by bilirubin (P53-DO-I Santa Cruz Biotechnology) (Figure 12B).

3.4 Bilirubin-induced DNA damage is reversed by antioxidant treatment

To demonstrate the involvement of oxidative stress in bilirubin induced DNA damage, cells were co-treated with N-Acetyl cysteine (NAC). NAC is the most commonly used antioxidant, which reduces oxidative stress by acting as a precursor of glutathione. In this set of experiments, SH SH 5Y cells were exposed to 140 nM Bf for different time intervals (8h, 24h, 30h and 48h).

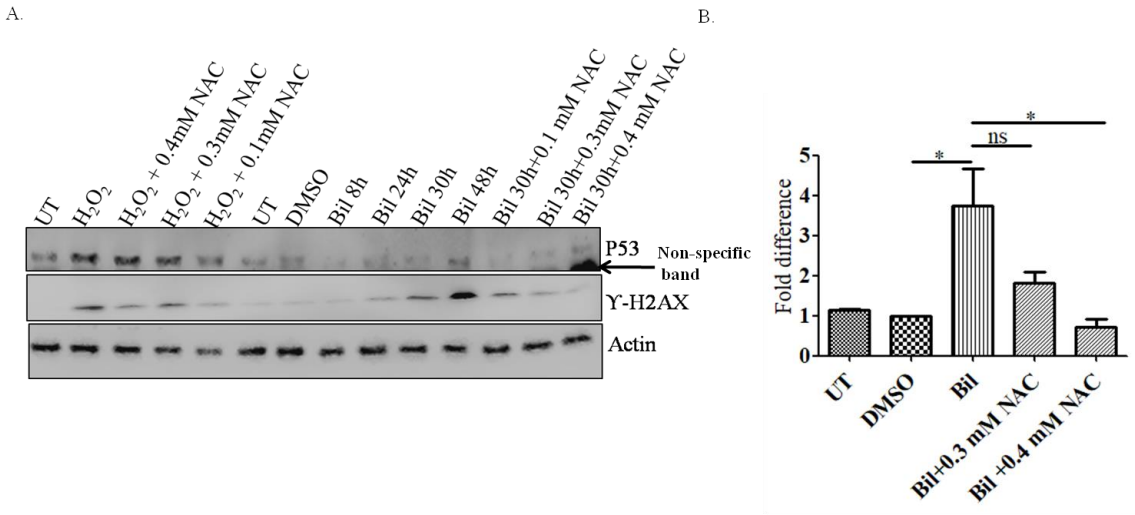

Figure 13. Western Blot analysis to check DNA damage reversal by NAC treatment. SH SY 5Y cells were treated with 140 nM bilirubin for different time intervals (8-48h). DMSO acts as solvent for bilirubin and was added as control. For antioxidant (NAC) treatment, cells were pre treated with different doses of NAC for 1h followed by co-treatment with bilirubin for 30h. A). DNA damage was assessed by checking the levels of γH2AX using Western Blot. Graph represents the quantification from 2 independent experiments (Panel B). Values are represented as mean ± SD. * represents $P < 0.05$, ns represents non-significant. One-way ANOVA Bonferroni's *post hoc* test was used to perform statistical analysis.

In the case of the NAC treatment experiment, to determine the role of oxidative stress in bilirubin-induced DNA damage, the experimental time-point of 30 h of bilirubin exposure was selected. In this experiment, cells were exposed to different doses of NAC for 1h followed by co-treatment with bilirubin for 30h. As shown in Figure 13, bilirubin treatment led to time-dependent increase in DNA damage (compare DMSO with Bil 8h-48h). The level of P53 remained unaffected after bilirubin treatment confirming the results of Figure 12B. However, when cells were co-treated with NAC, bilirubin-induced DNA damage was reversed by the treatment in a dose dependent manner (compare Bil 30h with Bil 30h + 0.1 mM NAC, Bil 30h + 0.3 mM NAC, and Bil 30h + 0.4 mM NAC). This result strongly suggests the involvement of oxidative stress in bilirubin induced DNA damage.

3.5 Bilirubin-induced DNA damage foci decreased after NAC treatment

In order to confirm the Western Blot analysis results, immunofluorescence analysis was done to detect the γH2AX foci formation after bilirubin treatment. In these experiments, SH SY 5Y cells were pre-exposed with NAC for 1h followed by co-treatment with bilirubin for 30h as described in the previous experiment (Figure 13).

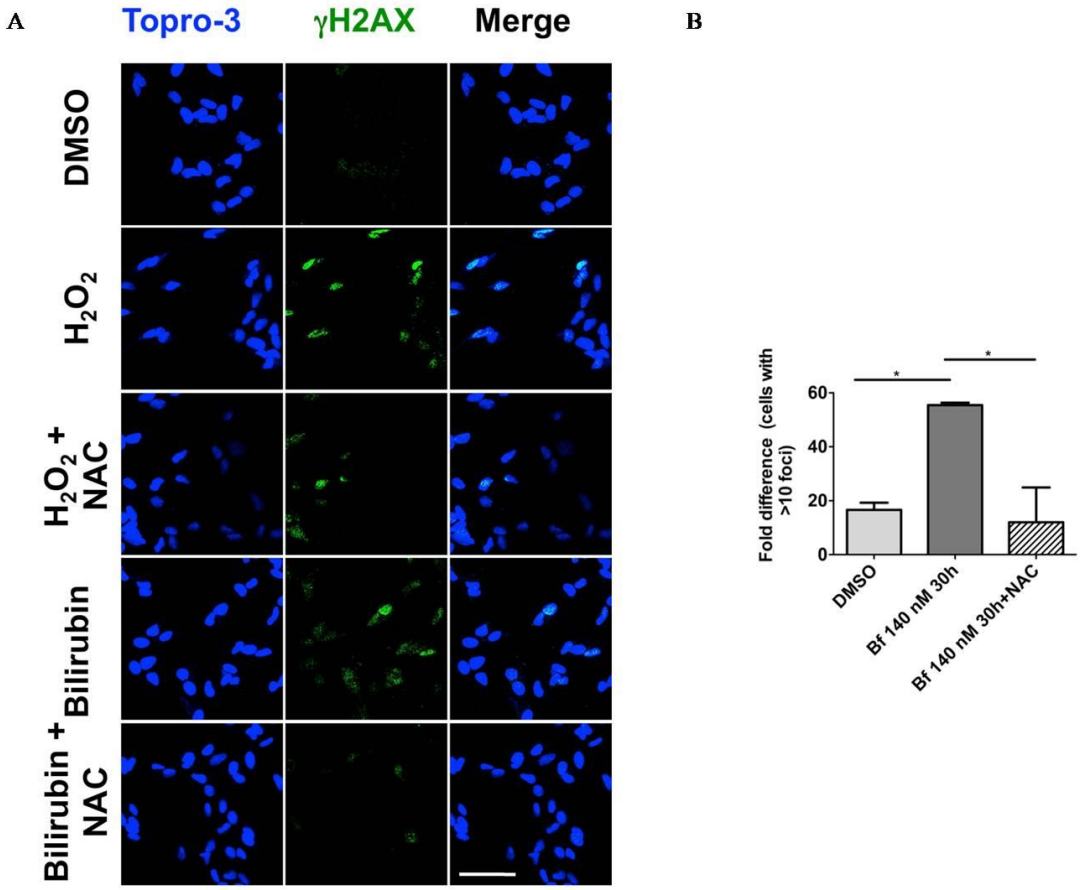

Figure 14. Immunofluorescence analysis to check bilirubin induced DNA damage reversal by NAC treatment. SH SY 5Y cells were treated with 0.4 mM NAC for 1h followed by co-treatment with bilirubin for additional 30h. A). Immunofluorescence analysis was done to check the presence of DNA damage foci. Graph represents the quantification from 2 independent experiments (Panel B). Values are represented as mean ± SD. * represents $P < 0.05$. One-way ANOVA Bonferroni 's *post hoc* test was used to perform statistical analysis. Scale bar represents 30 µM.

Treated cells were fixed, permeabilized and stained with an anti γH2AX-specific antibody. As shown in Figure 14, bilirubin treatment led to a significant increase in γH2AX foci formation in cells ($P < 0.05$-One Way ANOVA). Co-treatment with NAC reversed the DNA damage as shown by reduced γH2AX foci formation in NAC co-treated cells. The immunofluorescence results along with the Western Blot result in Figure 13, demonstrated the involvement of oxidative stress in bilirubin-induced DNA damage.

3.6 Bilirubin-induced toxicity in HeLa DR GFP cells

To investigate the role of bilirubin in HR, we took advantage of the HeLa DR GFP stable cell line. These cells contain a single copy of a homologous recombination reporter construct (an inactive GFP gene plus a duplicated, truncated, GFP fragment) inserted in the genome (see section 1.9.3). Transfection of these cells with a plasmid encoding the Isce1 restriction enzyme leads to the generation of a DSB in the upstream inactive GFP fragment. DSB formation activates HR between the upstream inactive version of GFP and the downstream truncated GFP, resulting in a full length, wild-type, GFP cDNA. The total number of GFP positive cells after FACS analysis corresponds to cells that have undergone HR (Cuozzo et al., 2007).

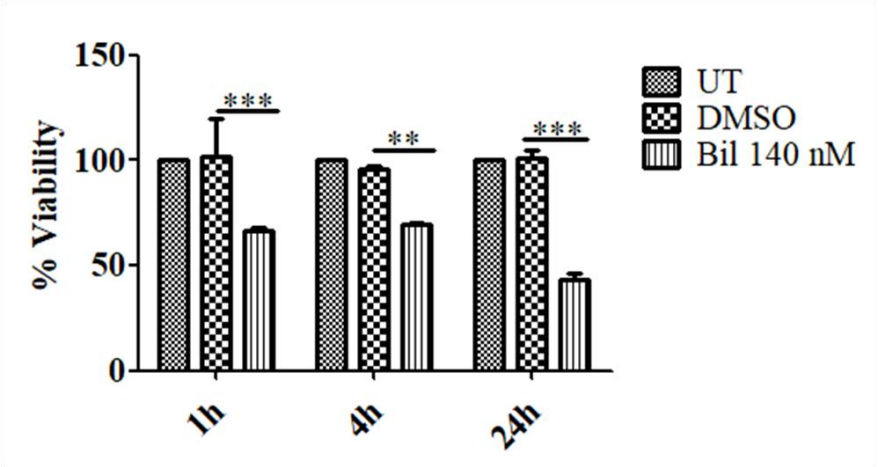

Figure 15. MTT test to check the viability of HeLa DR GFP cells. HeLa DR GFP cells were treated with 140 nM Bf for different time intervals ranging from 1h, 4h and 24h. Cell viability was assessed using MTT reagent corresponding to respective time point. Viability of untreated cells were considered as 100%. DMSO acts as a solvent for bilirubin and used as a control. Values are represented as mean ± SD. ** represents $P < 0.01$, *** represents $P < 0.001$. Two way ANOVA with Bonferroni's *post hoc* test was applied to perform statistical analysis.

HeLa DR GFP cells were exposed to bilirubin from 1h to 24h. Cell viability was assessed by the MTT test at the different time points. Treatment with 140 nM bilirubin led to 30% reduction in cellular viability after 1h and 4h of treatment. The effect of bilirubin became more severe after 24h of treatment, with 60% reduction in cellular viability (Figure 15).

Based on these observations, 140 nM Bf was used to do further experiments. However, in the dose-response experiments lower doses were also used in order to find the optimal Bf concentration that can modulate homologous recombination.

3.7 Time-course effect of Bilirubin on HR

The HeLa DR GFP stable cell line was used to study the effects of bilirubin on homologous recombination. In this experiment, HeLa DR GFP cells were transfected with the Isce1 plasmid and bilirubin was added for different time points ranging from 24-66h. The IsceI plasmid codes for the IsceI endonuclease, which generates a DSB in the reporter construct, resulting in the reconstitution of the GFP open reading frame after homology directed repair (Cuozzo et al., 2007). Cells were analysed for GFP fluorescence by FACS analysis 72h after transfection.

As shown in Figure 16, bilirubin treatment followed by Isce1 transfection led to a trend towards time-dependent increase in GFP positive cells. Interestingly, bilirubin itself did not stimulate the homologous recombination (compare UT and UT+Bil in FACS raw data, Figure 16, Panel B). However, in the presence of double stranded breaks, bilirubin treatment led to time dependent increase in the number of GFP positive cells,clearly suggesting the modulation of HR by

bilirubin (compare Isce1 DMSO and Isce1 Bil treatments, Figure 16, Panels B& C). Since transfection efficiency was normalised with the transfection efficiency of a different well, existence of lot of variability results in non-significant difference between different conditions when analysed using One-way ANOVA.

3.8 Dose-response effect of Bilirubin on HR

To determine the optimal dose of bilirubin resulting in an increase in HR, HeLa DR GFP cells were treated with bilirubin ranging from 10 nM to 140 nM for 66h after co-transfection with the Isce1-coding plasmid and a second plasmid encoding for renilla luciferase, which was used as control for transfection efficiency.

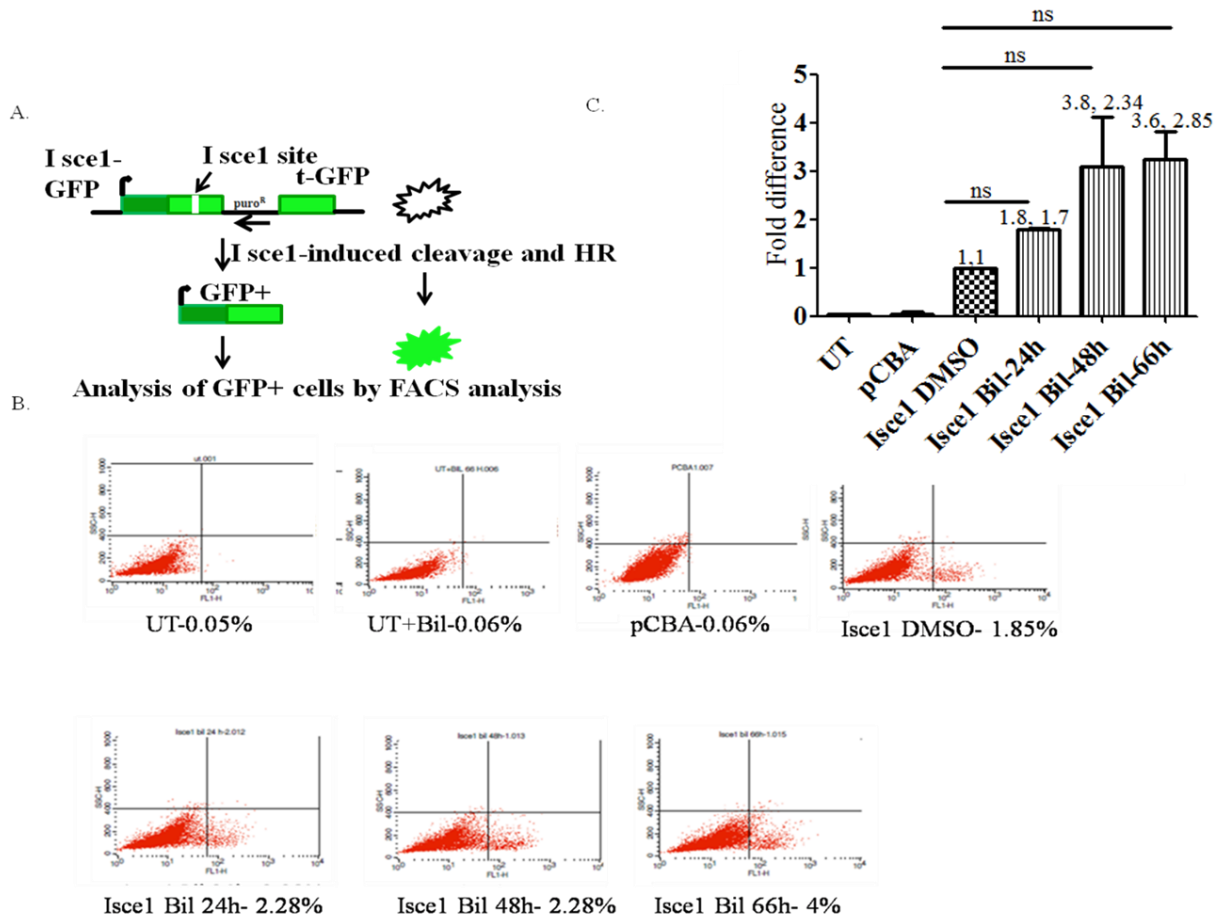

Figure 16. Time course effect of bilirubin on Homologous Recombination. HeLa DR GFP cells were transfected with plasmid encoding Isce1. After 6-7h of transfection, 140 nM Bf was added to cells for different time intervals ranging from 24-66h. DMSO acts as solvent for bilirubin and was added as control. Cells were analysed for GFP fluorescence by FACS analysis 72h after transfection (Panel B). Panel C, represents quantification from 2 independent experiments. eGFP in parallel well was used to normalise for differences in transfection efficiency. Every condition was done in duplicates in each experiment. Values are represented as mean ± SD. ns represents non-significant. One-way ANOVA Bonferroni 's *post hoc* test was used to perform statistical analysis.

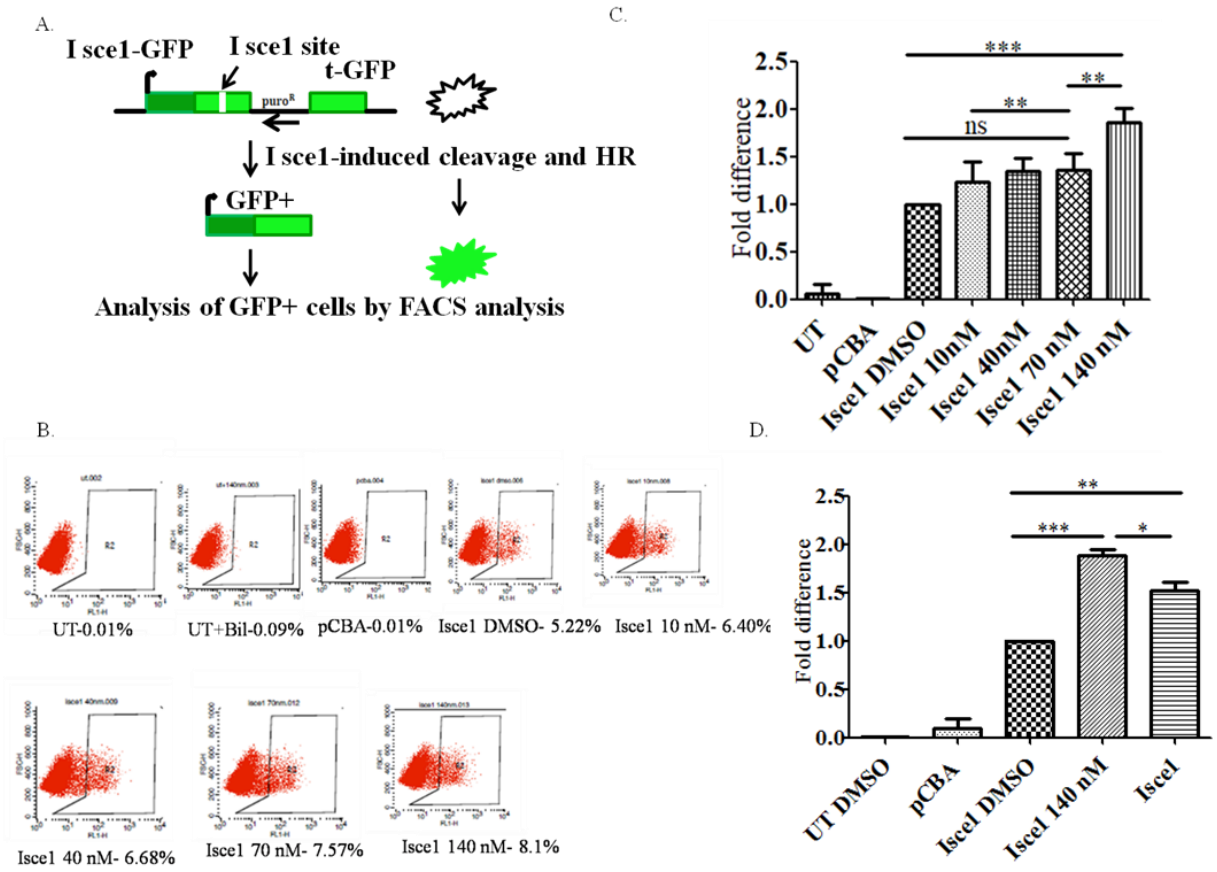

Figure 17. Dose response effect of bilirubin on Homologous recombination. HeLa DR GFP cells were co-transfected with plasmid encoding Isce1 (pCBA Isce1) and renilla (pHRG TK Renilla). After 6-7h of transfection, different doses of Bf (10-140 nM) was added to cells. DMSO acts as solvent for bilirubin and was added as control. Cells were analyzed for GFP expression by FACS analysis 72h post-transfection (Panel B). Panel C, represents quantification from 3 independent experiments. Panel D shows the effect of DMSO on HR. Data was normalised to renilla activity corresponds to same well. Values are represented as mean ± SD. *** represents $P < .001$, ** represents $P < .01$, * represents $P < .05$ and ns represents non-significant. One-way ANOVA with Bonferroni's *post hoc* test was done to perform the statistical analysis.

In this strategy, the percentage of GFP cells in a particular well was normalised with the transfection efficiency of the same well. In Figure 16, data was normalised to the transfection efficiency corresponds to a parallel well. Thus, the data obtained after normalisation may present higher variabiltiy, as can be seen in the bar graph. In this experiment, transfected cells were collected 72h after transfection, and half of the cell suspension was used to determine the transfection efficiency by measuring renilla luciferase activity, and the other half analysed for GFP expression by FACS analysis (Figure 17). I observed a dose-dependent increase in HR starting at 40 nM, with maximum increase at 140 nM (Figure 17, Panel B& C). Panel D in Figure 17 shows the effect of DMSO on HR. Bilirubin addition leads to significant increase in HR (compare Isce1 DMSO and Isce Bil), as observed in Panels B and C. DMSO addition does not result in DNA damage and, it apparently results in a significant decrease in HR (compare Isce1 DMSO and Isce1). This result confirm that the effect observed in Panel B is not due to the effect of DMSO on HR.

3.9 Bilirubin-induced HR is reversed after treatment with NAC

In order to demonstrate the role of oxidative stress behind bilirubin-induced modulation in HR, HeLa DR GFP cells were transfected with the Isce1-coding plasmid and a second plasmid encoding for renilla, which was used as control for transfection efficiency.

Cells were pre-exposed with 2 mM NAC for 1h followed by co-treatment with 140 nM Bf for 66 h. Fresh NAC was added to the culture media after every 24 h. Cells were analyzed for GFP fluorescence by FACS analysis 72 h after transfection. As shown in Figure 18, bilirubin treatment led to an increase in GFP positive cells, confirming the results

of Figure 17. However, co-treatment with NAC reduced the proportion of GFP positive cells, strongly suggesting the involvement of oxidative stress behind bilirubin induced modulation of HR.

3.10 Bilirubin does not alter cell cycle profile of HeLa DR GFP cells

Bilirubin-induced oxidative stress might affects the cell cycle of HeLa DR GFP cells. To investigate cell cycle of HeLa DR GFP cells, they were treated with bilirubin for 48h and cell cycle was analyzed.

Cell cycle analysis was performed in the HeLa DR GFP cells, with no perturbation in any phase of cell cycle by quantification of DNA content using different DNA binding dyes (Propidium Iodide) by FACS analysis. It is one of the most commonly method used to analyse the cell cycle profile of any living cell. These DNA dyes bind stoichiometrically to the DNA i.e. according to the amount of DNA present in the cells. Cells that are in S phase have more DNA than cells in G1, will take up proportionally more dye and will fluoresce more brightly until they have doubled their DNA content. The cells in G2 will be approximately twice as bright as cells in G1. As seen in Figure 19 (Panel A & B), treatment with bilirubin had no apparent effect on any phase of cell cycle, in contrast to a previous study done in SH SY 5Y cells (Deganuto et al., 2010).

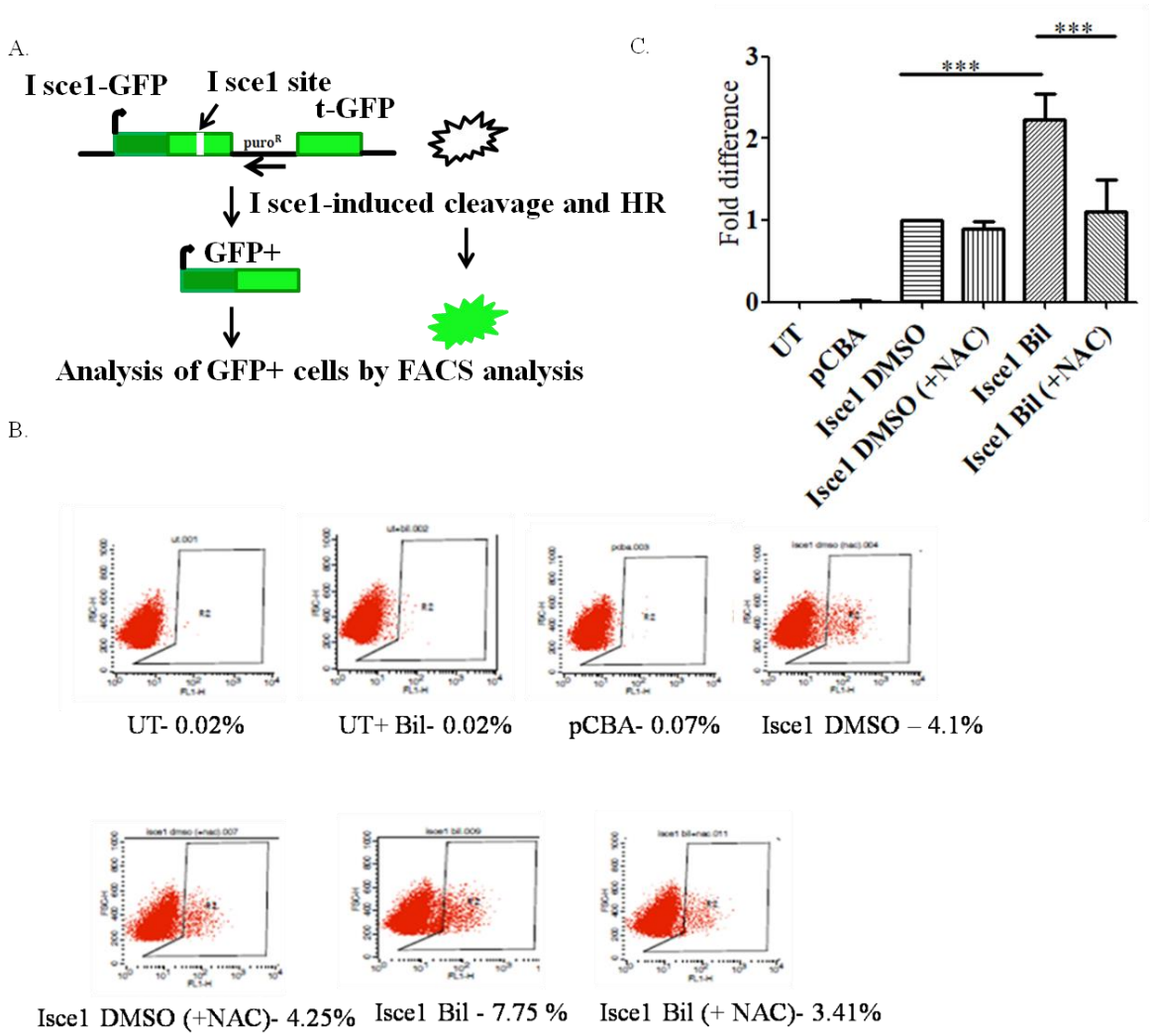

Figure 18. Effect of antioxidant (NAC) treatment on bilirubin induced Homologous recombination. HeLa DR GFP cells were co-transfected with plasmid encoding Isce1 (pCBA Isce1) and renilla (pHRG TK Renilla). After 6-7h of transfection, 140 nM Bf was added to cells. DMSO acts as solvent for bilirubin and was added as control. In the case of NAC treatment, cells were pretreated with 2mM NAC for 1h before bilirubin treatment followed by co-treatment along with bilirubin. Fresh NAC was added every 24h. Cells were analyzed for GFP expression by FACS analysis 72h post-transfection (Panel C). Panel B, represents quantification from 3 independent experiments. Data was normalised to renilla activity corresponds to same well. Each condition was done in duplicate. Values are represented as mean ± SD. *** represents $P < 0.001$. One-way ANOVA with Bonferroni's *post hoc* test was applied to perform statistical analysis.

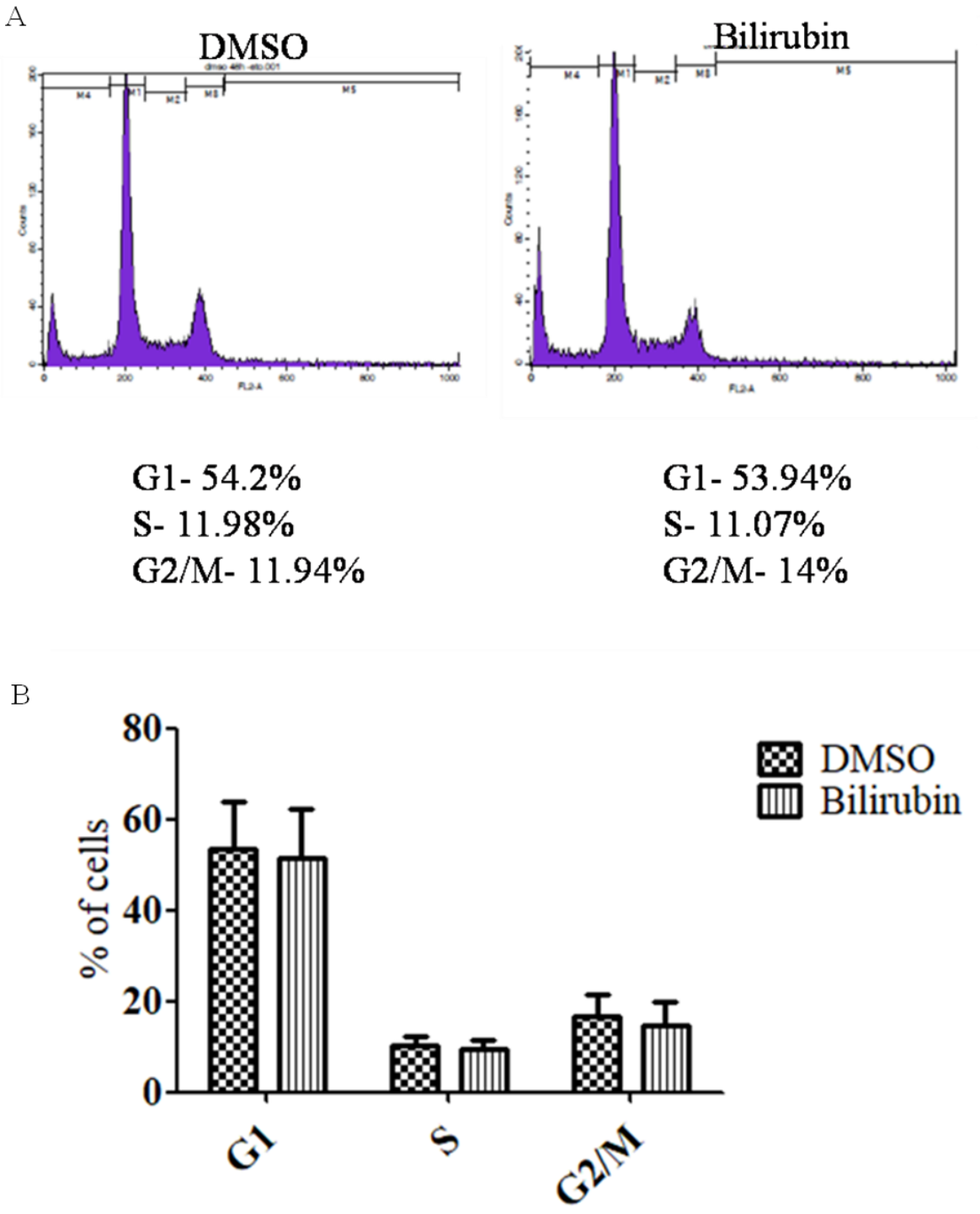

Figure 19. Cell cycle analysis of HeLa DR GFP cells after bilirubin treatment. HeLa DR GFP cells were treated with 140 nM Bf for 48h. DMSO acts as solvent for bilirubin and was added as control. Cell cycle analysis was done using Propidium Iodide (PI) staining (Panel A). Graph represents quantification from 3 independent experiments (Panel B).

3.11 Bilirubin induces DNA damage in HeLa cells

Based on the findings from our previous results, here we determined the presence of DNA damage by measuring the levels of γH2AX by Western Blot analysis in HeLa DR-GFP cells after bilirubin treatment. In these experiments, HeLa DR GFP cells were transfected with Isce1 plasmid and bilirubin was added after 6h. Cells were harvested 72h after transfection and DNA damage was assessed by assessing the levels of γH2AX.

As can be seen in Figure 20, treatment with bilirubin led to DNA damage in HeLa DR GFP cells. These results further confirmed our previous results in Figure 12-14.

3.12 Bilirubin induces DNA damage foci formation in HeLa cells

I further confirmed the bilirubin-mediated increase in DNA damage in HeLa cells by immunofluorescence analysis. During DNA damage, phosphorylated γH2AX form DNA damage foci in the nucleus which could be detected by IF with the anti phosphorylated γH2AX antibody. As can be seen in Figure 21, bilirubin treatment led to increase in the number of cells having more than ten γH2AX foci, thus, confirming our Western Blot result from Figure 20.

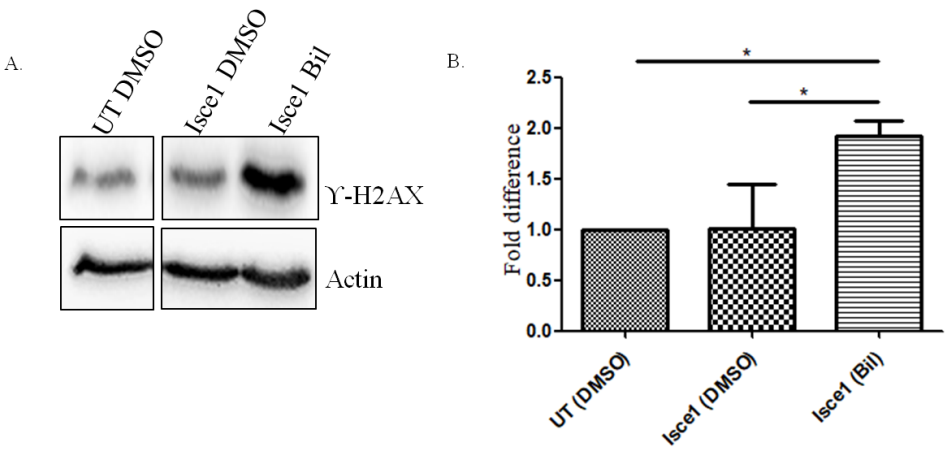

Figure 20. Bilirubin induced DNA damage in HeLa DR GFP cells. HeLa DR GFP cells were transfected with plasmid encoding Isce1 (pCBA Isce1). After 6-7h of transfection, 140 nM Bf was added to cells. DMSO acts as solvent for bilirubin and was added as control. Cells were harvested 72h after transfection and DNA damage was assessed by checking the level of γH2AX (panel A). Graph in panel B, represents quantification from three independent experiments and statistical analysis was done using One-way ANOVA with Bonferroni's *post hoc* test. Values are represented as mean ± SD. * represents $P < 0.05$.

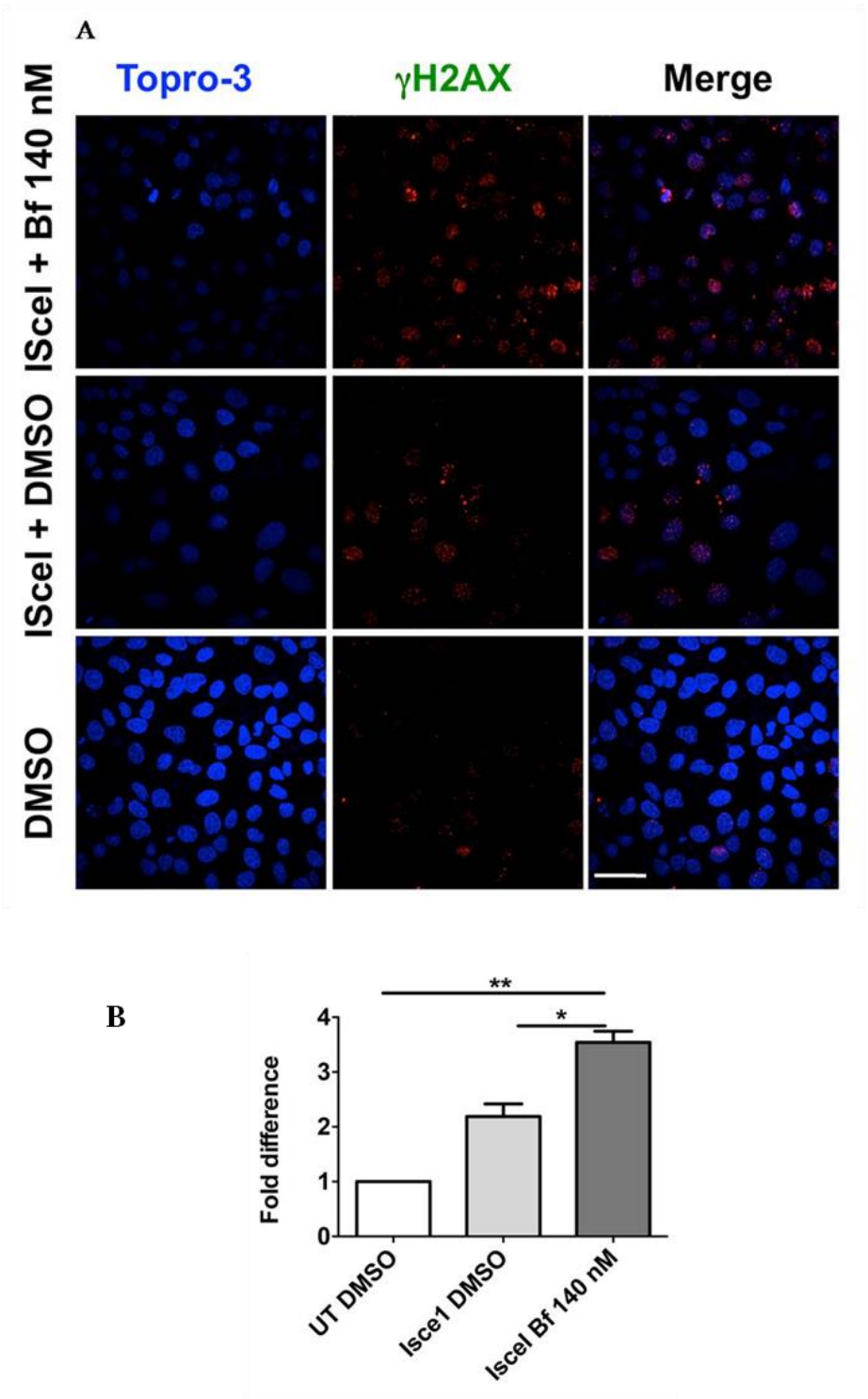

Figure 21. Bilirubin induced DNA damage foci formation in HeLa DR GFP cells. HeLa DR GFP cells cells were transfected with plasmid encoding Isce1 (pCBA Isce1). After 6-7 hours of transfection, 140 nM Bf was added to cells. DMSO acts as solvent for bilirubin and was added as control. Immunofluorescence analysis was done after 72h to check the presence of γH2AX foci. Values are represented as mean ± SD. Graph in panel B, represents quantification from two independent experiments and statistical analysis was done using One- way ANOVA with Bonferroni's *post hoc* test. * represents $P < 0.05$, ** represents $P < 0.01$. Scale bar represents 30 µM.

3.13 Bilirubin modulates the NHEJ pathway in HeLa cells

In order to determine whether bilirubin may also modulate NHEJ, which is another pathway that can get activated after DNA damage. In order to study NHEJ , I have used the pIM EJ5-GFP plasmid, as described in Section 1.9.5.

This plasmid consists of a promoterless GFP fragment preceded by a puromycin resistant cassette. A promoter is present upstream of the promycin resistance cassette. Two Isce1 site flank the puromycin cassette. Due to the absence of the promoter immediate upstream of GFP fragment, this plasmid does not express the GFP protein.

Isce1 enzyme induced breaks at the two Isce1 sites stimulates NHEJ followed by restoration of GFP expression. In this experiment, HeLa cells were co-transfected with the NHEJ substrate vector (pIM EJ5-GFP), a plasmid encoding Isce1 and a plasmid encoding renilla luciferase (pHRG-TK Renilla-transfection efficiency control). The pCBA plasmid was used as negative control.

Bilirubin was added 6-7h after transfection and cells were analysed for GFP fluorescence by FACS analysis 72h after transfection. Isce1 transfection led to significant increase in the number of GFP positive cells, suggesting the activation of NHEJ by Isce1-induced DSBs. However, addition of bilirubin significantly increased the number of GFP positive cells suggesting the activation of NHEJ by bilirubin.

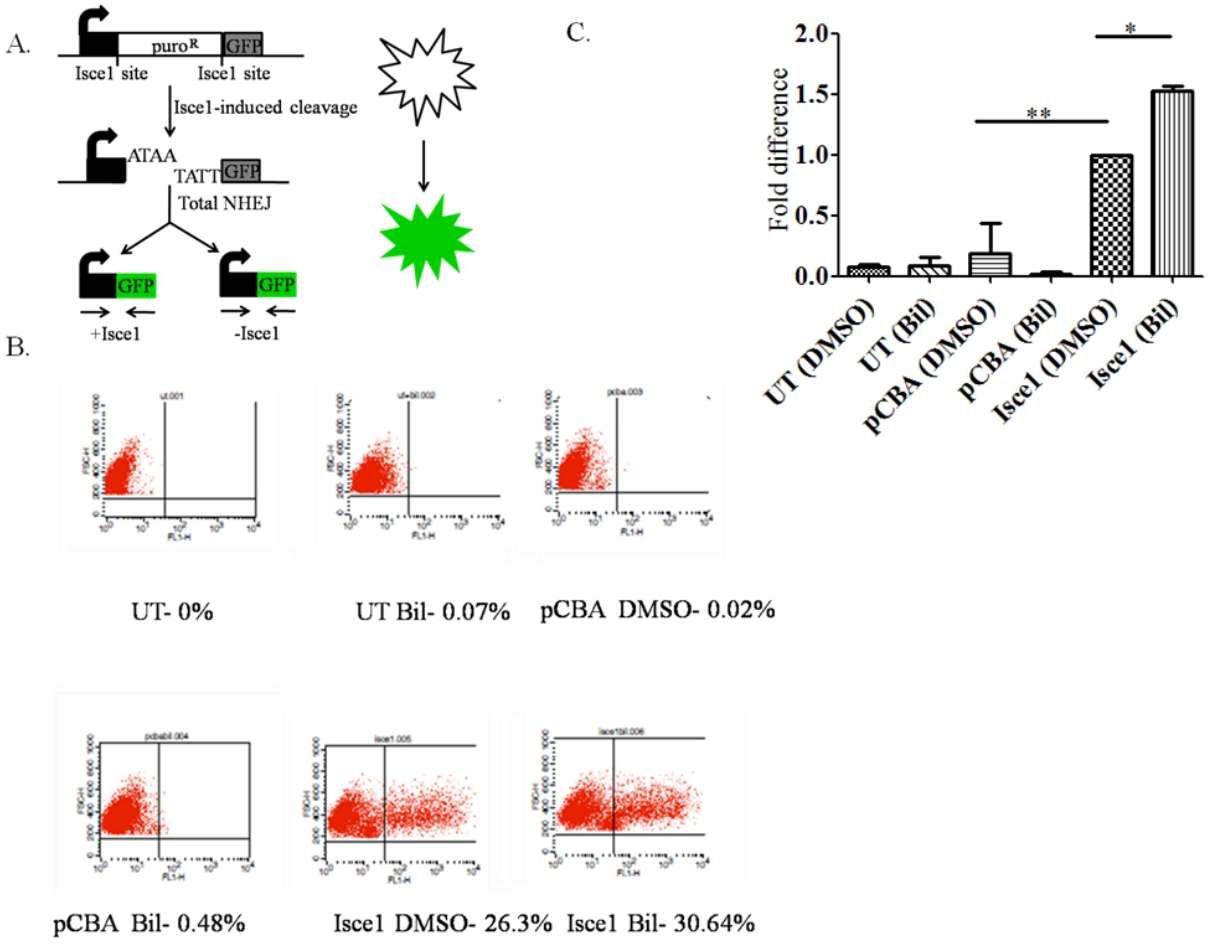

Figure 22. Effect of Bilirubin on Non-Homologous End Joining (NHEJ). HeLa cells were co-transfected with pIM EJ5-GFP plasmid, plasmid encoding Isce1 (pCBA Isce1) and renilla plasmid (pHRG TK-renilla). After 6-7h of transfection, 140 nM Bf was added to cells. DMSO acts as solvent for bilirubin and was added as control. Cells were analysed for GFP expression 72 after transfection (Panel B). Panel C, represents quantification from 2 independent experiments. Data was normalised using renilla activity corresponding to same well. Values are represented as mean ± SD.** represents P <0.01, * represents P <0.05. One-way ANOVA Bonferroni 's *post hoc* test was used to perform statistical analysis.

3.14 Effect of bilirubin on etoposide induced DNA damage.

Based on our previous results on bilirubin induced modulation of HR and NHEJ, we wanted to investigate the effect of bilirubin on DNA damage induced by a strong DNA damaging reagent, Etoposide. Etoposide acts by binding to DNA and DNA topoisomerase II, thereby inhibiting DNA re-ligation and causing DNA breaks. In this experiments, cells were pre-exposed with 140 nM of Bf for 24 h. After 24 h, bilirubin was removed and 100 µM etoposide was added for 2 h. After 2 h, etoposide was removed and fresh bilirubin was added for different time intervals ranging from 0-48 h. Cells were harvested at respective time intervals and the presence of DNA damage was investigated by checking the levels of γH2AX. As can be seen in Figure 23, addition of etoposide leads to extensive DNA damage (compare Lanes 2 and 3). The etoposide induced DNA damage repaired by cell over time up to 6 h (Lane 5). However, DNA damage started to accumulate after 24h of etoposide release, most probably due to the arrest of the cells in the G2/M phase (Schonn et al., 2010). However, when the same cells were treated with bilirubin after etoposide release, there was no accumulation of DNA damage at later time points (Compare lane 6-7 with lane 12-13). The reduced accumulation of DNA damage after bilirubin treatment may be due to completely different effect of bilirubin and etoposide on the cell cycle. Another possible reason of reduced accumulation of DNA damage in bilirubin treated cells may be due to repair of DNA breaks by bilirubin-induced modulation of DNA repair pathways. However, we did not followed this experiment further.

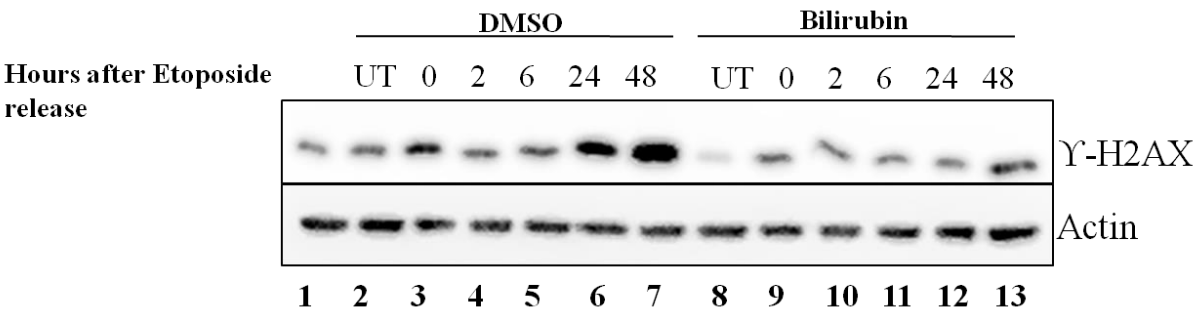

Figure 23. Effect of bilirubin on etoposide induced DNA damage. HeLa cells were treated with 140 nM Bf for 24h. After 24h, cells were treated with 100 µM etoposide for 2h. Etoposide was released from the cells and fresh bilirubin was addded for different time intervals. DNA damage analysis was done by cheking the level of γH2AX.

Section II

3.1 TALEN mediated correction of UGT1 KO mice

Our lab had generated several TALEN pairs targeting different restriction sites in the mutated Exon4 (mExon4) of the Ugt1 KO mice. This particular type of approach overcame the presence of allele specific single nucleotide polymorphisms (SNPs) and a pseudogene. Both these conditions restrict the use of surveyor assay for INDELs detection. In this work, the NcoI restriction site targeting TALEN pair was shown to be most active (Porro et al., 2014).

In this part of thesis, we decided to correct the endogenous mUgt1 locus by employing NcoI restriction site targeting TALEN. With the aim of correcting the one-base pair deletion at the exon 4 of the Ugt1 locus, mice were injected with the AAV virions expressing the TALEN pairs targeting the NcoI restriction site, along with the donor template as done before (Bedell et al., 2012). Our previous attempts to correct the endogenous loci by injecting 3 different Adeno-associated viruses (AAV) packaged with the right arm of TALEN, the left arm of TALEN and the donor template containing the corrected version of Exon 4 flanked by homology arms failed.

We decided to generate a new codon optimised AAV donor vector in order to eliminate cryptic splicing site that were present in the previous AAV donor vector construct. To generate the new pAAV donor vector, a DNA fragment containing the new codon optimised Exon 4 and flanking introns was syntesized and cloned into the pUC57 plasmid by a company. The pUC57 codon optimized Exon 4 plasmid was digested with BamH1 enzyme in order to release the insert (Figure 24B). The released Exon 4 fragment was cloned directly into the pBK plasmid without any purification step, since both plasmids have different

antibiotic resistance. Three different pBK codon optimised Exon 4 plasmids were screened by digestion with the BamH1 restriction enzyme. Only one clone out of 3 was positive for the presence of the correct insert (Figure 24C). Next, the new pAAV donor vector was generated from the old pAAV donor, after removal of Exon 4 from the pAAV old donor plasmid by BamHI digestion (Figure 24D). The plasmid vector backbone was directly ligated without purification step with codon-optimised Exon4 derived from PBK codon optimised Exon 4. After restriction digestion with NcoI, only one clone (Clone 7) gave the expected size of restriction fragments (4278, 1258, 1179, 95, and 30 bp; Figure 24E).

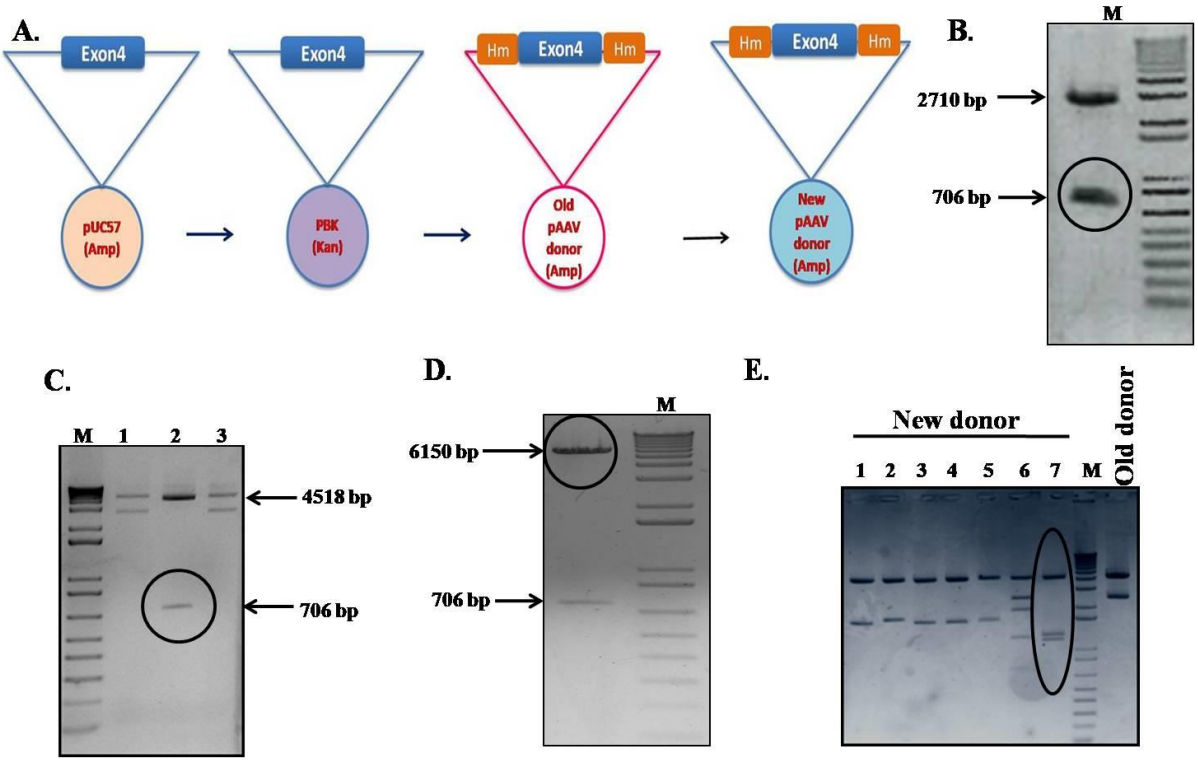

Figure 24. Sub-cloning of new codon optimised Exon 4 to generate the AAV donor vector. A). Strategy showing sub-cloning of codon-optimised Exon4 into the AAV vector. B). Restriction digestion of pUC57 containing the codon-optimised Exon4 with BamHI, for cloning the codon-optimised Exon4 into the BamHI-digested PBK vector.C). Restriction digestion of different clones of PBK-Exon4 with BamHI. D). Restriction digestion of old pAAV donor with BamH1 enzyme in order to replace the old Exon4 with codon optimised Exon4 to generate the new donor. E). Restriction digestion of different clones of pAAV new donor with NcoI.

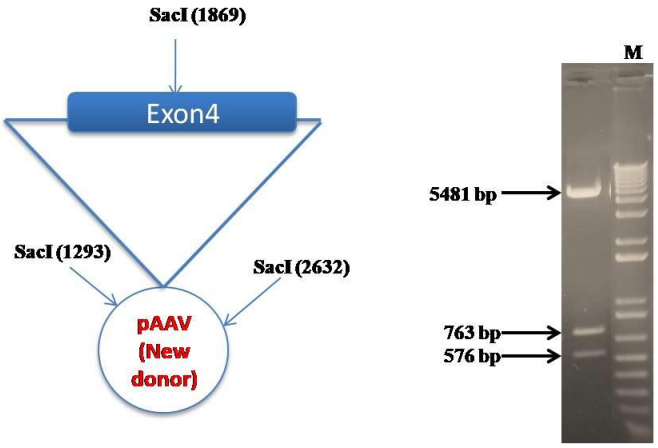

Figure 25. Orientation check of new AAV vector. The new pAAV donor vector clone 7 was digested with SacI restriction enzymes to give different size of restriction fragments.

Next, the sense orientation of pAAV new donor vector clone 7 was confirmed by SacI digestion (Figure 25). The pAAV new donor vector has three SacI restriction sites present at different locations in the plasmid. The digestion of pAAV new donor plasmid with sense orientation should give 3 different restriction fragments (5481, 763, 576 bp). This particular restriction digestion confirmed the sense-orientation of clone 7.

We also wanted to check the activity of the NcoI targeting TALEN pairs *in vivo* by injecting them into wild type mice. Genomic DNA was isolated from the liver of injected mice and genomic PCR was done using specific primers as shown in Figure 4A-B. Genomic PCR generated a PCR product of 1020 bp.

Genomic DNA from Ugt1 KO animals were used as a control to check the specificity of primers pairs and to exclude the amplification of the Ugt1 psedudogene, as discovered in our previous study (Porro et al., 2014). This PCR analysis showed that the primer pairs used in this PCR analysis are amplifying only the Ugt1 locus, and not the pseudogene (Figure 26C). The genomic PCR product was subjected to NcoI restriction digestion (Figure 26D) in order to detect fragments resistant to NcoI digestion, indicating NHEJ repair and mutation of the NcoI site. However, after repeated analysis of PCR analysis and restriction digestion, no NcoI resistant bands were seen. These results were non-conclusive. However, we do not have any information regarding expression of TALEN pairs *in vivo.*

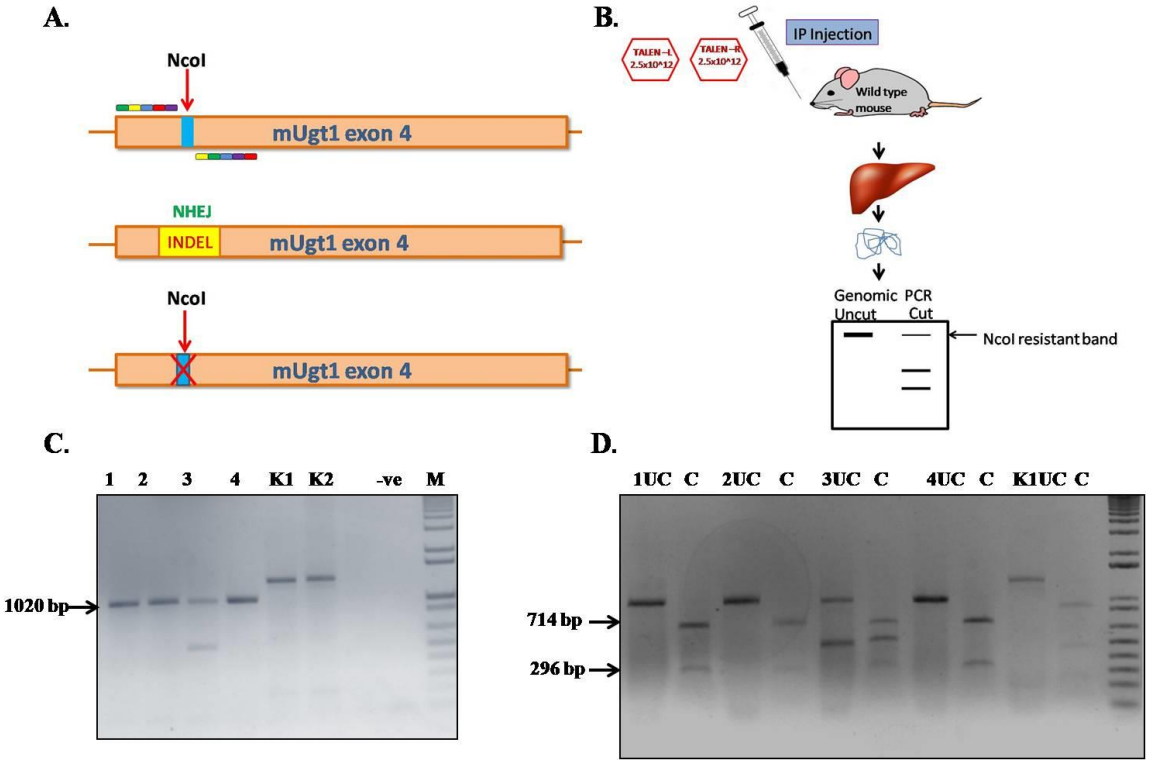

Figure 26. TALEN activity analysis by genomic PCR and restriction digestion. A)Schematic diagram showing NcoI restriction site in Exon4 of Ugt1 locus. The TALEN binding site flanking the NcoI restriction site is also shown. B). Schematic diagram showing the strategy used to check TALEN activity. C). Genomic PCR analysis showing amplification of Ugt1 Exon4 locus. The PCR product was separated in 1% agarose gel D). The genomic PCR product was then digested with NcoI restriction enzyme and the resulting product was separated in 1% agarose gel.

Next, we decided to modify the strategy and to use the *Staphylococcus aureus* CRISPR/Cas9 platform. This approach requires the administration of two AAV vectors (instead of the three AAVs required with the TALEN strategy), one containing the SaCas9 and the sgRNA, and the other one with the donor DNA, which should result in higher efficiency. We designed 4 difference gRNA targeting the Exon 4 of the Ugt1 gene locus and cloned them into the *S aureus* pX601 Cas9 vector. The clones positive for the presence of each gRNA were confirmed by sequencing analysis. In order to check the activity of each gRNA, a single stranded annealing (SSA) reporter was utilized. This reporter consists of luciferase gene interrupted by the Exon 4 derived from the Ugt1 gene locus. The Exon4 is flanked by direct repeated regions obtained from the luciferase gene. Induction of DSB at Exon 4 using site-specific nuclease stimulates recombination between the direct repeats, restoring luciferase activity, consequently loosing the Exon 4 (Figure 27A). In order to check the activity of different gRNAs, Hep3B cells were co-transfected with the SSA reporter vector, different concentrations of gRNAs and pHRG-Tk renilla plasmid. The cells were harvested 48 h after transfection and luciferase activity was measured using a luminometer. There was a dose-response increase in activity of all the gRNAs. Interstingly, the NcoI-TALEN pair was always more active than all the 4 gRNAs (Figure 27).

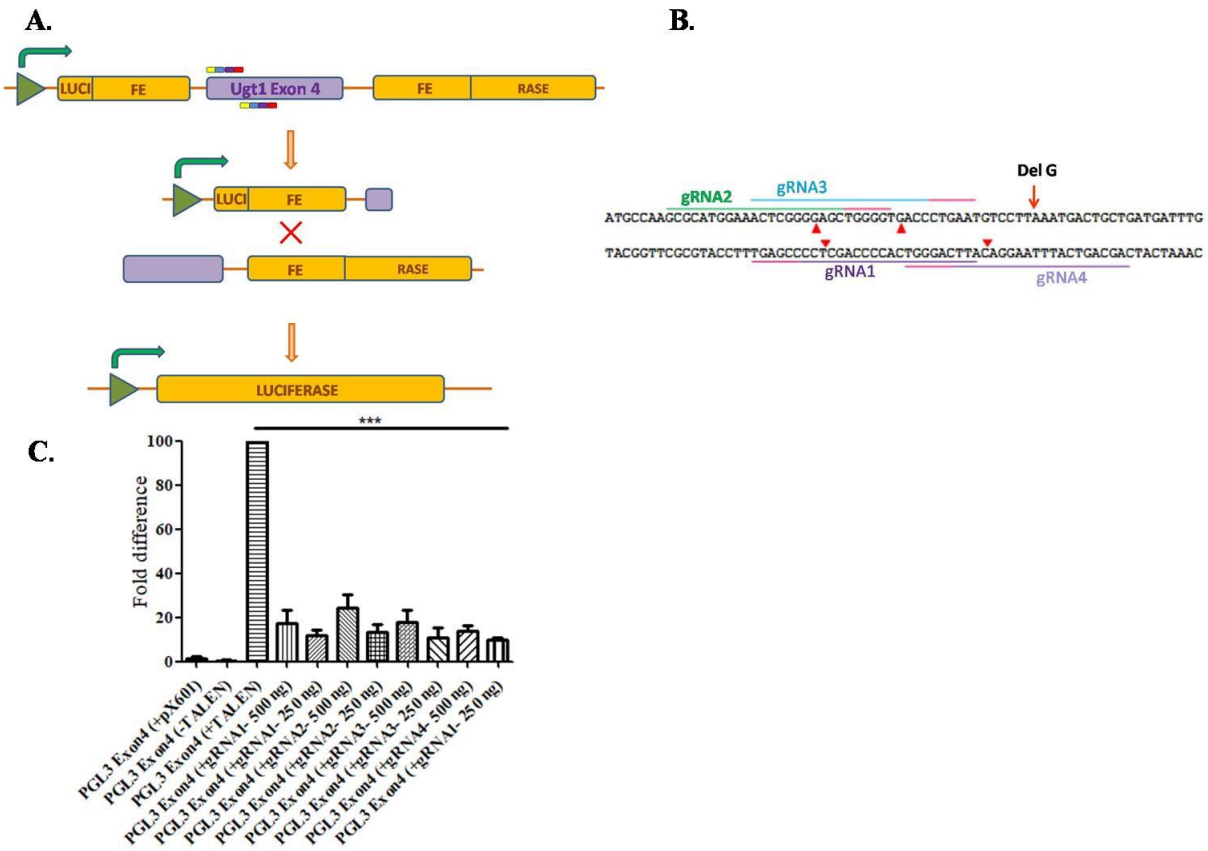

Figure 27. gRNA activity analysis in Hep3B cell line using a single stranded annealing (SSA) vector. A) Schematic diagram showing SSA vector used to check the activity of site-specific nucleases. B) This figure is showing the location of 4 different gRNAs targeting mUgt1 Exon4. C) The gRNA activity analysis after co-transfecting Hep3B cells with SSA vector, different concentrations of gRNAs and pHRG-Tk renilla vector. Data was normalised for transfection efficiency using renilla activity corresponds to same well. NcoI targeting TALEN pairs were used as positive control. ANOVA test with *Bonferroni's* correction was done to perform statistical analysis. *** represents $P<0.001$.

Next, activity of each NcoI targeted TALEN pair was determined using the SSA reporter. Hep3B cells were co-transfected with the SSA reporter vector, different concentrations of NcoI targeting TALEN pair and pHRG-Tk renilla plasmid. The cells were harvested 48h after transfection and luciferase activity was measured using a luminometer. There was a dose-response increase in activity of TALEN pairs (Figure 28).

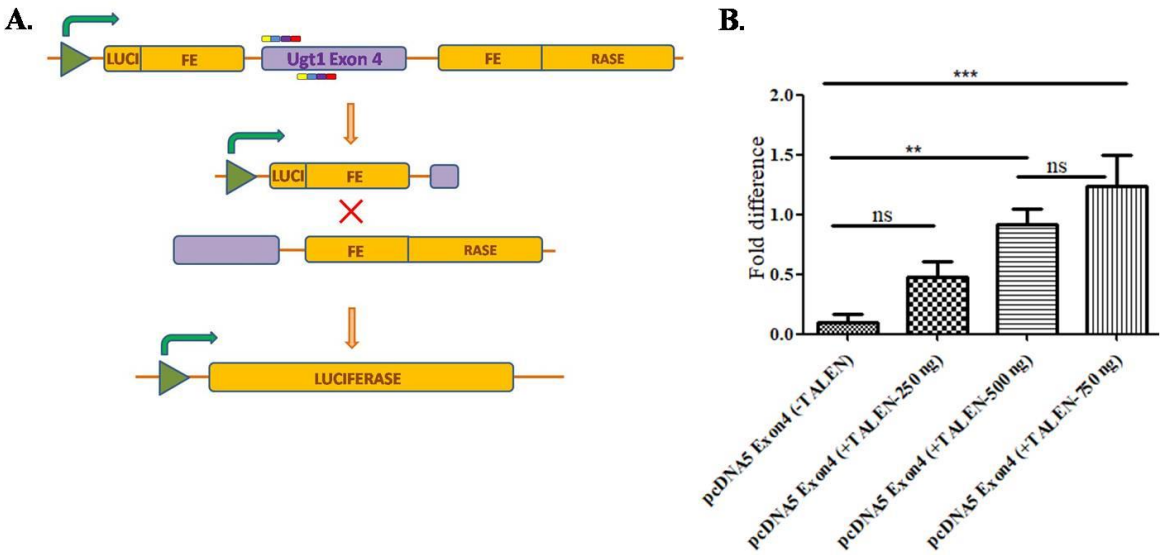

Figure 28. NcoI TALEN activity analysis in Hep3B cell line using a single stranded annealing (SSA) vector. A) Schematic diagram showing SSA vector used to check the activity of TALENs. B) This figure is showing the activity of TALENs using SSA vector after transecting different amount of TALEN pairs. Data was normalised for transfection efficiency using renilla activity corresponds to same well. ANOVA test with *Bonferroni's* correction was done to perform statistical analysis. *** represents $P<0.001$, ** represents $P<0.01$. ns represents non-significant.

3.2 Stable clone generation for miRNA screening

Different endonucleases such as TALEN and CRISPR/Cas9 system have been used to increase the frequency of HR. Although, endonuclease technology significantly increases HR, novel techniques are required to further increase the HR rate when used in combination with different endonucleases. We decided to perform a miRNA screening to find miRNA modulating HR. We planned to generate a stable Flp-IN Hek293 SSA reporter cell line. Two different types of stable clones were planned to be generated: the first one containing pcDNA5 Luc construct integrated, and the second one with the pcDNA5LuciFeExon4Ferase construct integrated. Both constructs were initially cloned in a pGL3 vector. For the purpose of Flp-IN stable clone generation, both the constructs were sub-cloned into the pcDNA5/FRT vector (Figure 29 & 30).

3.2.1 Subcloning of Luciferase and LuciFeExon4Ferase into pcDNA5/FRT plasmid

First, I sub-cloned the luciferase construct from the pGL3 luciferase vector into the pcDNA5/FRT plasmid, as shown in Figure 29A. The pGL3 Luciferase vector was digested with HindIII+ XbaI to release the 1651 bp fragment (Figure 29B). This fragment was then directly cloned into the pBK vector without purification step. The presence of the luciferase insert in the pBK plasmid was confirmed by HindIII+XbaI digestion (Figure 29C). Overall, 6 different plasmids were positive for the presence of luciferase. The luciferase insert obtained from the positive clone 2 was then ligated into the pcDNA5/FRT plasmid. The presence of the Luciferase gene in the pcDNA5/FRT plasmid was confirmed by HindIII+ PstI and HindIII+ SpeI restriction digestion.

Overall, 3 different plasmid were positive from all the screened plasmids (Figure 29D).

Next, I sub-cloned the luciFeExon4Ferase fragment using the strategy shown in Figure 30A. The pGL3 luciFeExon4Ferase was designed previously in our lab (Porro et al., 2014). The pGL3 luciFeExon4Ferase vector was digested with HindIII+ XbaI to release the 2967 bp fragment (Figure 30B). This fragment was directly cloned into the pBK vector without purification step. The presence of luciFeExon4Ferase insert in the pBK plasmid was confirmed by HindIII+XbaI digestion (Figure 30C).

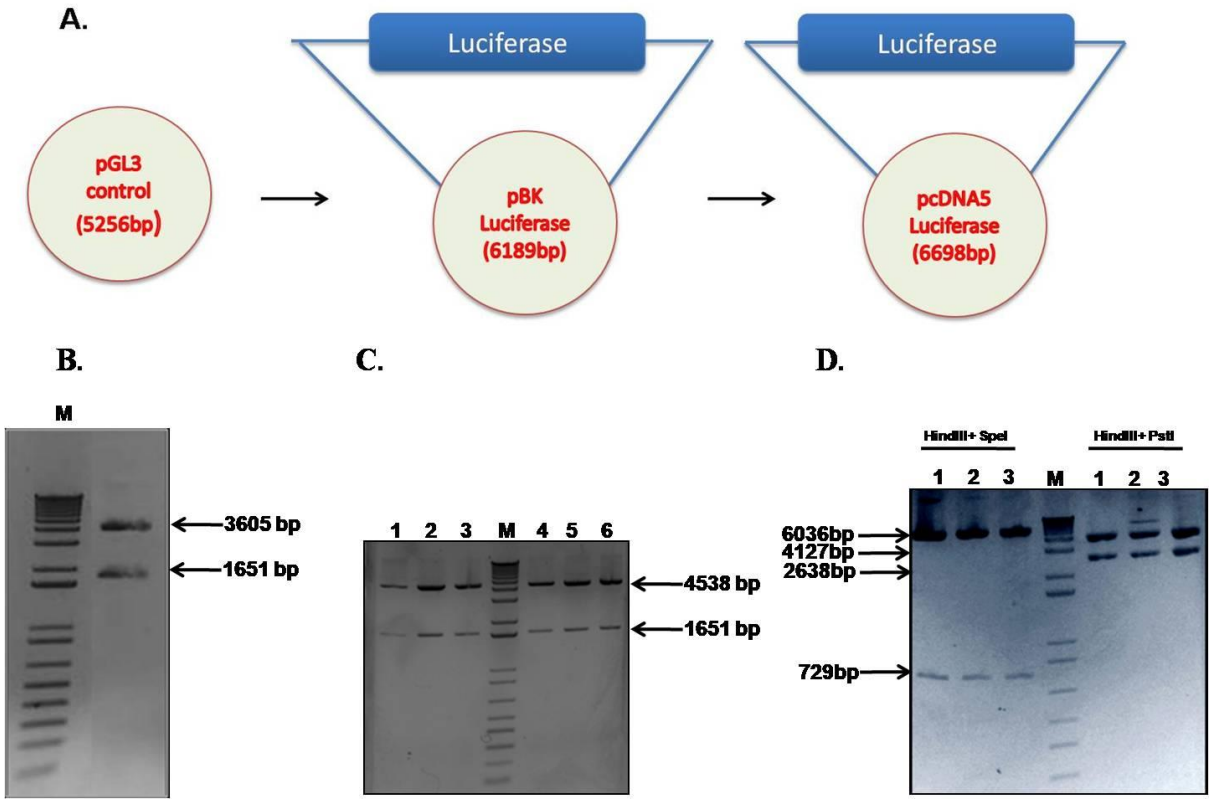

Figure 29. Sub-cloning of luciferase construct into pcDNA5/FRT plasmid. A). Strategy showing sub-cloning of the luciferase construct from pGL3 luciferase vector into the pcDNA5/FRT plasmid. B). Restriction digestion of pGL3 control vector. C). Restriction digestion of isolated clones to confirm the presence of the luciferase insert in the PBK plasmid. D). Restriction digestion of isolated clones to confirm the presence of luciferase insert in the pcDNA5/FRT plasmid.

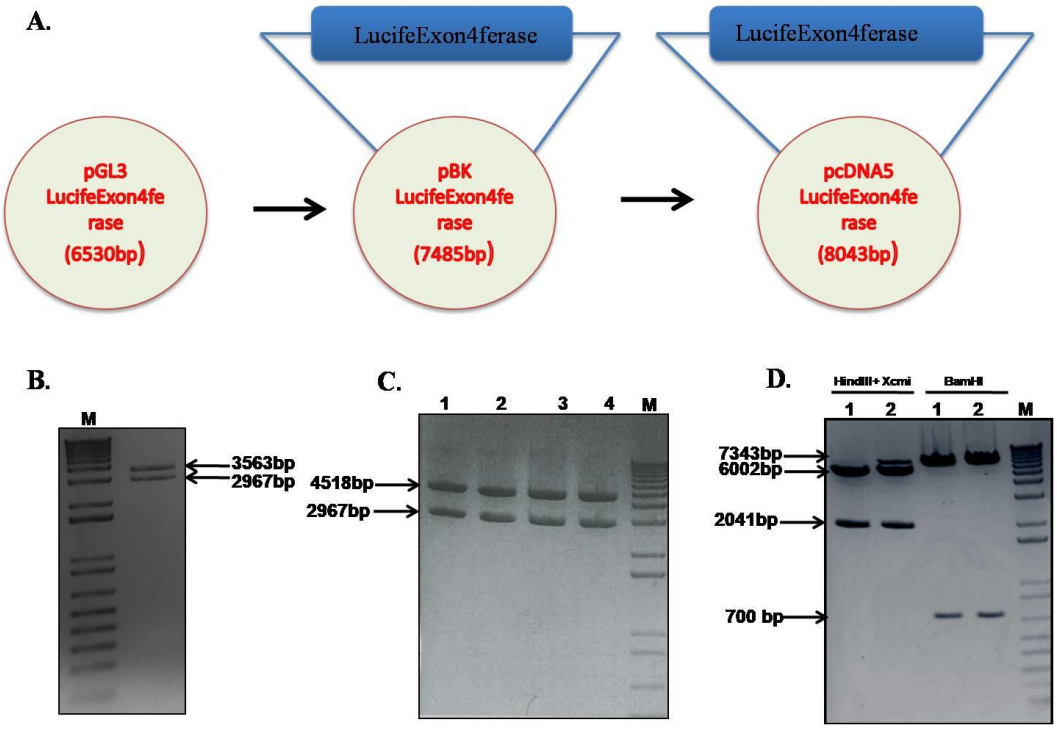

Figure 30. Sub-cloning of luciFeExon4Ferase construct into pcDNA5/FRT plasmid. A). Strategy showing sub-cloning of construct from pGL3 luciFeExon4Ferase vector into the pcDNA5/FRT plasmid. B). Restriction digestion of pGL3 luciFeExon4Ferasevector. C). Restriction digestion of isolated clones to confirm the presence of the LuciFeExon4Ferase fragment in the PBK plasmid. D). Restriction digestion of isolated clones to confirm the presence of the LuciFeExon4Ferase insert in the pcDNA5/FRT plasmid.

Overall, 4 different plasmids were positive for the presence of the luciFeExon4Ferase fragment. The luciFeExon4Ferase construct obtained from positive clone 2 was then cloned into the pcDNA5/FRT plasmid. The presence of luciFeExon4Ferase gene in the pcDNA5/FRT plasmid was confirmed by HindIII+ XcmI and BamHI restriction digestion. Overall, 2 different plasmids were positive from all the screened plasmid (Figure 30D).

3.2.2 Stable clone generation

As discussed above, we planned to generate Hek293 Flp-IN stable cell line for miRNA screening. However, we realised that Hek293 cells could not be used for miRNA screening because they get detached very easily from the wells during the automatic washing of the cells performed during the screening, by high-throughput screening facility. So, we decided to make the required stable clones in the Hep3B liver cell line, which do not detach during harsh washings. Since the Flp-IN system is not available in any liver cell line, we decided to generate the cell lines by transfection of the plasmids followed by selection, a procedure that is based on the random integration of the plasmids in the Hep3B genome.

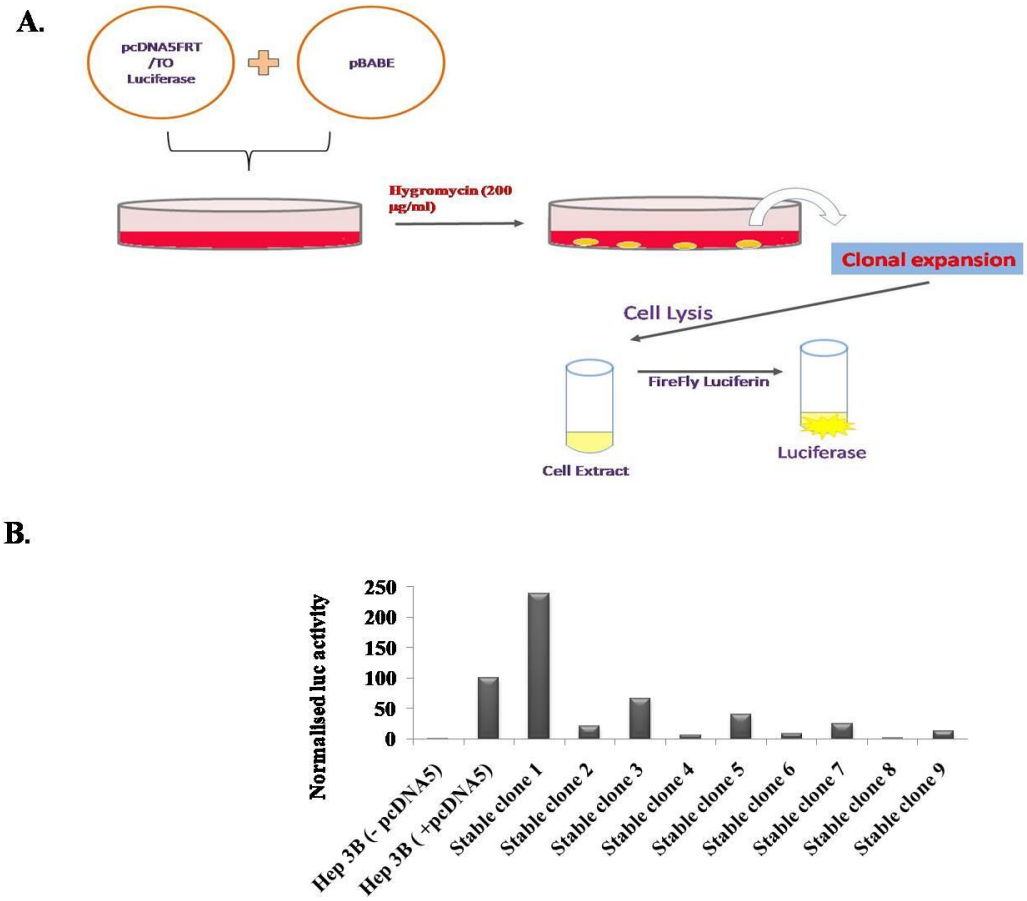

Figure 31. Hep3B luciferase stable clone generation. A). Strategy showing generation of Hep3B luciferase stable clone. B). Graph showing the normalised luciferase activity in different stable clones obtained. Hep3B cells transfected with pcDNA5 Exon4 plasmid acts as positive control in this experiment.

In order to generate Hep3B luciferase stable clones, cells were co-transfected with the pcDNA5Luciferase and pBABE plasmids. The pBABE plasmid was co-transfected in order to select the stable clones with the antibiotic geneticin, since pcDNA5/FRT plasmid does not contain any antibiotics resistance gene for selection.After selection for 10 days, different colonies were obtained, expanded and luciferase activity was checked in the different clones. From 9 stable clones, clone 1 has the highest luciferase activity followed by clone 3, clone 5 and clone 7 (Figure 31).

Next, we generated Hep3B luciFeExon4Ferase stable clones. To generate luciFeExon4Ferase stable clones, cells were co-transfected with pcDNA5 lucFeExon4Ferase and pBABE plasmid. After selection for 10 days, different colonies obtained were expanded and luciferase activity was checked in different clones after transfecting them with NcoI restriction site targeting TALEN pair. Among 11 clones obtained, clone 10 expressed the highest luciferase activity followed by clone 5 and clone 11. Although, clone 10 expresses the highest induction of luciferase activity after TALEN transfection, the presence of basal luciferase activity in untransfected cells may represent the intrachromosomal recombination due to integration of plasmid at several different locations in the genome (Figure 32).

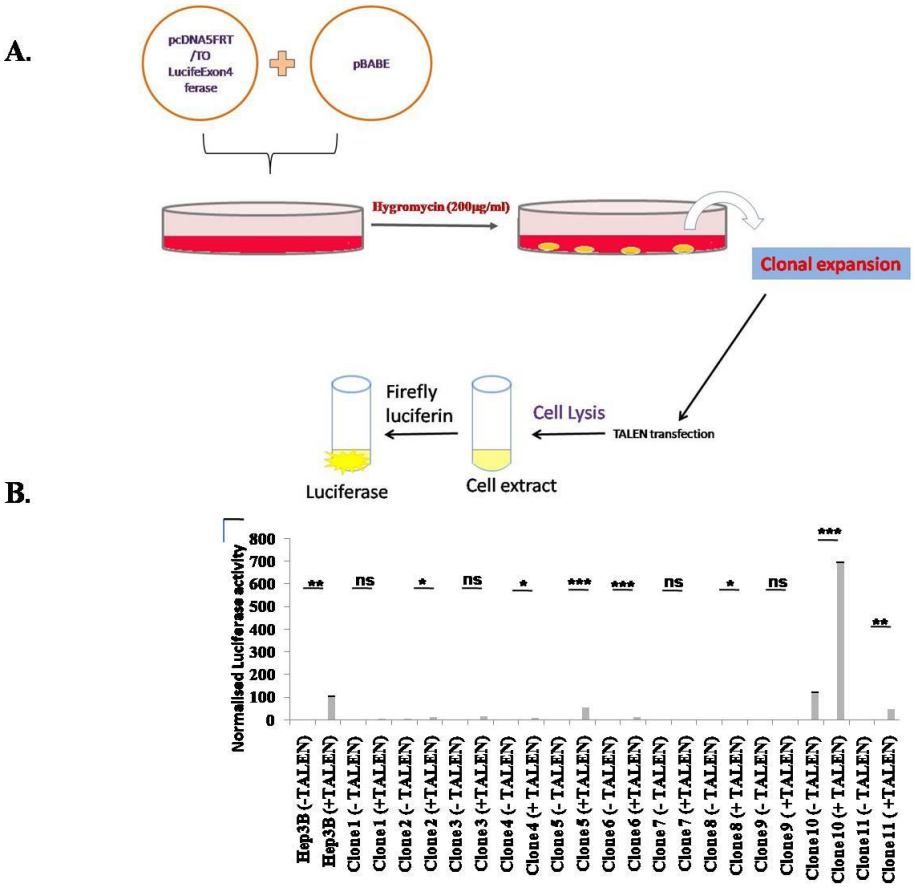

Figure 32. Hep3B lucFeExon4Ferase stable clone generation. A). Strategy showing generation of Hep3B lucFeExon4Ferase stable clone. B). Graph showing the normalised luciferase activity in different stable clones obtained after transfection with NcoI restriction site targeting TALEN pair and pHRG TK renilla plasmid. Hep3B cells co-transfected with pcDNA5 Exon4 plasmid, NcoI restriction site targeting TALEN pair and pHRG TK renilla plasmid acts as positive control in this experiment. Data was normalised to renilla activity corresponds to the same well. Student *t-test*was done to perform statistical analysis. * represents $P<0.05$, ** represents $P<0.01$, *** represents $P<0.001$, ns represents non-significant.

3.2.3 Cloning of luciferase and luciFeExon4Ferase in pcDNA3

The absence of mammalian antibiotic resistance in the pcDNA5/FRT plasmid forced us to clone the luciferase and luciFeExon4Ferase in the pcDNA3 vector, which contains the geneticin resistance gene.

In order to clone the luciferase construct in the pcDNA3 plasmid, the pBK luciferase plasmid from Figure 7 was utilized. The pBK luciferase construct was digested with HindIII+ XbaI to release the luciferase gene. The luciferase gene was then directly ligated into HindIII+XbaI digested pcDNA3 vector without purification step. The presence of the luciferase construct in pcDNA3 plasmid was confirmed by 3 different types of restriction digestions as shown in Figure 33.

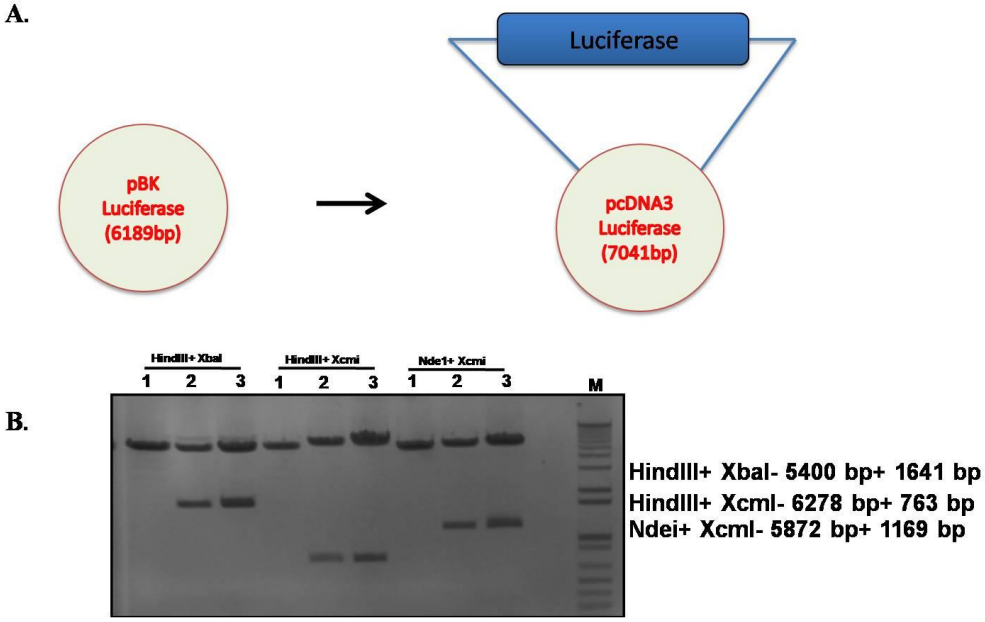

Figure 33. Sub-cloning of luciferase construct into pcDNA3. A). Strategy showing sub-clonng of luciferase construct from PBK luciferase contruct into pcDNA3 plasmid. B). Restriction digestion of final pcDNA3 luciferase plasmid with different restriction enzymes.

In order to clone the LuciFeExon4Ferase construct in the pcDNA3 plasmid, the pBK LuciFeExon4Ferase plasmid from Figure 8 was utilized. The pBK LuciFeExon4Ferase construct was digested with HindIII+ XbaI to release luciferase gene. The LuciFeExon4Ferase gene was than directly ligated into HindIII+XbaI digested pcDNA3 vector without purification step. The presence of the LuciFeExon4Ferase construct in pcDNA3 plasmid was confirmed by 3 different type of restriction digestion as shown in Figure 34.

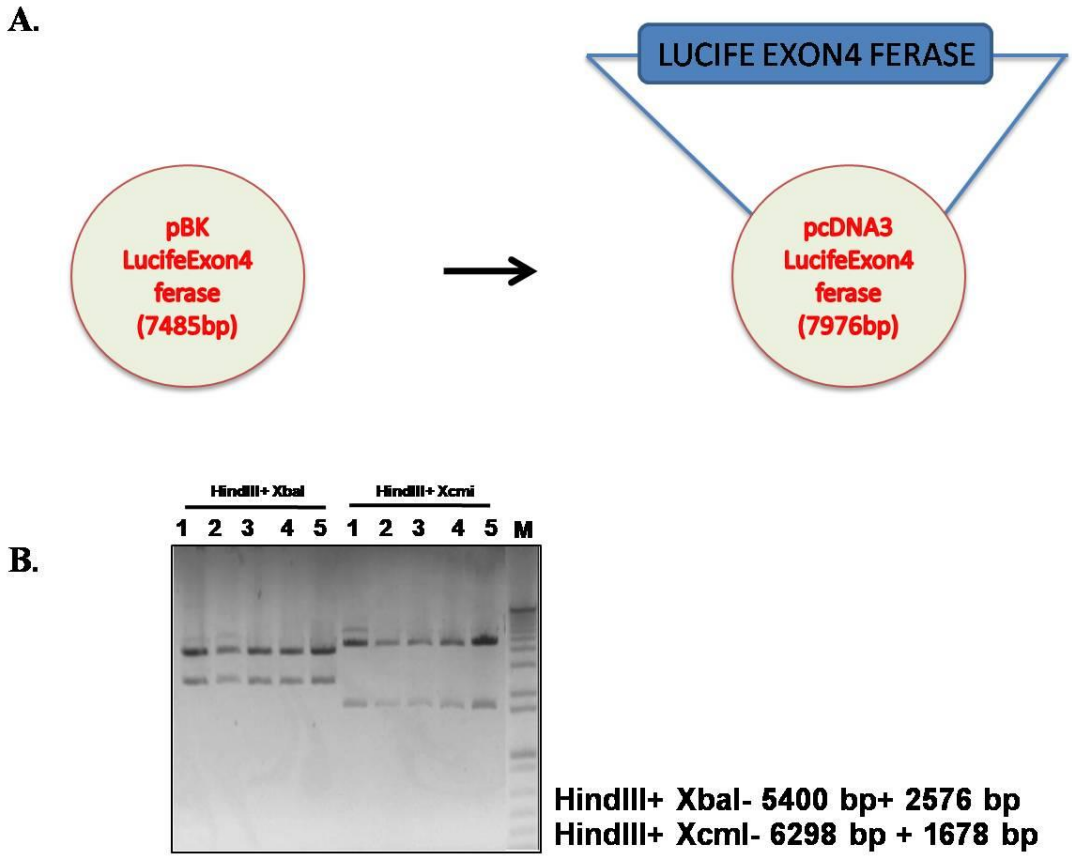

Figure 34. Sub-cloning of luciFeExon4Ferase construct into pcDNA3. A). Strategy showing sub-cloning of luciFeExon4Ferase construct from PBK luciFeExon4Ferase construct into pcDNA3 plasmid. B). Restriction digestion of final pcDNA3 luciFeExon4Ferase with different restriction enzymes.

DISCUSSION

Section I

Stocker and coworkers showed the beneficial and antioxidant properties of bilirubin at mildly elevated concentrations (Stocker et al., 1987). Conversely, elevated concentrations of bilirubin are responsible for the generation of oxidative stress. Increased oxidative stress leads to elevated synthesis of glutathione by cells (Giraudi et al., 2011). This study also proved that oxidative stress is a major determinant of bilirubin-induced neurotoxicity. Similarly, several *in vitro* and *in vivo* studies, including ours, have shown, induction of oxidative stress by bilirubin (Bortolussi et al., 2015; Brito et al., 2004; Cesaratto et al., 2007; Daood et al., 2012; Deganuto et al., 2010; Oakes and Bend, 2005; Seubert et al., 2002).

The present thesis work shows the effect of bilirubin on DNA damage and repair pathways, using two different cell line models (SH SY 5Y and HeLa). This work also showed the direct involvement of oxidative stress in DNA damage, and activation of HR and NHEJ.

4.1 Bilirubin induced DNA damage

In this study, bilirubin cytotoxicity was investigated in the neuroblastoma SH SY 5Y cell line after treatment with a clinically relevant Bf concentration, as reported in neonates with bilirubin encephalopathy (Ostrow et al., 2003). *In vivo* studies in Ugt1 KO mice showed immature Purkinje cells being the most severely affected in the cerebellum due to bilirubin toxicity (Bortolussi et al., 2014a). SH SY 5Y cells were used in this study because of their immature neuronal characteristics (ability to proliferate, expression of immature neuronal markers). Bilirubin treatment decreased cellular viability as measured by the MTT assay. The decrease in viability of cells was accompanied by the increase in the level of the double-stranded break marker, ϒ-H2AX.

NAC co-treatment results strongly demonstrated the role of oxidative stress in the bilirubin induced DNA damage.

To the best of our knowledge, bilirubin induced DNA damage has never been studied in patients with Crigler-Najjar syndrome. Previous studies performed in peripheral blood cells derived from babies with neonatal hyperbilirubinemia demonstrated the presence of DNA damage after intensive phototherapy treatment. However, the study results were controversial when DNA damage was compared between untreated (or pre-phototherapy) jaundiced babies with control normal groups (Karadag et al., 2010; Karakukcu et al., 2009 ; Ramy et al., 2016; Tatli et al., 2008; Yahia et al., 2015). Additionally, all these studies were done in peripheral blood cells that may have different sensitivity to bilirubin-induced toxicity when compared with neuronal cells.

Work done by other labs showed increased level of 8-OH G level in neonates with lower bilirubin level (Basu et al., 2014). Peripheral blood mononuclear cells (PBMCs) treated with bilirubin showed higher rate of DNA strand breakage (Khan and Poduval, 2012). MTT assay confirmed the bilirubin induced toxicity in SH SY 5Y cells (Qaisiya et al., 2017a; Qaisiya et al., 2014). Prolonged exposure (more than 4h) activates some type of protective mechanism in SH SY 5Y cells (Tiribelli's lab, unpublished results). We showed a time dependent induction of DNA damage after bilirubin treatment. DNA damage starts 24h post-bilirubin treatment that further accumulates over time. Previous study also showed accumulation of ϒ-H2AX foci after 24h of bilirubin treatment. BrDU labelling and pulse-chase experiments showed slower progression of cells through the S-phase post-bilirubin treatment (Deganuto et al., 2010). Our NAC co-treatment results proved the direct role of oxidative stress in bilirubin induced DNA damage. Bilirubin exposure leads to

higher levels of the marker of oxidative DNA damage 8-OH G and abasic sites in SH SY 5Y cells (Deganuto et al., 2010). The co-treatment of SH SY 5Y cells with bilirubin and NAC increases the viability, suggesting oxidative stress as an important factor for bilirubin toxicity (Deganuto et al., 2010)

The bilirubin-induced DNA damage had no effect on the levels of P53. These results are in contrast to studies performed in colon cancer cells (Ollinger et al., 2007). Colon cancer cells up-regulate P53 levels after treatment with bilirubin. Cell cycle analysis showed the accumulation of cells in G1-phase of the cell cycle. However, DNA damage was never checked in that study (Ollinger et al., 2007). The differential levels of P53 regulation in two studies may be due to the use of cell lines with different origins (SH SY 5Y vs Colon cancer cell line). However, we cannot rule out the possible activation of P53 independent sub-pathways. Other sub-pathways of DNA damage response were not addressed in this study. Bilirubin acts as a pro-oxidant at high Bf levels and kills neuronal cells. Neuronal cells are extremely susceptible to oxidative stress due to low GSH storage (Brito et al., 2008b). Reduced expression of antioxidant enzymes like superoxide dismutase, catalase, and glutathione peroxidase, compared to other tissues, accompanied by higher levels of unsaturated fatty acids that are prime target of lipid peroxidation, make neuronal cells extremely susceptible to oxidative stress (Aoyama et al., 2008). *In vivo* studies in hyperbilirubinemic mice showed cerebellum as the most severely affected part of the brain due to its post-natal development (Bortolussi et al., 2014a; Conlee and Shapiro, 1997). Studies from our group also showed the impairment of anti-oxidant defenses in the cerebellum of mutant mice (Bortolussi et al., 2015), strongly supporting the hypothesis of increased oxidative stress in those animals, consequent to hyperbilirubinemia. However, further

studies are required to determine the extent of DNA damage in the cerebellum of those animals.

The work presented in this thesis showed the potential DNA damaging activity of bilirubin. These results are particularly important for persons with hyperbilirubinemia conditions, which may put them at risk of mutagenesis and tumor development. Although no significant DNA damage was evident in Gilbert patients and Gunn rats (Wallner et al., 2013), we lack information from patients with cronically higher plasma bilirubin levels, such as Crigler-Najjar type I and type II patients. In many cases, these patients undergo liver transplantation early during life, restricting the availability of information regarding potential carcinogenesis due to uncontrolled hyperbilirubinemia for a longer period of time.

The analysis of potential carcinogenesis is also limited by the life-long immunosuppression to avoid organ rejection, which increases the risk of cancer development. (Haagsma et al., 2001; Herrero et al., 2005). Our results may prove to be important for CNS patients who have not undergone liver transplantation during early age. These patients may get exposed to chronic high level of bilirubin, with sporadic spikes of very high levels of plasma bilirubin, due to decreased efficiency of phototherapy during growth and puberty (Sellier et al., 2012), putting them at risk of DNA damage. In fact, the accumulation of DNA lesions in other scenarios contributes to neuronal cell death (Chan, 2001), a phenomenon observed in specific regions of the brain both in hyperbilirubinemic patients and rodent animal models (Bortolussi et al., 2014a; Bortolussi et al., 2015; Shapiro et al., 2006).

4.2 Effect of bilirubin on DNA repair pathway

In this study, we have shown for the first time the effect of bilirubin on HR and NHEJ. We started these experiments based on our previous observations that TALEN that were very efficient in cell lines, did not apparently function *in vivo*, in the liver of hyperbilirubinemic Ugt1 knockout animals. So, eventually, based on these observations, we investigated the effects of bilirubin on HR and NHEJ pathways. We hypothesized the bilirubin may acts as negative regulator of DNA repair in Ugt1 KO mice due to several reasons, such as, probable effect on cell cycle, reduction in expression of some of the DNA repair proteins and preventing the loading of repair proteins onto the damaged DNA template.

Bilirubin-induced toxicity in HeLa DR GFP cells was confirmed by the MTT assay. Previous studies also showed the toxicity of bilirubin in HeLa cells (Cesaratto et al., 2007). As discussed before, exposure to bilirubin leads to oxidative stress in human cells. Here, in contrary to our expectations, we showed dose-and time-dependent increase in HR by bilirubin. Treatment with the antioxidant NAC demonstrates the involvement of oxidative stress in the modulation of HR. Treatment with bilirubin also modulated the NHEJ pathway. DNA damage analysis in HeLa cells showed the induction of DNA damage after treatment with bilirubin. Investigation of the effect of bilirubin on cell cycle showed no effect on any phase of the cell cycle.

The work presented in this thesis showed dose-dependent induction of HR by bilirubin, with maximum increase (1.8-2 folds) at pathologically relevant Bf concentration, i.e., 140 nM Bf. The modulation of HR by NAC proved the role of oxidative stress in HR. Studies in yeast, *Saccharomycess cerevisiae* showed important role of HR in recovery of

cells from oxidative DNA damage (Hayashi and Umezu, 2017; Yi et al., 2016). Similarly, N, N- dimethylformamide-induced oxidative stress leads to oxidative DNA damage and induction of HR in human cells (Wang et al., 2016). Another study showed the importance of HR in the rescue of stalled replication forks due to endogenous oxidative stress (Wilhelm et al., 2016). DNA damage analysis showed induction of DNA damage by bilirubin in HeLa cells, as seen in SH SY 5Y cell in this work and another study (Deganuto et al., 2010). However, cell cycle analysis of HeLa cells post bilirubin treatment showed unperturbed cell cycle phases. These results are in contrast to the results shown in previous study using SH SY 5Y cells (Deganuto et al., 2010). We hypothesize that modulation of HR is a general mechanism that gets activated after induction of DNA damage by bilirubin. Another pathway of DSB repair that can be activated after DNA damage is NHEJ. Indeed, using a non-homologous recombination substrate, we have also shown modulation of NHEJ by bilirubin. However, the *in vivo* scenario may be completely different. Our study is supported by other studies in prostate cancer. This study showed NHEJ as a main player behind gene fusion in prostate cancer by inflammation-induced oxidative stress (Mani et al., 2016). Similarly, another study showed activation of NHEJ by oxidative stress (Sharma et al., 2016).

Our recent work in Ugt1 KO mice showed different susceptibility of brain and liver tissues to high bilirubin levels. In this mouse model, there was a time dependent increase in DNA damage in cerebellum, with no DNA damage in liver tissues (unpublished results from Dr. Muro's group). These results are particularly important, proved that different tissues respond differentially to bilirubin induced oxidative stress.

In conclusion, bilirubin-induced oxidative stress leads to DNA damage in neuronal cells. In addition, bilirubin-induced DNA damage has a general effect on both types of DNA repair pathways: HR and NHEJ pathway in HeLa cells.

4.3 Future directions

In the future, more detailed analysis of the signalling mechanisms activated by bilirubin induced DNA damage in SH SY 5Y and HeLa cells will be done. More specifically, activation of the two most important kinases and their different downstream targets that gets activated after ssDNA (ATR) and dsDNA (ATM) breaks will be studied.

In addition, more detailed analysis on the DNA damaging activity of bilirubin will be performed in neonate mice of the hyperbilirubinemic model generated in our lab (Bortolussi et al., 2012). The most interesting organs to analyse are the cerebellum and the liver. The cerebellum represents the most severely affected part in the brain, consequent to increased bilirubin-induced toxicity during its post-natal development. However, we do not rule out the presence of DNA damage in other brain regions. DNA damage by bilirubin could be also present in the liver of jaundiced mice, consequent to the high level of tissue bilirubin present in the acute phases of the disease, which is approximately 10 fold of the concentration found in the cerebellum (Bortolussi et al., 2014b).

Many different pathways are activated by bilirubin both in vitro and in vivo leading to neurodegeneration and brain damage, such as inflammation, oxidative stress and ER stress, but how DNA damage interacts with those mechanisms is not yet defined. Treatment of hyperbilirubinemic mice with NAC may also provide very important mechanistic information of bilirubin toxicity *in vivo*.

Section II

In this part of thesis, we planned to work on two different projects. In the first project, we planned to correct the one-base deletion present in the Ugt1 knockout strain using NcoI restriction site targeting TALEN pair previously designed and tested in our laboratory (Porro et al., 2014). In the second project, we decided to perform hi-throughput miRNA screening to find out miRNAs modulating HR in a liver cell line. The HR modulating miRNA discovered in the hi-throughput screening was further planned to be tested *in vivo* in order to increase the gene-targeting efficiency *in vivo*.

4.4 TALEN mediated correction of Ugt1 Knockout mice model

Our previous attempts to correct the Ugt1 knockout model using previously tested NcoI targeting TALEN pairs failed. We hypothesized that the failure could be due to two main problems. First, we hypothesized that during previous attempts, the pAAV donor vector used by us possibly had some cryptic splicing site. This led us to design new human-codon optimized donor vector. In this work, we successfully cloned the new donor DNA in the rAAV vector. This new donor vector was not tested *in vivo*, as the TALEN activity was very low in vivo. Secondly, we hypothesized that the TALEN activity *in vivo* was very low compared to our previous *in vitro* studies. So, we decided to check the activity of NcoI targeting TALEN pair *in vivo*. In order to check the activity of TALENs *in vivo*, wild type mice were injected with AAV virus encapsulating NcoI restriction site targeting TALEN pair. Genomic PCR followed by NcoI site restriction analysis from the genomic DNA derived from the liver of injected animals showed the absence of any NcoI resistant band. However, this result cannot explain

the low or absent activity of TALENs *in vivo*, given the high activity observed in vivo using the reporter system. Several different types of analysis could have been done to analyse the functionality of TALENs *in vivo*. One of the possible experiment that could have been done was checking the expression of TALEN in liver of mice after injection. Real time qPCR was one of the options to check the expression of TALEN pair in the liver of injected mice. However, real time qPCR was impossible to perform in order to check the expression of TALEN due to high level of similarity between right and left arm of TALENs. Another possibility to check the expression of TALENs in liver is by tagging TALEN pairs with two different tags such as FLAG and HA tag. Unfortunately, we used the Golden-Gate system (Cermak et al., 2011) to generate the TALENS, which did not have plasmids containing the tags in the TALEN pairs.

Due to several non-conclusive results, we decided to stop this project. We also planned to test the CRISPR/Cas9 system to correct the Ugt1 KO mice. The design and cloning of 4 different gRNAs was done. The activity of all the gRNAs was tested using the reporter vector used in our previous work to check the activity of TALEN. Unexpectedly, the activity of all the 4 gRNAs in transfected cells was always lower than NcoI targeting TALENs. The reason for the lower gRNA activity compared to TALEN was not clear; therefore, we decided not to proceed with the CRISPR/Cas9 system to correct the Ugt1 mutation in the KO mouse strain.

4.5 Hi-throughput miRNA screening to identify novel modulators of homologous recombination

To perform hi-throughput miRNA screening, we decided to prepare the FlipIN HEK293 stable cell line using reporter vector designed by our lab during our previous study (Porro et al., 2014). So, we subcloned the reporter insert into the pcDNA5/FRT plasmid to make FlipIN stable cell clones. However, later on we realized that HEK293 cells could not be used for hi-throughput screening due to the partial removal of cells from the wells during transfection and other processing events, necessary during the miRNA highthroughput analysis procedure. So, we decided to generate the stable clones in Hep3B background. In parallel, cloning of reporter insert was done in pcDNA3 vector also due to the fact that pcDNA5/FRT plasmid that we cloned previously does not contain any antibiotic resistance gene. Several different stable clones were generated and the luciferase activity of all the clones was checked after TALEN transfection.

Later on, through literature search, we discovered that the reporter plasmid used to generate stable clones, is mainly repaired by the single stranded annealing (SSA) mechanisms instead of HR (Bhargava et al., 2016). In parallel, another member of the laboratory prepared a substrate specific for analyzing HR events, but since the recombination efficiency appeared to be too low to be used in a screening analysis, we decided to interrupt this project. The correct strategy that we should be using from the beginning to perform hi-througput screening in DR-GFP stable cell clones used extensively in HR research field. However, these cells are not of liver origin and results may not be directly applicable in a liver context, requiring further confirmation experiments.

CONCLUSIONS

Better understanding of the mechanisms responsible for bilirubin-induced neurotoxicity is very important for the treatment and management of BIND. Oxidative stress is one of the main mechanisms responsible for bilirubin-induced neurotoxicity.

In the first part of this thesis, I have shown the time-dependent increase in DNA damage in neuronal cell line after treatment with bilirubin. Treatment with the antioxidant NAC reduced DNA damage, strongly suggesting the key role of oxidative stress in bilirubin-induced DNA damage.

In the second part of this thesis, I have shown the effect of bilirubin on DSB repair pathways. Bilirubin treatment led to dose-dependent increase in homologous recombination. NAC treatment reversed the increase in HR, which suggests the important role of oxidative stress behind the bilirubin-induced increase in HR. DNA damage analysis showed the increase in DNA damage after bilirubin treatment also in HeLa cells. Furthermore, bilirubin treatment also modulated NHEJ. Based on these result, I conclude that treatment with bilirubin led to increased DNA damage, which further activated both the NHEJ and HR DSB repair pathways.

BIBLIOGRAPHY

Ahel, I., Rass, U., El-Khamisy, S.F., Katyal, S., Clements, P.M., McKinnon, P.J., Caldecott, K.W., and West, S.C. (2006). The neurodegenerative disease protein aprataxin resolves abortive DNA ligation intermediates. Nature *443*, 713-716.

Ahlfors, C.E., Marshall, G.D., Wolcott, D.K., Olson, D.C., and Van Overmeire, B. (2006). Measurement of unbound bilirubin by the peroxidase test using Zone Fluidics. Clinica chimica acta; international journal of clinical chemistry *365*, 78-85.

Ahlfors, C.E., and Wennberg, R.P. (2004). Bilirubin-albumin binding and neonatal jaundice. Seminars in perinatology *28*, 334-339.

Amin, S.B., Ahlfors, C., Orlando, M.S., Dalzell, L.E., Merle, K.S., and Guillet, R. (2001). Bilirubin and serial auditory brainstem responses in premature infants. Pediatrics *107*, 664-670.

Amin, S.B., and Lamola, A.A. (2011). Newborn jaundice technologies: unbound bilirubin and bilirubin binding capacity in neonates. Seminars in perinatology *35*, 134-140.

Andres, S.N., Vergnes, A., Ristic, D., Wyman, C., Modesti, M., and Junop, M. (2012). A human XRCC4-XLF complex bridges DNA. Nucleic acids research *40*, 1868-1878.

Anguela, X.M., Sharma, R., Doyon, Y., Miller, J.C., Li, H., Haurigot, V., Rohde, M.E., Wong, S.Y., Davidson, R.J., Zhou, S.*, et al.* (2013). Robust ZFN-mediated genome editing in adult hemophilic mice. Blood *122*, 3283-3287.

Aoyama, K., Watabe, M., and Nakaki, T. (2008). Regulation of neuronal glutathione synthesis. Journal of pharmacological sciences *108*, 227-238.

Arias, I.M. (1962). Chronic unconjugated hyperbilirubinemia without overt signs of hemolysis in adolescents and adults. The Journal of clinical investigation *41*, 2233-2245.

Asad, S.F., Singh, S., Ahmad, A., and Hadi, S.M. (1999). Bilirubin-Cu(II) complex degrades DNA. Biochimica et biophysica acta *1428*, 201-208.

Auclair, C., Hakim, J., Boivin, P., Troube, H., and Boucherot, J. (1976). Bilirubin and paranitrophenol glucuronyl transferase activities of the liver in patients with Gilbert's syndrome An attempt at a biochemical breakdown of the Gilbert's syndrome. Enzyme *21*, 97-107.

Bae, K.H., Kwon, Y.D., Shin, H.C., Hwang, M.S., Ryu, E.H., Park, K.S., Yang, H.Y., Lee, D.K., Lee, Y., Park, J.*, et al.* (2003). Human zinc fingers as building blocks in the construction of artificial transcription factors. Nature biotechnology *21*, 275-280.

Barateiro, A., Chen, S., Yueh, M.F., Fernandes, A., Domingues, H.S., Relvas, J., Barbier, O., Nguyen, N., Tukey, R.H., and Brites, D. (2016). Reduced Myelination and Increased Glia Reactivity Resulting from Severe Neonatal Hyperbilirubinemia. Molecular pharmacology *89*, 84-93.

Barateiro, A., Vaz, A.R., Silva, S.L., Fernandes, A., and Brites, D. (2012). ER stress, mitochondrial dysfunction and calpain/JNK activation are involved in oligodendrocyte precursor cell death by unconjugated bilirubin. Neuromolecular medicine *14*, 285-302.

Barrangou, R., Fremaux, C., Deveau, H., Richards, M., Boyaval, P., Moineau, S., Romero, D.A., and Horvath, P. (2007). CRISPR provides acquired resistance against viruses in prokaryotes. Science *315*, 1709-1712.

Bartek, J., and Lukas, J. (2007). DNA damage checkpoints: from initiation to recovery or adaptation. Current opinion in cell biology *19*, 238-245.

Basu, S., De, D., Dev Khanna, H., and Kumar, A. (2014). Lipid peroxidation, DNA damage and total antioxidant status in neonatal hyperbilirubinemia. Journal of perinatology : official journal of the California Perinatal Association *34*, 519-523.

Baumann, P., and West, S.C. (1998). DNA end-joining catalyzed by human cell-free extracts. Proceedings of the National Academy of Sciences of the United States of America *95*, 14066-14070.

Bedell, V.M., Wang, Y., Campbell, J.M., Poshusta, T.L., Starker, C.G., Krug, R.G., 2nd, Tan, W., Penheiter, S.G., Ma, A.C., Leung, A.Y.*, et al.* (2012). In vivo genome editing using a high-efficiency TALEN system. Nature *491*, 114-118.

Beerli, R.R., Dreier, B., and Barbas, C.F., 3rd (2000). Positive and negative regulation of endogenous genes by designed transcription factors. Proceedings of the National Academy of Sciences of the United States of America *97*, 1495-1500.

Bennardo, N., Cheng, A., Huang, N., and Stark, J.M. (2008). Alternative-NHEJ is a mechanistically distinct pathway of mammalian chromosome break repair. PLoS genetics *4*, e1000110.

Bernstein, J., and Landing, B.H. (1962). Extraneural lesions associated with neonatal hyperbilirubinemia and kernicterus. The American journal of pathology *40*, 371-391.

Bhargava, R., Onyango, D.O., and Stark, J.M. (2016). Regulation of Single-Strand Annealing and its Role in Genome Maintenance. Trends in genetics : TIG *32*, 566-575.

Bhutani, V.K., and Wong, R.J. (2013). Bilirubin neurotoxicity in preterm infants: risk and prevention. Journal of clinical neonatology *2*, 61-69.

Birben, E., Sahiner, U.M., Sackesen, C., Erzurum, S., and Kalayci, O. (2012). Oxidative stress and antioxidant defense. The World Allergy Organization journal *5*, 9-19.

Boch, J., Scholze, H., Schornack, S., Landgraf, A., Hahn, S., Kay, S., Lahaye, T., Nickstadt, A., and Bonas, U. (2009). Breaking the code of DNA binding specificity of TAL-type III effectors. Science *326*, 1509-1512.

Borges, H.L., Linden, R., and Wang, J.Y. (2008). DNA damage-induced cell death: lessons from the central nervous system. Cell Res *18*, 17-26.

Bortolussi, G., Baj, G., Vodret, S., Viviani, G., Bittolo, T., and Muro, A.F. (2014a). Age-dependent pattern of cerebellar susceptibility to bilirubin neurotoxicity in vivo in mice. Disease models & mechanisms *7*, 1057-1068.

Bortolussi, G., Codarin, E., Antoniali, G., Vascotto, C., Vodret, S., Arena, S., Cesaratto, L., Scaloni, A., Tell, G., and Muro, A.F. (2015). Impairment of enzymatic antioxidant defenses is associated with bilirubin-induced neuronal cell death in the cerebellum of Ugt1 KO mice. Cell death & disease *6*, e1739.

Bortolussi, G., Zentilin, L., Baj, G., Giraudi, P., Bellarosa, C., Giacca, M., Tiribelli, C., and Muro, A.F. (2012). Rescue of bilirubin-induced neonatal lethality in a mouse model of Crigler-Najjar syndrome type I by AAV9-mediated gene transfer. FASEB journal : official publication of the Federation of American Societies for Experimental Biology *26*, 1052-1063.

Bortolussi, G., Zentillin, L., Vanikova, J., Bockor, L., Bellarosa, C., Mancarella, A., Vianello, E., Tiribelli, C., Giacca, M., Vitek, L*., et al.* (2014b). Life-long correction of hyperbilirubinemia with a neonatal liver-specific AAV-mediated gene transfer in a lethal mouse model of Crigler-Najjar Syndrome. Human gene therapy *25*, 844-855.

Bosma, P.J. (2003). Inherited disorders of bilirubin metabolism. Journal of hepatology *38*, 107-117.

Bosma, P.J., Chowdhury, J.R., Bakker, C., Gantla, S., de Boer, A., Oostra, B.A., Lindhout, D., Tytgat, G.N., Jansen, P.L., Oude Elferink, R.P*., et al.* (1995). The genetic basis of the reduced expression of bilirubin UDP-glucuronosyltransferase 1 in Gilbert's syndrome. The New England journal of medicine *333*, 1171-1175.

Boulton, S.J., and Jackson, S.P. (1996). Identification of a Saccharomyces cerevisiae Ku80 homologue: roles in DNA double strand break rejoining and in telomeric maintenance. Nucleic acids research *24*, 4639-4648.

Brettschneider, J., Del Tredici, K., Lee, V.M., and Trojanowski, J.Q. (2015). Spreading of pathology in neurodegenerative diseases: a focus on human studies. Nature reviews Neuroscience *16*, 109-120.

Briggs, A.W., Rios, X., Chari, R., Yang, L., Zhang, F., Mali, P., and Church, G.M. (2012). Iterative capped assembly: rapid and scalable synthesis of repeat-module DNA such as TAL effectors from individual monomers. Nucleic acids research *40*, e117.

Brito, M.A., Brites, D., and Butterfield, D.A. (2004). A link between hyperbilirubinemia, oxidative stress and injury to neocortical synaptosomes. Brain research *1026*, 33-43.

Brito, M.A., Lima, S., Fernandes, A., Falcao, A.S., Silva, R.F., Butterfield, D.A., and Brites, D. (2008a). Bilirubin injury to neurons: contribution of oxidative stress and rescue by glycoursodeoxycholic acid. Neurotoxicology *29*, 259-269.

Brito, M.A., Rosa, A.I., Falcao, A.S., Fernandes, A., Silva, R.F., Butterfield, D.A., and Brites, D. (2008b). Unconjugated bilirubin differentially affects the redox status of neuronal and astroglial cells. Neurobiology of disease *29*, 30-40.

Brodersen, P., and Voinnet, O. (2009). Revisiting the principles of microRNA target recognition and mode of action. Nature reviews Molecular cell biology *10*, 141-148.

Brooks, P.J. (2000). Brain atrophy and neuronal loss in alcoholism: a role for DNA damage? Neurochemistry international *37*, 403-412.

Caldecott, K.W. (2008). Single-strand break repair and genetic disease. Nature reviews Genetics *9*, 619-631.

Calligaris, R., Bellarosa, C., Foti, R., Roncaglia, P., Giraudi, P., Krmac, H., Tiribelli, C., and Gustincich, S. (2009). A transcriptome analysis identifies molecular effectors of unconjugated bilirubin in human neuroblastoma SH-SY5Y cells. BMC genomics *10*, 543.

Cary, R.B., Peterson, S.R., Wang, J., Bear, D.G., Bradbury, E.M., and Chen, D.J. (1997). DNA looping by Ku and the DNA-dependent protein kinase. Proceedings of the National Academy of Sciences of the United States of America *94*, 4267-4272.

Cejka, P., Cannavo, E., Polaczek, P., Masuda-Sasa, T., Pokharel, S., Campbell, J.L., and Kowalczykowski, S.C. (2010). DNA end resection by Dna2-Sgs1-RPA and its stimulation by Top3-Rmi1 and Mre11-Rad50-Xrs2. Nature *467*, 112-116.

Cermak, T., Doyle, E.L., Christian, M., Wang, L., Zhang, Y., Schmidt, C., Baller, J.A., Somia, N.V., Bogdanove, A.J., and Voytas, D.F. (2011). Efficient design and assembly of custom TALEN and other TAL effector-based constructs for DNA targeting. Nucleic acids research *39*, e82.

Cesaratto, L., Calligaris, S.D., Vascotto, C., Deganuto, M., Bellarosa, C., Quadrifoglio, F., Ostrow, J.D., Tiribelli, C., and Tell, G. (2007). Bilirubin-induced cell toxicity involves PTEN activation through an APE1/Ref-1-dependent pathway. Journal of molecular medicine *85*, 1099-1112.

Chan, P.H. (2001). Reactive oxygen radicals in signaling and damage in the ischemic brain. Journal of cerebral blood flow and metabolism : official journal of the International Society of Cerebral Blood Flow and Metabolism *21*, 2-14.

Chevalier, B.S., and Stoddard, B.L. (2001). Homing endonucleases: structural and functional insight into the catalysts of intron/intein mobility. Nucleic acids research *29*, 3757-3774.

Cho, H.Y., Jedlicka, A.E., Reddy, S.P., Kensler, T.W., Yamamoto, M., Zhang, L.Y., and Kleeberger, S.R. (2002). Role of NRF2 in protection against hyperoxic lung injury in mice. American journal of respiratory cell and molecular biology *26*, 175-182.

Choi, Y.E., Pan, Y., Park, E., Konstantinopoulos, P., De, S., D'Andrea, A., and Chowdhury, D. (2014). MicroRNAs down-regulate homologous recombination in the G1 phase of cycling cells to maintain genomic stability. eLife *3*, e02445.

Choo, Y., and Klug, A. (1994). Toward a code for the interactions of zinc fingers with DNA: selection of randomized fingers displayed on phage. Proceedings of the National Academy of Sciences of the United States of America *91*, 11163-11167.

Chylinski, K., Makarova, K.S., Charpentier, E., and Koonin, E.V. (2014). Classification and evolution of type II CRISPR-Cas systems. Nucleic acids research *42*, 6091-6105.

Cimprich, K.A., and Cortez, D. (2008). ATR: an essential regulator of genome integrity. Nature reviews Molecular cell biology *9*, 616-627.

Cong, L., Ran, F.A., Cox, D., Lin, S., Barretto, R., Habib, N., Hsu, P.D., Wu, X., Jiang, W., Marraffini, L.A.*, et al.* (2013). Multiplex genome engineering using CRISPR/Cas systems. Science *339*, 819-823.

Conlee, J.W., and Shapiro, S.M. (1997). Development of cerebellar hypoplasia in jaundiced Gunn rats: a quantitative light microscopic analysis. Acta neuropathologica *93*, 450-460.
Cooper, M.P., Machwe, A., Orren, D.K., Brosh, R.M., Ramsden, D., and Bohr, V.A. (2000). Ku complex interacts with and stimulates the Werner protein. Genes & development *14*, 907-912.

Coppede, F., and Migliore, L. (2015). DNA damage in neurodegenerative diseases. Mutat Res *776*, 84-97.

Costantini, S., Woodbine, L., Andreoli, L., Jeggo, P.A., and Vindigni, A. (2007). Interaction of the Ku heterodimer with the DNA ligase IV/Xrcc4 complex and its regulation by DNA-PK. DNA repair *6*, 712-722.

Crigler, J.F., Jr., and Najjar, V.A. (1952). Congenital familial nonhemolytic jaundice with kernicterus. Pediatrics *10*, 169-180.

Cuozzo, C., Porcellini, A., Angrisano, T., Morano, A., Lee, B., Di Pardo, A., Messina, S., Iuliano, R., Fusco, A., Santillo, M.R.*, et al.* (2007). DNA damage, homology-directed repair, and DNA methylation. PLoS genetics *3*, e110.

Damia, G., and D'Incalci, M. (2007). Targeting DNA repair as a promising approach in cancer therapy. European journal of cancer *43*, 1791-1801.

Daood, M.J., Hoyson, M., and Watchko, J.F. (2012). Lipid peroxidation is not the primary mechanism of bilirubin-induced neurologic dysfunction in jaundiced Gunn rat pups. Pediatric research *72*, 455-459.

David, S.S., O'Shea, V.L., and Kundu, S. (2007). Base-excision repair of oxidative DNA damage. Nature *447*, 941-950.

Davis, A.J., and Chen, D.J. (2013). DNA double strand break repair via non-homologous end-joining. Translational cancer research *2*, 130-143.

Deganuto, M., Cesaratto, L., Bellarosa, C., Calligaris, R., Vilotti, S., Renzone, G., Foti, R., Scaloni, A., Gustincich, S., Quadrifoglio, F.*, et al.* (2010). A proteomic approach to the bilirubin-induced toxicity in neuronal cells reveals a protective function of DJ-1 protein. Proteomics *10*, 1645-1657.

Deng, D., Yan, C., Pan, X., Mahfouz, M., Wang, J., Zhu, J.K., Shi, Y., and Yan, N. (2012). Structural basis for sequence-specific recognition of DNA by TAL effectors. Science *335*, 720-723.

Desjarlais, J.R., and Berg, J.M. (1992). Toward rules relating zinc finger protein sequences and DNA binding site preferences. Proceedings of the National Academy of Sciences of the United States of America *89*, 7345-7349.

Doyle, K.M., Kennedy, D., Gorman, A.M., Gupta, S., Healy, S.J., and Samali, A. (2011). Unfolded proteins and endoplasmic reticulum stress in neurodegenerative disorders. Journal of cellular and molecular medicine *15*, 2025-2039.

Dupuy, A., Valton, J., Leduc, S., Armier, J., Galetto, R., Gouble, A., Lebuhotel, C., Stary, A., Paques, F., Duchateau, P*., et al.* (2013). Targeted gene therapy of xeroderma pigmentosum cells using meganuclease and TALEN. PloS one *8*, e78678.

Erlinger, S., Arias, I.M., and Dhumeaux, D. (2014). Inherited disorders of bilirubin transport and conjugation: new insights into molecular mechanisms and consequences. Gastroenterology *146*, 1625-1638.

Eulalio, A., Mano, M., Dal Ferro, M., Zentilin, L., Sinagra, G., Zacchigna, S., and Giacca, M. (2012). Functional screening identifies miRNAs inducing cardiac regeneration. Nature *492*, 376-381.
\
Falcao, A.S., Silva, R.F., Fernandes, A., Brito, M.A., and Brites, D. (2007). Influence of hypoxia and ischemia preconditioning on bilirubin damage to astrocytes. Brain research *1149*, 191-199.

Fanning, E., Klimovich, V., and Nager, A.R. (2006). A dynamic model for replication protein A (RPA) function in DNA processing pathways. Nucleic acids research *34*, 4126-4137.

Ferguson, D.O., and Holloman, W.K. (1996). Recombinational repair of gaps in DNA is asymmetric in Ustilago maydis and can be explained by a migrating D-loop model. Proceedings of the National Academy of Sciences of the United States of America *93*, 5419-5424.

Fernandes, A., and Brites, D. (2009). Contribution of inflammatory processes to nerve cell toxicity by bilirubin and efficacy of potential therapeutic agents. Current pharmaceutical design *15*, 2915-2926.
Fernandes, A., Falcao, A.S., Abranches, E., Bekman, E., Henrique, D., Lanier, L.M., and Brites, D. (2009). Bilirubin as a determinant for altered neurogenesis, neuritogenesis, and synaptogenesis. Developmental neurobiology *69*, 568-582.

Fernandes, A., Falcao, A.S., Silva, R.F., Brito, M.A., and Brites, D. (2007). MAPKs are key players in mediating cytokine release and cell death induced by unconjugated bilirubin in cultured rat cortical astrocytes. The European journal of neuroscience *25*, 1058-1068.

Fernandes, A., Falcao, A.S., Silva, R.F., Gordo, A.C., Gama, M.J., Brito, M.A., and Brites, D. (2006). Inflammatory signalling pathways involved in astroglial activation by unconjugated bilirubin. Journal of neurochemistry *96*, 1667-1679.

Fernandes, A., Silva, R.F., Falcao, A.S., Brito, M.A., and Brites, D. (2004). Cytokine production, glutamate release and cell death in rat cultured astrocytes treated with unconjugated bilirubin and LPS. Journal of neuroimmunology *153*, 64-75.

Fisher, M.B., Paine, M.F., Strelevitz, T.J., and Wrighton, S.A. (2001). The role of hepatic and extrahepatic UDP-glucuronosyltransferases in human drug metabolism. Drug metabolism reviews *33*, 273-297.

Fonseca, S.G., Gromada, J., and Urano, F. (2011). Endoplasmic reticulum stress and pancreatic beta-cell death. Trends in endocrinology and metabolism: TEM *22*, 266-274.

Frank-Cannon, T.C., Alto, L.T., McAlpine, F.E., and Tansey, M.G. (2009). Does neuroinflammation fan the flame in neurodegenerative diseases? Molecular neurodegeneration *4*, 47.

Frock, R.L., Hu, J., Meyers, R.M., Ho, Y.J., Kii, E., and Alt, F.W. (2015). Genome-wide detection of DNA double-stranded breaks induced by engineered nucleases. Nature biotechnology *33*, 179-186.

Fujiwara, R., Chen, S., Karin, M., and Tukey, R.H. (2012). Reduced expression of UGT1A1 in intestines of humanized UGT1 mice via inactivation of NF-kappaB leads to hyperbilirubinemia. Gastroenterology *142*, 109-118 e102.
Fujiwara, R., Maruo, Y., Chen, S., and Tukey, R.H. (2015). Role of extrahepatic UDP-glucuronosyltransferase 1A1: Advances in understanding breast milk-induced neonatal hyperbilirubinemia. Toxicology and applied pharmacology *289*, 124-132.

Gabbita, S.P., Lovell, M.A., and Markesbery, W.R. (1998). Increased nuclear DNA oxidation in the brain in Alzheimer's disease. Journal of neurochemistry *71*, 2034-2040.

Gasparini, P., Lovat, F., Fassan, M., Casadei, L., Cascione, L., Jacob, N.K., Carasi, S., Palmieri, D., Costinean, S., Shapiro, C.L*., et al.* (2014). Protective role of miR-155 in breast cancer through RAD51 targeting impairs homologous recombination after irradiation. Proceedings of the National Academy of Sciences of the United States of America *111*, 4536-4541.

Gersbach, C.A., Gaj, T., and Barbas, C.F., 3rd (2014). Synthetic zinc finger proteins: the advent of targeted gene regulation and genome modification technologies. Accounts of chemical research *47*, 2309-2318.

Giraudi, P.J., Bellarosa, C., Coda-Zabetta, C.D., Peruzzo, P., and Tiribelli, C. (2011). Functional induction of the cystine-glutamate exchanger system Xc(-) activity in SH-SY5Y cells by unconjugated bilirubin. PloS one *6*, e29078.

Gordo, A.C., Falcao, A.S., Fernandes, A., Brito, M.A., Silva, R.F., and Brites, D. (2006). Unconjugated bilirubin activates and damages microglia. Journal of neuroscience research *84*, 194-201.

Grawunder, U., Wilm, M., Wu, X., Kulesza, P., Wilson, T.E., Mann, M., and Lieber, M.R. (1997). Activity of DNA ligase IV stimulated by complex formation with XRCC4 protein in mammalian cells. Nature *388*, 492-495.

Greco, C., Arnolda, G., Boo, N.Y., Iskander, I.F., Okolo, A.A., Rohsiswatmo, R., Shapiro, S.M., Watchko, J., Wennberg, R.P., Tiribelli, C*., et al.* (2016). Neonatal Jaundice in Low- and Middle-Income Countries: Lessons and Future Directions from the 2015 Don Ostrow Trieste Yellow Retreat. Neonatology *110*, 172-180.

Grundy, G.J., Rulten, S.L., Zeng, Z., Arribas-Bosacoma, R., Iles, N., Manley, K., Oliver, A., and Caldecott, K.W. (2013). APLF promotes the assembly and activity of non-homologous end joining protein complexes. The EMBO journal *32*, 112-125.

Gupta, A., Christensen, R.G., Rayla, A.L., Lakshmanan, A., Stormo, G.D., and Wolfe, S.A. (2012). An optimized two-finger archive for ZFN-mediated gene targeting. Nature methods *9*, 588-590.

Gurlevik, E., Schache, P., Goez, A., Kloos, A., Woller, N., Armbrecht, N., Manns, M.P., Kubicka, S., and Kuhnel, F. (2013). Meganuclease-mediated virus self-cleavage facilitates tumor-specific virus replication. Molecular therapy : the journal of the American Society of Gene Therapy *21*, 1738-1748.

Haagsma, E.B., Hagens, V.E., Schaapveld, M., van den Berg, A.P., de Vries, E.G., Klompmaker, I.J., Slooff, M.J., and Jansen, P.L. (2001). Increased cancer risk after liver transplantation: a population-based study. Journal of hepatology *34*, 84-91.

Hammel, M., Rey, M., Yu, Y., Mani, R.S., Classen, S., Liu, M., Pique, M.E., Fang, S., Mahaney, B.L., Weinfeld, M*., et al.* (2011). XRCC4 protein interactions with XRCC4-like factor (XLF) create an extended grooved scaffold for DNA ligation and double strand break repair. The Journal of biological chemistry *286*, 32638-32650.
Hammel, M., Yu, Y., Fang, S., Lees-Miller, S.P., and Tainer, J.A. (2010). XLF regulates filament architecture of the XRCC4.ligase IV complex. Structure *18*, 1431-1442.

Harper, J.W., and Elledge, S.J. (2007). The DNA damage response: ten years after. Molecular cell *28*, 739-745.

Harrison, J.C., and Haber, J.E. (2006). Surviving the breakup: the DNA damage checkpoint. Annual review of genetics *40*, 209-235.

Harvey, B.K., Richie, C.T., Hoffer, B.J., and Airavaara, M. (2011). Transgenic animal models of neurodegeneration based on human genetic studies. Journal of neural transmission *118*, 27-45.

Haustein, M.D., Read, D.J., Steinert, J.R., Pilati, N., Dinsdale, D., and Forsythe, I.D. (2010). Acute hyperbilirubinaemia induces presynaptic neurodegeneration at a central glutamatergic synapse. The Journal of physiology *588*, 4683-4693.

Hayashi, M., and Umezu, K. (2017). Homologous recombination is required for recovery from oxidative DNA damage. Genes & genetic systems *92*, 73-80.

He, L., and Hannon, G.J. (2004). MicroRNAs: small RNAs with a big role in gene regulation. Nature reviews Genetics *5*, 522-531.

Herrero, J.I., Lorenzo, M., Quiroga, J., Sangro, B., Pardo, F., Rotellar, F., Alvarez-Cienfuegos, J., and Prieto, J. (2005). De Novo neoplasia after liver transplantation: an analysis of risk factors and influence on survival. Liver transplantation : official publication of the American Association for the Study of Liver Diseases and the International Liver Transplantation Society *11*, 89-97.

Heyer, W.D., Ehmsen, K.T., and Liu, J. (2010). Regulation of homologous recombination in eukaryotes. Annual review of genetics *44*, 113-139.

Hockemeyer, D., Wang, H., Kiani, S., Lai, C.S., Gao, Q., Cassady, J.P., Cost, G.J., Zhang, L., Santiago, Y., Miller, J.C*., et al.* (2011). Genetic engineering of human pluripotent cells using TALE nucleases. Nature biotechnology *29*, 731-734.

Hoeijmakers, J.H. (2001). Genome maintenance mechanisms for preventing cancer. Nature *411*, 366-374.

Holkers, M., Maggio, I., Liu, J., Janssen, J.M., Miselli, F., Mussolino, C., Recchia, A., Cathomen, T., and Goncalves, M.A. (2013). Differential integrity of TALE nuclease genes following adenoviral and lentiviral vector gene transfer into human cells. Nucleic acids research *41*, e63.

Huen, M.S., and Chen, J. (2010). Assembly of checkpoint and repair machineries at DNA damage sites. Trends in biochemical sciences *35*, 101-108.

Ihara, H., Hashizume, N., Shimizu, N., and Aoki, T. (1999). Threshold concentration of unbound bilirubin to induce neurological deficits in a patient with type I Crigler-Najjar syndrome. Annals of clinical biochemistry *36 (Pt 3)*, 347-352.

Jackson, S.P., and Bartek, J. (2009). The DNA-damage response in human biology and disease. Nature *461*, 1071-1078.
Jangi, S., Otterbein, L., and Robson, S. (2013). The molecular basis for the immunomodulatory activities of unconjugated bilirubin. The international journal of biochemistry & cell biology *45*, 2843-2851.

Jasin, M. (1996). Genetic manipulation of genomes with rare-cutting endonucleases. Trends in genetics : TIG *12*, 224-228.

Jemnitz, K., Heredi-Szabo, K., Janossy, J., Ioja, E., Vereczkey, L., and Krajcsi, P. (2010). ABCC2/Abcc2: a multispecific transporter with dominant excretory functions. Drug metabolism reviews *42*, 402-436.

Jinek, M., Chylinski, K., Fonfara, I., Hauer, M., Doudna, J.A., and Charpentier, E. (2012). A programmable dual-RNA-guided DNA endonuclease in adaptive bacterial immunity. Science *337*, 816-821.

Jinek, M., East, A., Cheng, A., Lin, S., Ma, E., and Doudna, J. (2013). RNA-programmed genome editing in human cells. eLife *2*, e00471.

Jiricny, J. (2006). The multifaceted mismatch-repair system. Nature reviews Molecular cell biology *7*, 335-346.

Jung, B.J., Yoo, H.S., Shin, S., Park, Y.J., and Jeon, S.M. (2017). Dysregulation of NRF2 in Cancer: from Molecular Mechanisms to Therapeutic Opportunities. Biomolecules & therapeutics.

Kanno, S., Kuzuoka, H., Sasao, S., Hong, Z., Lan, L., Nakajima, S., and Yasui, A. (2007). A novel human AP endonuclease with conserved zinc-finger-like motifs involved in DNA strand break responses. The EMBO journal *26*, 2094-2103.

Kaplan, M., and Hammerman, C. (2005). Understanding severe hyperbilirubinemia and preventing kernicterus: adjuncts in the interpretation of neonatal serum bilirubin. Clinica chimica acta; international journal of clinical chemistry *356*, 9-21.

Kaplan, M., Hammerman, C., Renbaum, P., Klein, G., and Levy-Lahad, E. (2000). Gilbert's syndrome and hyperbilirubinaemia in ABO-incompatible neonates. Lancet *356*, 652-653.

Kaplan, M., Renbaum, P., Levy-Lahad, E., Hammerman, C., Lahad, A., and Beutler, E. (1997). Gilbert syndrome and glucose-6-phosphate dehydrogenase deficiency: a dose-dependent genetic interaction crucial to neonatal hyperbilirubinemia. Proceedings of the National Academy of Sciences of the United States of America *94*, 12128-12132.

Karadag, A., Demirin, H., Dogan, D.G., Aslan, M., and Tatli, M.M. (2010). Phototherapy, hyperbilirubinemia and genotoxicity in newborns. Mutation research *697*, 68; author reply 69.

Karakukcu, C., Ustdal, M., Ozturk, A., Baskol, G., and Saraymen, R. (2009). Assessment of DNA damage and plasma catalase activity in healthy term hyperbilirubinemic infants receiving phototherapy. Mutation research *680*, 12-16.

Kastan, M.B., and Bartek, J. (2004). Cell-cycle checkpoints and cancer. Nature *432*, 316-323.

Kawanishi, S., and Hiraku, Y. (2006). Oxidative and nitrative DNA damage as biomarker for carcinogenesis with special reference to inflammation. Antioxidants & redox signaling *8*, 1047-1058.

Keppler, D. (2011). Multidrug resistance proteins (MRPs, ABCCs): importance for pathophysiology and drug therapy. Handbook of experimental pharmacology, 299-323.

Khan, N.M., and Poduval, T.B. (2012). Bilirubin augments radiation injury and leads to increased infection and mortality in mice: molecular mechanisms. Free radical biology & medicine *53*, 1152-1169.

Khanna, K.K., and Jackson, S.P. (2001). DNA double-strand breaks: signaling, repair and the cancer connection. Nature genetics *27*, 247-254.

Kigerl, K.A., Gensel, J.C., Ankeny, D.P., Alexander, J.K., Donnelly, D.J., and Popovich, P.G. (2009). Identification of two distinct macrophage subsets with divergent effects causing either neurotoxicity or regeneration in the injured mouse spinal cord. The Journal of neuroscience : the official journal of the Society for Neuroscience *29*, 13435-13444.

Kim, Y.G., and Chandrasegaran, S. (1994). Chimeric restriction endonuclease. Proceedings of the National Academy of Sciences of the United States of America *91*, 883-887.

Kulkarni, A., and Wilson, D.M., 3rd (2008). The involvement of DNA-damage and -repair defects in neurological dysfunction. American journal of human genetics *82*, 539-566.

Kuma, A., Hatano, M., Matsui, M., Yamamoto, A., Nakaya, H., Yoshimori, T., Ohsumi, Y., Tokuhisa, T., and Mizushima, N. (2004). The role of autophagy during the early neonatal starvation period. Nature *432*, 1032-1036.

Kumar, A., Pant, P., Basu, S., Rao, G.R., and Khanna, H.D. (2007). Oxidative stress in neonatal hyperbilirubinemia. Journal of tropical pediatrics *53*, 69-71.

Kusumoto, R., Dawut, L., Marchetti, C., Wan Lee, J., Vindigni, A., Ramsden, D., and Bohr, V.A. (2008). Werner protein cooperates with the XRCC4-DNA ligase IV complex in end-processing. Biochemistry *47*, 7548-7556.

Lauer, B.J., and Spector, N.D. (2011). Hyperbilirubinemia in the newborn. Pediatrics in review *32*, 341-349.

Lee, J.H., Ghirlando, R., Bhaskara, V., Hoffmeyer, M.R., Gu, J., and Paull, T.T. (2003). Regulation of Mre11/Rad50 by Nbs1: effects on nucleotide-dependent DNA binding and association with ataxia-telangiectasia-like disorder mutant complexes. The Journal of biological chemistry *278*, 45171-45181.

Lee, M.S., Gippert, G.P., Soman, K.V., Case, D.A., and Wright, P.E. (1989). Three-dimensional solution structure of a single zinc finger DNA-binding domain. Science *245*, 635-637.

Li, L., Wu, L.P., and Chandrasegaran, S. (1992). Functional domains in Fok I restriction endonuclease. Proceedings of the National Academy of Sciences of the United States of America *89*, 4275-4279.

Li, S., Kanno, S., Watanabe, R., Ogiwara, H., Kohno, T., Watanabe, G., Yasui, A., and Lieber, M.R. (2011). Polynucleotide kinase and aprataxin-like forkhead-associated protein (PALF) acts as both a single-stranded DNA endonuclease and a single-stranded DNA 3' exonuclease and can participate in DNA end joining in a biochemical system. The Journal of biological chemistry *286*, 36368-36377.
Li, Y., Guo, Y., Tang, J., Jiang, J., and Chen, Z. (2014). New insights into the roles of CHOP-induced apoptosis in ER stress. Acta biochimica et biophysica Sinica *46*, 629-640.

Liang, F., Romanienko, P.J., Weaver, D.T., Jeggo, P.A., and Jasin, M. (1996). Chromosomal double-strand break repair in Ku80-deficient cells. Proceedings of the National Academy of Sciences of the United States of America *93*, 8929-8933.

Liaury, K., Miyaoka, T., Tsumori, T., Furuya, M., Wake, R., Ieda, M., Tsuchie, K., Taki, M., Ishihara, K., Tanra, A.J*., et al.* (2012). Morphological features of microglial cells in the hippocampal dentate gyrus of Gunn rat: a possible schizophrenia animal model. Journal of neuroinflammation *9*, 56.

Lieber, M.R. (2008). The mechanism of human nonhomologous DNA end joining. The Journal of biological chemistry *283*, 1-5.

Liu, G., Su, L., Hao, X., Zhong, N., Zhong, D., Singhal, S., and Liu, X. (2012). Salermide up-regulates death receptor 5 expression through the ATF4-ATF3-CHOP axis and leads to apoptosis in human cancer cells. Journal of cellular and molecular medicine *16*, 1618-1628.

Ljungman, M., and Lane, D.P. (2004). Transcription - guarding the genome by sensing DNA damage. Nature reviews Cancer *4*, 727-737.

Lombardo, A., Genovese, P., Beausejour, C.M., Colleoni, S., Lee, Y.L., Kim, K.A., Ando, D., Urnov, F.D., Galli, C., Gregory, P.D*., et al.* (2007). Gene editing in human stem cells using zinc finger nucleases and integrase-defective lentiviral vector delivery. Nature biotechnology *25*, 1298-1306.

London, I.M., West, R., Shemin, D., and Rittenberg, D. (1950). On the origin of bile pigment in normal man. The Journal of biological chemistry *184*, 351-358.

Ma, Y., Pannicke, U., Schwarz, K., and Lieber, M.R. (2002). Hairpin opening and overhang processing by an Artemis/DNA-dependent protein kinase complex in nonhomologous end joining and V(D)J recombination. Cell *108*, 781-794.

Macrae, C.J., McCulloch, R.D., Ylanko, J., Durocher, D., and Koch, C.A. (2008). APLF (C2orf13) facilitates nonhomologous end-joining and undergoes ATM-dependent hyperphosphorylation following ionizing radiation. DNA repair *7*, 292-302.

Maeder, M.L., and Gersbach, C.A. (2016). Genome-editing Technologies for Gene and Cell Therapy. Molecular therapy : the journal of the American Society of Gene Therapy *24*, 430-446.

Maeder, M.L., Thibodeau-Beganny, S., Osiak, A., Wright, D.A., Anthony, R.M., Eichtinger, M., Jiang, T., Foley, J.E., Winfrey, R.J., Townsend, J.A*., et al.* (2008). Rapid "open-source" engineering of customized zinc-finger nucleases for highly efficient gene modification. Molecular cell *31*, 294-301.

Maki, T., Sato, T., and Sato, T. (1962). A study on the activity of beta-glucuronidase in bile in connection with precipitation of calcium bilirubinate. The Tohoku journal of experimental medicine *77*, 179-186.

Maki, T., Sato, T., Yamaguchi, I., and Saito, Y. (1964). Autopsy Incidence of Gallstones in Japan. The Tohoku journal of experimental medicine *84*, 37-45.

Malhotra, J.D., and Kaufman, R.J. (2007). Endoplasmic reticulum stress and oxidative stress: a vicious cycle or a double-edged sword? Antioxidants & redox signaling *9*, 2277-2293.

Mali, P., Yang, L., Esvelt, K.M., Aach, J., Guell, M., DiCarlo, J.E., Norville, J.E., and Church, G.M. (2013). RNA-guided human genome engineering via Cas9. Science *339*, 823-826.

Malivert, L., Ropars, V., Nunez, M., Drevet, P., Miron, S., Faure, G., Guerois, R., Mornon, J.P., Revy, P., Charbonnier, J.B*., et al.* (2010). Delineation of the Xrcc4-interacting region in the globular head domain of cernunnos/XLF. The Journal of biological chemistry *285*, 26475-26483.

Mani, R.S., Amin, M.A., Li, X., Kalyana-Sundaram, S., Veeneman, B.A., Wang, L., Ghosh, A., Aslam, A., Ramanand, S.G., Rabquer, B.J*., et al.* (2016). Inflammation-Induced Oxidative Stress Mediates Gene Fusion Formation in Prostate Cancer. Cell reports *17*, 2620-2631.

Mari, P.O., Florea, B.I., Persengiev, S.P., Verkaik, N.S., Bruggenwirth, H.T., Modesti, M., Giglia-Mari, G., Bezstarosti, K., Demmers, J.A., Luider, T.M*., et al.* (2006). Dynamic assembly

of end-joining complexes requires interaction between Ku70/80 and XRCC4. Proceedings of the National Academy of Sciences of the United States of America *103*, 18597-18602.

Martinez, F.O., Gordon, S., Locati, M., and Mantovani, A. (2006). Transcriptional profiling of the human monocyte-to-macrophage differentiation and polarization: new molecules and patterns of gene expression. Journal of immunology *177*, 7303-7311.

Mattson, M.P. (2000). Apoptosis in neurodegenerative disorders. Nature reviews Molecular cell biology *1*, 120-129.

McCord, J.M. (2000). The evolution of free radicals and oxidative stress. The American journal of medicine *108*, 652-659.

McVey, M., and Lee, S.E. (2008). MMEJ repair of double-strand breaks (director's cut): deleted sequences and alternative endings. Trends in genetics : TIG *24*, 529-538.

Mikoshiba, K., Kohsaka, S., Takamatsu, K., and Tsukada, Y. (1980). Cerebellar hypoplasia in the Gunn rat with hereditary hyperbilirubinemia: immunohistochemical and neurochemical studies. Journal of neurochemistry *35*, 1309-1318.

Miller, J.C., Tan, S., Qiao, G., Barlow, K.A., Wang, J., Xia, D.F., Meng, X., Paschon, D.E., Leung, E., Hinkley, S.J.*, et al.* (2011). A TALE nuclease architecture for efficient genome editing. Nature biotechnology *29*, 143-148.

Moehle, E.A., Rock, J.M., Lee, Y.L., Jouvenot, Y., DeKelver, R.C., Gregory, P.D., Urnov, F.D., and Holmes, M.C. (2007). Targeted gene addition into a specified location in the human genome using designed zinc finger nucleases. Proceedings of the National Academy of Sciences of the United States of America *104*, 3055-3060.

Moerschel, S.K., Cianciaruso, L.B., and Tracy, L.R. (2008). A practical approach to neonatal jaundice. American family physician *77*, 1255-1262.

Monaghan, G., Ryan, M., Seddon, R., Hume, R., and Burchell, B. (1996). Genetic variation in bilirubin UPD-glucuronosyltransferase gene promoter and Gilbert's syndrome. Lancet *347*, 578-581.

Moon, A.F., Garcia-Diaz, M., Batra, V.K., Beard, W.A., Bebenek, K., Kunkel, T.A., Wilson, S.H., and Pedersen, L.C. (2007). The X family portrait: structural insights into biological functions of X family polymerases. DNA repair *6*, 1709-1725.

Morbitzer, R., Elsaesser, J., Hausner, J., and Lahaye, T. (2011). Assembly of custom TALE-type DNA binding domains by modular cloning. Nucleic acids research *39*, 5790-5799.

Morioka, I., Nakamura, H., Koda, T., Yokota, T., Okada, H., Katayama, Y., Kunikata, T., Kondo, M., Nakamura, M., Hosono, S.*, et al.* (2015). Current incidence of clinical kernicterus in preterm infants in Japan. Pediatrics international : official journal of the Japan Pediatric Society *57*, 494-497.

Moskwa, P., Buffa, F.M., Pan, Y., Panchakshari, R., Gottipati, P., Muschel, R.J., Beech, J., Kulshrestha, R., Abdelmohsen, K., Weinstock, D.M.*, et al.* (2011). miR-182-mediated downregulation of BRCA1 impacts DNA repair and sensitivity to PARP inhibitors. Molecular cell *41*, 210-220.

\

Mullaart, E., Boerrigter, M.E., Ravid, R., Swaab, D.F., and Vijg, J. (1990). Increased levels of DNA breaks in cerebral cortex of Alzheimer's disease patients. Neurobiol Aging *11*, 169-173.

Mussolino, C., Morbitzer, R., Lutge, F., Dannemann, N., Lahaye, T., and Cathomen, T. (2011). A novel TALE nuclease scaffold enables high genome editing activity in combination with low toxicity. Nucleic acids research *39*, 9283-9293.

Nassif, N., Penney, J., Pal, S., Engels, W.R., and Gloor, G.B. (1994). Efficient copying of nonhomologous sequences from ectopic sites via P-element-induced gap repair. Molecular and cellular biology *14*, 1613-1625.

Nguyen, T., Nioi, P., and Pickett, C.B. (2009). The Nrf2-antioxidant response element signaling pathway and its activation by oxidative stress. The Journal of biological chemistry *284*, 13291-13295.

Nguyen, T., Sherratt, P.J., and Pickett, C.B. (2003). Regulatory mechanisms controlling gene expression mediated by the antioxidant response element. Annual review of pharmacology and toxicology *43*, 233-260.

Nick McElhinny, S.A., Havener, J.M., Garcia-Diaz, M., Juarez, R., Bebenek, K., Kee, B.L., Blanco, L., Kunkel, T.A., and Ramsden, D.A. (2005). A gradient of template dependence defines distinct biological roles for family X polymerases in nonhomologous end joining. Molecular cell *19*, 357-366.

Nick McElhinny, S.A., Snowden, C.M., McCarville, J., and Ramsden, D.A. (2000). Ku recruits the XRCC4-ligase IV complex to DNA ends. Molecular and cellular biology *20*, 2996-3003.

Niu, H., Chung, W.H., Zhu, Z., Kwon, Y., Zhao, W., Chi, P., Prakash, R., Seong, C., Liu, D., Lu, L*., et al.* (2010). Mechanism of the ATP-dependent DNA end-resection machinery from Saccharomyces cerevisiae. Nature *467*, 108-111.

Oakes, G.H., and Bend, J.R. (2005). Early steps in bilirubin-mediated apoptosis in murine hepatoma (Hepa 1c1c7) cells are characterized by aryl hydrocarbon receptor-independent oxidative stress and activation of the mitochondrial pathway. Journal of biochemical and molecular toxicology *19*, 244-255.

Oakes, G.H., and Bend, J.R. (2010). Global changes in gene regulation demonstrate that unconjugated bilirubin is able to upregulate and activate select components of the endoplasmic reticulum stress response pathway. Journal of biochemical and molecular toxicology *24*, 73-88.

Olive, P.L., and Banath, J.P. (2006). The comet assay: a method to measure DNA damage in individual cells. Nature protocols *1*, 23-29.

Ollinger, R., Kogler, P., Troppmair, J., Hermann, M., Wurm, M., Drasche, A., Konigsrainer, I., Amberger, A., Weiss, H., Ofner, D*., et al.* (2007). Bilirubin inhibits tumor cell growth via activation of ERK. Cell cycle *6*, 3078-3085.

Olusanya, B.O., Ogunlesi, T.A., and Slusher, T.M. (2014). Why is kernicterus still a major cause of death and disability in low-income and middle-income countries? Archives of disease in childhood *99*, 1117-1121.

Ostrow, J.D., Mukerjee, P., and Tiribelli, C. (1994). Structure and binding of unconjugated bilirubin: relevance for physiological and pathophysiological function. Journal of lipid research *35*, 1715-1737.
Ostrow, J.D., Pascolo, L., Brites, D., and Tiribelli, C. (2004). Molecular basis of bilirubin-induced neurotoxicity. Trends in molecular medicine *10*, 65-70.

Ostrow, J.D., Pascolo, L., and Tiribelli, C. (2003). Reassessment of the unbound concentrations of unconjugated bilirubin in relation to neurotoxicity in vitro. Pediatric research *54*, 98-104.

Owens, D., and Evans, J. (1975). Population studies on Gilbert's syndrome. Journal of medical genetics *12*, 152-156.

Palmela, I., Sasaki, H., Cardoso, F.L., Moutinho, M., Kim, K.S., Brites, D., and Brito, M.A. (2012). Time-dependent dual effects of high levels of unconjugated bilirubin on the human blood-brain barrier lining. Frontiers in cellular neuroscience *6*, 22.

Paull, T.T., and Gellert, M. (1999). Nbs1 potentiates ATP-driven DNA unwinding and endonuclease cleavage by the Mre11/Rad50 complex. Genes & development *13*, 1276-1288.

Pavletich, N.P., and Pabo, C.O. (1991). Zinc finger-DNA recognition: crystal structure of a Zif268-DNA complex at 2.1 A. Science *252*, 809-817.

Perry, J.J., Yannone, S.M., Holden, L.G., Hitomi, C., Asaithamby, A., Han, S., Cooper, P.K., Chen, D.J., and Tainer, J.A. (2006). WRN exonuclease structure and molecular mechanism imply an editing role in DNA end processing. Nature structural & molecular biology *13*, 414-422.

Peter, M.E., Hadji, A., Murmann, A.E., Brockway, S., Putzbach, W., Pattanayak, A., and Ceppi, P. (2015). The role of CD95 and CD95 ligand in cancer. Cell death and differentiation *22*, 549-559.

Petzold, A., Tisdall, M.M., Girbes, A.R., Martinian, L., Thom, M., Kitchen, N., and Smith, M. (2011). In vivo monitoring of neuronal loss in traumatic brain injury: a microdialysis study. Brain : a journal of neurology *134*, 464-483.

Pierce, A.J., Johnson, R.D., Thompson, L.H., and Jasin, M. (1999). XRCC3 promotes homology-directed repair of DNA damage in mammalian cells. Genes & development *13*, 2633-2638.

Porro, F., Bockor, L., De Caneva, A., Bortolussi, G., and Muro, A.F. (2014). Generation of Ugt1-deficient murine liver cell lines using TALEN technology. PloS one *9*, e104816.

Pothof, J., Verkaik, N.S., van, I.W., Wiemer, E.A., Ta, V.T., van der Horst, G.T., Jaspers, N.G., van Gent, D.C., Hoeijmakers, J.H., and Persengiev, S.P. (2009). MicroRNA-mediated gene silencing modulates the UV-induced DNA-damage response. The EMBO journal *28*, 2090-2099.

Povirk, L.F., Zhou, T., Zhou, R., Cowan, M.J., and Yannone, S.M. (2007). Processing of 3'-phosphoglycolate-terminated DNA double strand breaks by Artemis nuclease. The Journal of biological chemistry *282*, 3547-3558.

Qaisiya, M., Brischetto, C., Jasprova, J., Vitek, L., Tiribelli, C., and Bellarosa, C. (2017a). Bilirubin-induced ER stress contributes to the inflammatory response and apoptosis in neuronal cells. Archives of toxicology *91*, 1847-1858.

Qaisiya, M., Coda Zabetta, C.D., Bellarosa, C., and Tiribelli, C. (2014). Bilirubin mediated oxidative stress involves antioxidant response activation via Nrf2 pathway. Cellular signalling *26*, 512-520.

Qaisiya, M., Mardesic, P., Pastore, B., Tiribelli, C., and Bellarosa, C. (2017b). The activation of autophagy protects neurons and astrocytes against bilirubin-induced cytotoxicity. Neuroscience letters *661*, 96-103.

Ramadan, K., Shevelev, I.V., Maga, G., and Hubscher, U. (2004). De novo DNA synthesis by human DNA polymerase lambda, DNA polymerase mu and terminal deoxyribonucleotidyl transferase. Journal of molecular biology *339*, 395-404.

Ramy, N., Ghany, E.A., Alsharany, W., Nada, A., Darwish, R.K., Rabie, W.A., and Aly, H. (2016). Jaundice, phototherapy and DNA damage in full-term neonates. Journal of perinatology : official journal of the California Perinatal Association *36*, 132-136.

Rass, U., Ahel, I., and West, S.C. (2007). Defective DNA repair and neurodegenerative disease. Cell *130*, 991-1004.

Rebar, E.J., and Pabo, C.O. (1994). Zinc finger phage: affinity selection of fingers with new DNA-binding specificities. Science *263*, 671-673.

Refaey, M.E., McGee-Lawrence, M.E., Fulzele, S., Kennedy, E.J., Bollag, W.B., Elsalanty, M., Zhong, Q., Ding, K.H., Bendzunas, N.G., Shi, X.M.*, et al.* (2017). Kynurenine, a Tryptophan Metabolite That Accumulates With Age, Induces Bone Loss. Journal of bone and mineral research : the official journal of the American Society for Bone and Mineral Research *32*, 2182-2193.

Renkawitz, J., Lademann, C.A., and Jentsch, S. (2014). Mechanisms and principles of homology search during recombination. Nature reviews Molecular cell biology *15*, 369-383.

Reyon, D., Tsai, S.Q., Khayter, C., Foden, J.A., Sander, J.D., and Joung, J.K. (2012). FLASH assembly of TALENs for high-throughput genome editing. Nature biotechnology *30*, 460-465.

Riley, T., Sontag, E., Chen, P., and Levine, A. (2008). Transcriptional control of human p53-regulated genes. Nature reviews Molecular cell biology *9*, 402-412.

Roberts, S.A., Strande, N., Burkhalter, M.D., Strom, C., Havener, J.M., Hasty, P., and Ramsden, D.A. (2010). Ku is a 5'-dRP/AP lyase that excises nucleotide damage near broken ends. Nature *464*, 1214-1217.

Roca, L., Calligaris, S., Wennberg, R.P., Ahlfors, C.E., Malik, S.G., Ostrow, J.D., and Tiribelli, C. (2006). Factors affecting the binding of bilirubin to serum albumins: validation and application of the peroxidase method. Pediatric research *60*, 724-728.

Rodrigues, C.M., Sola, S., Silva, R., and Brites, D. (2000). Bilirubin and amyloid-beta peptide induce cytochrome c release through mitochondrial membrane permeabilization. Mol Med *6*, 936-946.

Rosen, L.E., Morrison, H.A., Masri, S., Brown, M.J., Springstubb, B., Sussman, D., Stoddard, B.L., and Seligman, L.M. (2006). Homing endonuclease I-CreI derivatives with novel DNA target specificities. Nucleic acids research *34*, 4791-4800.

Rubinsztein, D.C., Ravikumar, B., Acevedo-Arozena, A., Imarisio, S., O'Kane, C.J., and Brown, S.D. (2005). Dyneins, autophagy, aggregation and neurodegeneration. Autophagy *1*, 177-178.

Rupaimoole, R., and Slack, F.J. (2017). MicroRNA therapeutics: towards a new era for the management of cancer and other diseases. Nature reviews Drug discovery *16*, 203-222.

San Filippo, J., Sung, P., and Klein, H. (2008). Mechanism of eukaryotic homologous recombination. Annual review of biochemistry *77*, 229-257.
\
Sander, J.D., Cade, L., Khayter, C., Reyon, D., Peterson, R.T., Joung, J.K., and Yeh, J.R. (2011a). Targeted gene disruption in somatic zebrafish cells using engineered TALENs. Nature biotechnology *29*, 697-698.

Sander, J.D., Dahlborg, E.J., Goodwin, M.J., Cade, L., Zhang, F., Cifuentes, D., Curtin, S.J., Blackburn, J.S., Thibodeau-Beganny, S., Qi, Y.*, et al.* (2011b). Selection-free zinc-finger-nuclease engineering by context-dependent assembly (CoDA). Nature methods *8*, 67-69.

Sartori, A.A., Lukas, C., Coates, J., Mistrik, M., Fu, S., Bartek, J., Baer, R., Lukas, J., and Jackson, S.P. (2007). Human CtIP promotes DNA end resection. Nature *450*, 509-514.

Schmid-Burgk, J.L., Schmidt, T., Kaiser, V., Honing, K., and Hornung, V. (2013). A ligation-independent cloning technique for high-throughput assembly of transcription activator-like effector genes. Nature biotechnology *31*, 76-81.

Schonn, I., Hennesen, J., and Dartsch, D.C. (2010). Cellular responses to etoposide: cell death despite cell cycle arrest and repair of DNA damage. Apoptosis *15*, 162-172.

Scott, R.C., Juhasz, G., and Neufeld, T.P. (2007). Direct induction of autophagy by Atg1 inhibits cell growth and induces apoptotic cell death. Current biology : CB *17*, 1-11.

Segal, D.J., Dreier, B., Beerli, R.R., and Barbas, C.F., 3rd (1999). Toward controlling gene expression at will: selection and design of zinc finger domains recognizing each of the 5'-GNN-3' DNA target sequences. Proceedings of the National Academy of Sciences of the United States of America *96*, 2758-2763.

Sellier, A.L., Labrune, P., Kwon, T., Boudjemline, A.M., Deschenes, G., and Gajdos, V. (2012). Successful plasmapheresis for acute and severe unconjugated hyperbilirubinemia in a child with crigler najjar type I syndrome. JIMD reports *2*, 33-36.

Seubert, J.M., Darmon, A.J., El-Kadi, A.O., D'Souza, S.J., and Bend, J.R. (2002). Apoptosis in murine hepatoma hepa 1c1c7 wild-type, C12, and C4 cells mediated by bilirubin. Molecular pharmacology *62*, 257-264.

Shah, Z., Chawla, A., Patkar, D., and Pungaonkar, S. (2003). MRI in kernicterus. Australasian radiology *47*, 55-57.

Shapiro, S.M. (2003). Bilirubin toxicity in the developing nervous system. Pediatric neurology *29*, 410-421.

Shapiro, S.M. (2010). Chronic bilirubin encephalopathy: diagnosis and outcome. Seminars in fetal & neonatal medicine *15*, 157-163.

Shapiro, S.M., Bhutani, V.K., and Johnson, L. (2006). Hyperbilirubinemia and kernicterus. Clinics in perinatology *33*, 387-410.

Shapiro, S.M., and Nakamura, H. (2001). Bilirubin and the auditory system. Journal of perinatology : official journal of the California Perinatal Association *21 Suppl 1*, S52-55; discussion S59-62.

Sharma, A., Singh, K., and Almasan, A. (2012). Histone H2AX phosphorylation: a marker for DNA damage. Methods Mol Biol *920*, 613-626.

Sharma, R., Anguela, X.M., Doyon, Y., Wechsler, T., DeKelver, R.C., Sproul, S., Paschon, D.E., Miller, J.C., Davidson, R.J., Shivak, D*., et al.* (2015). In vivo genome editing of the albumin locus as a platform for protein replacement therapy. Blood *126*, 1777-1784.

Sharma, V., Collins, L.B., Chen, T.H., Herr, N., Takeda, S., Sun, W., Swenberg, J.A., and Nakamura, J. (2016). Oxidative stress at low levels can induce clustered DNA lesions leading to NHEJ mediated mutations. Oncotarget *7*, 25377-25390.

Shen, Y.N., Bae, I.S., Park, G.H., Choi, H.S., Lee, K.H., and Kim, S.H. (2018). MicroRNA-196b enhances the radiosensitivity of SNU-638 gastric cancer cells by targeting RAD23B. Biomedicine & pharmacotherapy = Biomedecine & pharmacotherapie *105*, 362-369.

Shibata, A. (2017). Regulation of repair pathway choice at two-ended DNA double-strand breaks. Mutation research *803-805*, 51-55.

Shiloh, Y. (2003). ATM and related protein kinases: safeguarding genome integrity. Nature reviews Cancer *3*, 155-168.

Shinohara, A., Ogawa, H., and Ogawa, T. (1992). Rad51 protein involved in repair and recombination in S. cerevisiae is a RecA-like protein. Cell *69*, 457-470.

Silva, R.F., Rodrigues, C.M., and Brites, D. (2001). Bilirubin-induced apoptosis in cultured rat neural cells is aggravated by chenodeoxycholic acid but prevented by ursodeoxycholic acid. Journal of hepatology *34*, 402-408.

Silva, S.L., Vaz, A.R., Barateiro, A., Falcao, A.S., Fernandes, A., Brito, M.A., Silva, R.F., and Brites, D. (2010). Features of bilirubin-induced reactive microglia: from phagocytosis to inflammation. Neurobiology of disease *40*, 663-675.

Sinaasappel, M., and Jansen, P.L. (1991). The differential diagnosis of Crigler-Najjar disease, types 1 and 2, by bile pigment analysis. Gastroenterology *100*, 783-789.

Smith, J., Bibikova, M., Whitby, F.G., Reddy, A.R., Chandrasegaran, S., and Carroll, D. (2000). Requirements for double-strand cleavage by chimeric restriction enzymes with zinc finger DNA-recognition domains. Nucleic acids research *28*, 3361-3369.

Smith, J., Grizot, S., Arnould, S., Duclert, A., Epinat, J.C., Chames, P., Prieto, J., Redondo, P., Blanco, F.J., Bravo, J.*, et al.* (2006). A combinatorial approach to create artificial homing endonucleases cleaving chosen sequences. Nucleic acids research *34*, e149.

Smitherman, H., Stark, A.R., and Bhutani, V.K. (2006). Early recognition of neonatal hyperbilirubinemia and its emergent management. Seminars in fetal & neonatal medicine *11*, 214-224.

Sternberg, S.H., Redding, S., Jinek, M., Greene, E.C., and Doudna, J.A. (2014). DNA interrogation by the CRISPR RNA-guided endonuclease Cas9. Nature *507*, 62-67.

Sticova, E., and Jirsa, M. (2013). New insights in bilirubin metabolism and their clinical implications. World journal of gastroenterology *19*, 6398-6407.

Stocker, R., Yamamoto, Y., McDonagh, A.F., Glazer, A.N., and Ames, B.N. (1987). Bilirubin is an antioxidant of possible physiological importance. Science *235*, 1043-1046.

Stracker, T.H., and Petrini, J.H. (2011). The MRE11 complex: starting from the ends. Nature reviews Molecular cell biology *12*, 90-103.

Suberbielle, E., Sanchez, P.E., Kravitz, A.V., Wang, X., Ho, K., Eilertson, K., Devidze, N., Kreitzer, A.C., and Mucke, L. (2013). Physiologic brain activity causes DNA double-strand breaks in neurons, with exacerbation by amyloid-beta. Nat Neurosci *16*, 613-621.

Sumida, K., Kawana, M., Kouno, E., Itoh, T., Takano, S., Narawa, T., Tukey, R.H., and Fujiwara, R. (2013). Importance of UDP-glucuronosyltransferase 1A1 expression in skin and its induction by UVB in neonatal hyperbilirubinemia. Molecular pharmacology *84*, 679-686.

Symington, L.S., and Gautier, J. (2011). Double-strand break end resection and repair pathway choice. Annual review of genetics *45*, 247-271.

Takata, M., Sasaki, M.S., Sonoda, E., Morrison, C., Hashimoto, M., Utsumi, H., Yamaguchi-Iwai, Y., Shinohara, A., and Takeda, S. (1998). Homologous recombination and non-homologous end-joining pathways of DNA double-strand break repair have overlapping roles in the maintenance of chromosomal integrity in vertebrate cells. The EMBO journal *17*, 5497-5508.

Tatli, M.M., Minnet, C., Kocyigit, A., and Karadag, A. (2008). Phototherapy increases DNA damage in lymphocytes of hyperbilirubinemic neonates. Mutation research *654*, 93-95.

Tebas, P., Stein, D., Tang, W.W., Frank, I., Wang, S.Q., Lee, G., Spratt, S.K., Surosky, R.T., Giedlin, M.A., Nichol, G.*, et al.* (2014). Gene editing of CCR5 in autologous CD4 T cells of persons infected with HIV. N Engl J Med *370*, 901-910.

Tell, G., and Gustincich, S. (2009). Redox state, oxidative stress, and molecular mechanisms of protective and toxic effects of bilirubin on cells. Current pharmaceutical design *15*, 2908-2914.

Travan, L., Lega, S., Crovella, S., Montico, M., Panontin, E., and Demarini, S. (2014). Severe neonatal hyperbilirubinemia and UGT1A1 promoter polymorphism. The Journal of pediatrics *165*, 42-45.

Trujillo, K.M., Roh, D.H., Chen, L., Van Komen, S., Tomkinson, A., and Sung, P. (2003). Yeast xrs2 binds DNA and helps target rad50 and mre11 to DNA ends. The Journal of biological chemistry *278*, 48957-48964.

Tupler, R., Perini, G., and Green, M.R. (2001). Expressing the human genome. Nature *409*, 832-833.

Uematsu, N., Weterings, E., Yano, K., Morotomi-Yano, K., Jakob, B., Taucher-Scholz, G., Mari, P.O., van Gent, D.C., Chen, B.P., and Chen, D.J. (2007). Autophosphorylation of DNA-PKCS regulates its dynamics at DNA double-strand breaks. The Journal of cell biology *177*, 219-229.

Urnov, F.D., Miller, J.C., Lee, Y.L., Beausejour, C.M., Rock, J.M., Augustus, S., Jamieson, A.C., Porteus, M.H., Gregory, P.D., and Holmes, M.C. (2005). Highly efficient endogenous human gene correction using designed zinc-finger nucleases. Nature *435*, 646-651.

Uttara, B., Singh, A.V., Zamboni, P., and Mahajan, R.T. (2009). Oxidative stress and neurodegenerative diseases: a review of upstream and downstream antioxidant therapeutic options. Current neuropharmacology *7*, 65-74.

Valko, M., Rhodes, C.J., Moncol, J., Izakovic, M., and Mazur, M. (2006). Free radicals, metals and antioxidants in oxidative stress-induced cancer. Chemico-biological interactions *160*, 1-40.

van de Steeg, E., Stranecky, V., Hartmannova, H., Noskova, L., Hrebicek, M., Wagenaar, E., van Esch, A., de Waart, D.R., Oude Elferink, R.P., Kenworthy, K.E*., et al.* (2012). Complete OATP1B1 and OATP1B3 deficiency causes human Rotor syndrome by interrupting conjugated bilirubin reuptake into the liver. The Journal of clinical investigation *122*, 519-528.

Vaz, A.R., Delgado-Esteban, M., Brito, M.A., Bolanos, J.P., Brites, D., and Almeida, A. (2010). Bilirubin selectively inhibits cytochrome c oxidase activity and induces apoptosis in immature cortical neurons: assessment of the protective effects of glycoursodeoxycholic acid. Journal of neurochemistry *112*, 56-65.

Vaz, A.R., Silva, S.L., Barateiro, A., Falcao, A.S., Fernandes, A., Brito, M.A., and Brites, D. (2011). Selective vulnerability of rat brain regions to unconjugated bilirubin. Molecular and cellular neurosciences *48*, 82-93.

Vitek, L., and Carey, M.C. (2003). Enterohepatic cycling of bilirubin as a cause of 'black' pigment gallstones in adult life. European journal of clinical investigation *33*, 799-810.

Vodret, S., Bortolussi, G., Jasprova, J., Vitek, L., and Muro, A.F. (2017). Inflammatory signature of cerebellar neurodegeneration during neonatal hyperbilirubinemia in Ugt1 (-/-) mouse model. Journal of neuroinflammation *14*, 64.

Vodret, S., Bortolussi, G., Schreuder, A.B., Jasprova, J., Vitek, L., Verkade, H.J., and Muro, A.F. (2015). Albumin administration prevents neurological damage and death in a mouse model of severe neonatal hyperbilirubinemia. Scientific reports *5*, 16203.

Wahid, F., Shehzad, A., Khan, T., and Kim, Y.Y. (2010). MicroRNAs: synthesis, mechanism, function, and recent clinical trials. Biochimica et biophysica acta *1803*, 1231-1243.

Wallner, M., Antl, N., Rittmannsberger, B., Schreidl, S., Najafi, K., Mullner, E., Molzer, C., Ferk, F., Knasmuller, S., Marculescu, R.*, et al.* (2013). Anti-genotoxic potential of bilirubin in vivo: damage to DNA in hyperbilirubinemic human and animal models. Cancer prevention research *6*, 1056-1063.

Wang, C., Yang, J., Lu, D., Fan, Y., Zhao, M., and Li, Z. (2016). Oxidative stress-related DNA damage and homologous recombination repairing induced by N,N-dimethylformamide. Journal of applied toxicology : JAT *36*, 936-945.

Wang, Y., Huang, J.W., Calses, P., Kemp, C.J., and Taniguchi, T. (2012). MiR-96 downregulates REV1 and RAD51 to promote cellular sensitivity to cisplatin and PARP inhibition. Cancer research *72*, 4037-4046.

Ward, I.M., and Chen, J. (2001). Histone H2AX is phosphorylated in an ATR-dependent manner in response to replicational stress. J Biol Chem *276*, 47759-47762.

Watchko, J.F. (2006). Kernicterus and the molecular mechanisms of bilirubin-induced CNS injury in newborns. Neuromolecular medicine *8*, 513-529.

Watchko, J.F., and Tiribelli, C. (2013). Bilirubin-induced neurologic damage--mechanisms and management approaches. The New England journal of medicine *369*, 2021-2030.

Wei, W., Ba, Z., Gao, M., Wu, Y., Ma, Y., Amiard, S., White, C.I., Rendtlew Danielsen, J.M., Yang, Y.G., and Qi, Y. (2012). A role for small RNAs in DNA double-strand break repair. Cell *149*, 101-112.

Weiner, A., Zauberman, N., and Minsky, A. (2009). Recombinational DNA repair in a cellular context: a search for the homology search. Nature reviews Microbiology *7*, 748-755.

Weissman, L., de Souza-Pinto, N.C., Stevnsner, T., and Bohr, V.A. (2007). DNA repair, mitochondria, and neurodegeneration. Neuroscience *145*, 1318-1329.

Wen, Y., Zhai, R.G., and Kim, M.D. (2013). The role of autophagy in Nmnat-mediated protection against hypoxia-induced dendrite degeneration. Molecular and cellular neurosciences *52*, 140-151.

Wennberg, R.P., Ahlfors, C.E., Bhutani, V.K., Johnson, L.H., and Shapiro, S.M. (2006). Toward understanding kernicterus: a challenge to improve the management of jaundiced newborns. Pediatrics *117*, 474-485.

Wennberg, R.P., Ahlfors, C.E., and Rasmussen, L.F. (1979). The pathochemistry of kernicterus. Early human development *3*, 353-372.

Wennberg, R.P., and Hance, A.J. (1986). Experimental bilirubin encephalopathy: importance of total bilirubin, protein binding, and blood-brain barrier. Pediatric research *20*, 789-792.

Weterings, E., and Chen, D.J. (2008). The endless tale of non-homologous end-joining. Cell research *18*, 114-124.

Wilhelm, T., Ragu, S., Magdalou, I., Machon, C., Dardillac, E., Techer, H., Guitton, J., Debatisse, M., and Lopez, B.S. (2016). Slow Replication Fork Velocity of Homologous Recombination-Defective Cells Results from Endogenous Oxidative Stress. PLoS genetics *12*, e1006007.

Williams, R.S., Williams, J.S., and Tainer, J.A. (2007). Mre11-Rad50-Nbs1 is a keystone complex connecting DNA repair machinery, double-strand break signaling, and the chromatin template. Biochemistry and cell biology = Biochimie et biologie cellulaire *85*, 509-520.

Yaffe, S.J., Levy, G., Matsuzawa, T., and Baliah, T. (1966). Enhancement of glucuronide-conjugating capacity in a hyperbilirubinemic infant due to apparent enzyme induction by phenobarbital. The New England journal of medicine *275*, 1461-1466.

Yahia, S., Shabaan, A.E., Gouida, M., El-Ghanam, D., Eldegla, H., El-Bakary, A., and Abdel-Hady, H. (2015). Influence of hyperbilirubinemia and phototherapy on markers of genotoxicity and apoptosis in full-term infants. European journal of pediatrics *174*, 459-464.

Yano, K., Morotomi-Yano, K., Wang, S.Y., Uematsu, N., Lee, K.J., Asaithamby, A., Weterings, E., and Chen, D.J. (2008). Ku recruits XLF to DNA double-strand breaks. EMBO reports *9*, 91-96.

Yi, D.G., Kim, M.J., Choi, J.E., Lee, J., Jung, J., Huh, W.K., and Chung, W.H. (2016). Yap1 and Skn7 genetically interact with Rad51 in response to oxidative stress and DNA double-strand break in Saccharomyces cerevisiae. Free radical biology & medicine *101*, 424-433.

Yueh, M.F., Chen, S., Nguyen, N., and Tukey, R.H. (2014). Developmental onset of bilirubin-induced neurotoxicity involves Toll-like receptor 2-dependent signaling in humanized UDP-glucuronosyltransferase1 mice. The Journal of biological chemistry *289*, 4699-4709.

Zhang, F., Cong, L., Lodato, S., Kosuri, S., Church, G.M., and Arlotta, P. (2011). Efficient construction of sequence-specific TAL effectors for modulating mammalian transcription. Nature biotechnology *29*, 149-153.